To Bernard —

Thank you very much for
all the help & encouragement.

Cliff

Investigations on the Role of Fluid During
Granulite Facies Metamorphism, Kigluaik
Mountains, Seward Peninsula, Alaska

by

Clifford Scott Todd

A thesis submitted in partial fulfillment
of the requirements for the degree of

Doctor of Philosophy

University of Washington

1992

Approved by _____
(Chairperson of Supervisory Committee)

Program Authorized
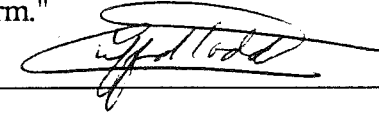to Offer Degree _____ Geological Sciences _____

Date _____ June 2, 1992 _____

Doctoral Dissertation

In presenting this dissertation in partial fulfillment of the requirements for the Doctoral degree at the University of Washington, I agree that the Library shall make its copies freely available for inspection. I further agree that extensive copying of this dissertation is allowable only for scholarly purposes, consistent with "fair use" as prescribed in the U.S. Copyright Law. Requests for copying or reproduction of this dissertation may be referred to University Microfilms, 1490 Eisenhower Place, P.O. Box 975, Ann Arbor, MI 48106, to whom the author has granted "the right to reproduce and sell (a) copies of the manuscript in microform and/or (b) printed copies of the manuscript made from microform."

Signature _____

Date ___2 June 1992_____

University of Washington

Abstract

Investigations on the Role of Fluid During Granulite Facies Metamorphism, Kigluaik Mountains, Seward Peninsula, Alaska

by Clifford Scott Todd

Chairperson of the Supervisory Committee: Professor Bernard W. Evans
Department of Geological Sciences

Flat-lying thick marble units acted as impermeable barriers to upward fluid flow in amphibolite to granulite grade rocks of the Kigluaik Mountains, Seward Peninsula, Alaska. The degree of impermeability can be related to the composition of the marble. The margin of a thick pure dolomite marble chemically reacted with underlying metasyenite to form a 2 cm thick border of calcite + forsterite. No fluid penetrated past this reaction front. The high temperatures at which this process occurred (nearly 800°C) allowed C and O isotopic interaction for an additional 2 cm by diffusion through the solid dolomite. A second marble with a higher silica content underwent more decarbonation, which enhanced porosity and lead to a greater extent of isotopic interaction. An estimate of fluid flux across the bottom of this marble layer based on the shape of the isotope profile is 1 cm^3/cm^2 directed down, out of the marble. At two other marble-gneiss contacts, steep isotopic gradients exist, coincident with the lithologic contacts, indicating very little cross-lithology fluid flux.

Fluid composition during metamorphism was locally controlled by lithology. At a contact where an homogeneous Hbl-bearing gneiss lies above a marble, Hbl in the gneiss reacted to form fine-grained granular Opx, Cpx, Pl and Kfs within 60 cm of the marble. The Hbl-bearing and Hbl-free gneiss assemblages are related by Bt and Hbl

dehydration reactions. These reactions were driven by a reduction in H_2O-activity due to dilution with CO_2 from the marble. Water-activity calculations based on biotite dehydration equilibria in the Hbl-free gneiss indicate a trend from 0.14 to 0.08 toward the marble. Mineral assemblages confirm that the marble was a source of high XCO_2 fluids. This example provides an indication of the limited role (60 cm) played by fluid movement in controlling mineral parageneses in this terrane.

It is concluded that there was no pervasive infiltration of C-O-H fluid across the thick, continuous, marble units of the amphibolite to granulite grade Kigluaik Group during peak metamorphism. Movement of volatile species and isotopic interaction between rocks during peak metamorphism was dominated by diffusive processes. No evidence for channelized fluid pathways through the marble units during peak metamorphism has been found. Therefore, heating of the terrane occurred by conduction, not advection via a fluid.

In granulite grade rocks of the Kigluaik Mountains, no peak metamorphic fluids survived as fluid inclusions. Retrograde CO_2-rich fluids were trapped late in the metamorphic cycle and have variable density around 0.5 g/cm^3. In amphibolite grade rocks, aqueous fluid inclusions may represent samples of near-peak metamorphic fluids. Density of these inclusions varies from 0.9 to 0.8 g/cm^3 with salinities less than 4 wt% NaCl equivalent.

TABLE OF CONTENTS

LIST OF FIGURES

LIST OF TABLES

ACKNOWLEDGMENTS

Chapter 1: Introduction and background

Definition of Problem

This paper is presented as a contribution to the ongoing debate concerning the role of fluid infiltration in deep-crustal granulite facies environments. In contrast to greenschist and amphibolite grade regional metamorphic environments where numerous recent phase equilibrium, reaction progress, and stable-isotope studies have demonstrated major involvement of fluid advection (e.g., Rumble et al. 1982, Tracy et al. 1983, Ferry 1984, 1986, Wickham and Taylor 1985, 1987, Hoisch 1991; Chamberlain and Rumble 1988, 1989), conclusions regarding fluid composition and fluxes during granulite-grade metamorphism appear to be in conflict (see Newton 1986). In lower crustal environments, it seems necessary to document the specific circumstances for each terrane (Peacock 1991); certainly, more case studies need to be presented in order to establish generalized models for the lower crust.

In any crustal environment, fluids play potentially major roles in the transfer of thermal energy (Brady 1988), as a catalyst (Rubie 1986), a medium of mass transfer (Fyfe et al. 1978), and an important factor in rheology (Etheridge et al. 1984). At deeper crustal levels, there are additional complexities related to the development and possible migration of partial melts, to the release of fluids from crystallizing magmas, and to the possible introduction of fluids from the upper mantle. While there is general agreement that granulite facies rocks were mostly hotter and drier than those with high-amphibolite facies parageneses, the role of the fluid phase during granulite grade metamorphism remains the subject of continued discussion. The present work concentrates on identifying and quantifying the composition, abundance and transport characteristics of fluid in a well-exposed, amphibolite to granulite grade metamorphic

terrane on the Seward Peninsula of Alaska. This is accomplished through the investigation of mineral assemblages and mineral chemistry, stable isotope geochemistry, and fluid inclusions.

Geologic Setting

Location

The Seward Peninsula is located in the western part of Alaska (figure 1.1), with the Bering Sea to the north, Norton Sound to the South and the Bering Straights to the west. The Peninsula is composed mostly of rolling hills covered by treeless tundra. Mountain ranges are present in the inland portions of the peninsula which expose more rugged terrain. The Kigluaik Mountains are one such range. Geologic exploration was initiated on the Peninsula when placer gold deposits were discovered on the beach at the town of Nome in 1897.

Previous Work

A good historical review of the geologic work done on the Seward Peninsula was presented by Till (1980) and Till and Dumoulin (1992) , and is briefly summarized here. Following the discovery of gold, the U.S. Geological Survey conducted several reconnaissance surveys on the Seward Peninsula (Brooks et al. 1901, Collier 1902, Collier et al. 1908, Smith 1908 1910, Moffit 1913). This lead to more focussed studies on the occurrence of economic mineral deposits (Harrington 1919a b, Cathcart 1922, Steidtmann and Cathcart 1922), continued mapping (Hummel 1962a b, Sainsbury et al. 1969 1972a b c d e f, Sainsbury 1969 1972, Miller et al. 1972, Hudson 1977, Robinson and Stevens 1984) and geophysical surveys (Cady 1977, Barnes and Hudson 1977). More recent work concerning metamorphic petrogenesis on the peninsula has

been initiated by groups from the University of Washington and the University of Alaska (Till 1980, Pollock 1982, Sturnick 1984, Forbes et al. 1984, Thurston 1985, Armstrong et al. 1986, Evans and Patrick 1987, Patrick 1987 1988, Lieberman 1988, Patrick and Lieberman 1988, Patrick and Evans 1989, Buxton 1990, Evans et al. 1992, Lieberman and Petrakakis 1992), with work also being conducted from Stanford University (Miller et al. 1992a, Calvert 1992).

Current Understanding

Rocks of the Seward Peninsula of Alaska can be divided into four groups based on their metamorphic grade (Pollock 1982): 1) low grade metasediments of the York Mountains, 2) blueschist/greenschist facies metasediments and meta-igneous rocks of the Nome Group, 3) amphibolite to granulite facies rocks (Kigluaik Group) of the Kigluaik, Bendeleben and Darby Mountains, 4) unmetamorphosed Cretaceous or younger sedimentary and igneous rocks (figure 1.1). The Nome Group is of Cretaceous metamorphic age (Armstrong et al. 1986). The schists are believed to be related to the high P/T rocks of the schist belt along the southern margin of the Brooks Range (Hitzman et al. 1986; Patrick 1988; Gottschalk 1990). The protoliths of the Nome Group were continental margin related carbonates, pelites, volcanics and calcareous sediments of preCambrian (?) to Devonian age (Till et al. 1986, Buxton 1990). Together with later intrusive bodies, this package underwent subduction beneath oceanic and island arc crust (Box 1985).

In three mountain ranges on the Seward Peninsula (Kigluaik, Darby and Bendeleben), uplifts or structural arches expose Barrovian-style metamorphic complexes formed by dynamo-thermal overprint on Nome Group schists (figure 1.1). The high grade rocks of the Kigluaik Mountains, which are stratigraphically and structurally continuous with the overlying Nome Group schists (figures 1.2, 1.3 and 1.4; also see

Patrick and Lieberman 1988), grade downward through biotite, staurolite, sillimanite, and sillimanite + K-feldspar zones into orthopyroxene-bearing gneisses in the most deeply exposed parts (Till 1980). The Kigluaik Group metasediments probably include rocks at least as old as late Proterozoic (Armstrong et al. 1986). Timing of the peak of high grade metamorphism is currently under investigation, but probably occurred around 109-103 Ma (Armstrong et al. 1986, Lieberman and Van der Heyden personal communication, J. Wright personal communication), with rapid cooling of the area occurring around 85 Ma (Turner et al. 1979, Miller et al. 1992a b, Amato et al. 1992).

In the most deeply exposed portion of the Kigluaik Mountains, maximum metamorphic conditions of approximately 800°C and 8 kbar (Lieberman 1988; Lieberman and Petrakakis 1992) were followed by decompression, as indicated by mineral replacements and petrogenetic grid considerations (Ky → Sil; Rt → Ilm; Bt + Sil → Crd; Grt → Opx + Pl; abbreviations in table 1.1). P-T conditions in the isograd region are as follows (Lieberman 1988): Sta 550°C 4 kbar, Sil 660°C 4.5 kbar, Sil+Kfs 725°C 5.5 kbar.

Description of Lithologic Units

An explanation of lithologies found in the Kigluaik Mountains is presented here (figure 1.4). Additional information can be found in Till (1980), Pollock (1982), Sturnick (1984), Lieberman (1988) and Calvert (1992).

Pelite above the Thompson Creek Orthogneiss (4th pelite)

A series of isograds occur within this unit (figures 1.2, 1.3 and 1.4). By increasing grade they are: Bt, Sta, Sil and Sil+Kfs. All isograds are parallel to lithologic layering. The first occurrence of biotite and staurolite is probably controlled by the bulk composition of the rock. The Bt isograd typically is at the boundary between a graphitic

quartzite and a biotite schist. The Sta isograd occupies the boundary between the biotite schist (which contains no Al-rich minerals) and a pelitic schist. In contrast, the Sil isograd is controlled by mineral reactions in which the outer portions of garnets reacted to form fine grained mats of sillimanite (Lieberman 1988). The Sil+Kfs isograd is controlled by the reaction:

$$Ms + Qtz \rightarrow Sil + Kfs + H_2O \qquad\qquad (1)$$

and occurs at the base of the unit, near the Thompson Creek orthogneiss (Till 1980). In the staurolite zone, peak metamorphic mineral assemblages include: Grt + Bt + Sta + Ms + Qtz, Bt + Sta + Ky + Ms + Qtz, and Bt + Ky + Crd + Ms + Qtz (figure 1.5). Upgrade of the Sil isograd the assemblage may be: Bt + Sta + Sil + Ms + Qtz or Grt + Bt + Sil + Qtz + Ms. Plagioclase and graphite are commonly present in all assemblages. Calculated water activities are around unity (Lieberman 1988). A compilation of mineral assemblage information from Kigluaik pelites can be found in Appendix I.

Pelites below the Thompson Creek Orthogneiss (1st, 2nd and 3rd pelites)

The typical peak metamorphic mineral assemblage in a pelitic schist is: Grt + Bt + Sil + Pl + Kfs + Qtz + Ilm ± Graph. In rare cases, graphite constitutes 80% of the rock. Calculated activities of H_2O are about 0.5 (Lieberman 1988). Figure 1.6 shows the effect of increasing grade on mineral compositions in the AFM assemblage Grt + Bt + Sil. The shift toward more Mg-rich compositions is driven by the continuous reaction:

$$Sil + Bt + Qtz \rightarrow Grt + Kfs + H_2O. \qquad\qquad (2)$$

In many samples from the 1st pelite, kyanite occurs as inclusions in garnet whereas sillimanite occurs in the matrix of the rock. Also, rutile commonly occurs as inclusions within garnet, but not in the matrix, where ilmenite is usually present. Both

of these relationships indicate a history of higher pressures prior to peak metamorphism via the respective reactions:

$$Ky \rightarrow Sil, \tag{3}$$

and:

$$Grt + Rt \rightarrow Sil + Qtz + Ilm. \tag{4}$$

In Kigluaik pelites it is not uncommon for small amounts of cordierite to occur along the biotite and sillimanite foliation, indicating retrograde decompression manifested by the continuous reaction:

$$Bt + Sil + Qtz \rightarrow Crd + Kfs + H_2O \pm melt. \tag{5}$$
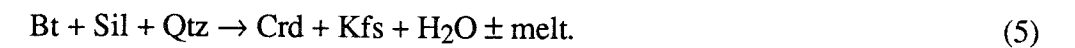
This reaction can be local in extent and garnet may not have participated in the reaction leading to some of the spuriously high temperatures obtained by the Grt-Bt Fe-Mg exchange thermometer obtained in the Kigluaik mountains by Lieberman (1988).

Staurolite is found as inclusions within garnet in pelites from all stratigraphic levels, although it is not found as a matrix mineral beyond the Sil+Kfs isograd. Some of these staurolites are accompanied by hercynite, a breakdown product of staurolite in the absence of quartz. These staurolites were stabilized to higher temperatures both by being separated from other reactants (Qtz ± Ms) by a mantle of garnet, and by a higher Zn content (up to 7% Zn end member). The spinel found with staurolite inclusions also has an elevated Zn content (~10% Zn end member).

Marbles

Pure dolomitic marbles are very coarse grained (up to 0.5 cm) and may be bluish-gray in color. Calcitic marbles tend to be whiter and finer grained (around 0.1 cm). Marbles are generally granoblastic with weak foliation defined by oriented micas, when present. Since there are very few marble layers in the isograd area, most marbles sampled are from approximately the same grade. By 800°C the buffer capacity of

marbles is nearly exhausted (figure 1.7). The peak metamorphic mineral assemblage is determined by the bulk composition of the rock. Most marble mineral assemblages can be described by the bold compatibility triangle in figure 1.7. Fluid compositions associated with marbles are discussed in chapter 3.

Metaperidotite

A metaperidotite unit occurs low in the stratigraphy (figure 1.4). This unit is distinctive in the field because of its orange color when weathered. It varies from about 3 m to 50 m thick. In places the metaperidotite unit is massive, and the foliation, defined by flattened discs of Opx, is concordant with the layering in nearby lithologies. In other places the metaperidotite unit is boudinaged with pegmatite or, rarely, marble filling the interstices of the jumbled, rounded blocks of metaperidotite. These blocks are typically several centimeters to one meter in diameter. The mineral assemblage in the metaperidotite is Fo + Opx + Cpx + Spl ± Phl ± Prg ± Grt remnants. A thorough investigation of the metaperidotite unit was done by Lieberman (1988). Associated with the metaperidotite, though not universally present, is a mafic gneiss. The assemblage is: Opx + Cpx + Pl + Ilm + Hbl + Bt + Grt.

Below the Peridotite (0th pelite)

The lowest part of the exposed stratigraphy in the Kigluaik Mountains is dominated by fine-grained felsic, intermediate and calcareous gneiss, with minor marble. These rocks are compositionally layered on a scale as small as centimeters. A common assemblage in calcareous gneiss is: Cpx + Pl + Qtz ± Tnt. In the few marbles sampled, the assemblage is: Cal + Fo ± Dol ± Spl ± Phl. The assemblage observed in felsic compositions is: Grt + Bi + Qtz + Pl ± Kfs ± Ilm ± Opx. Figure 1.8 depicts the mineral chemistry of one Opx-bearing lithology along with a sillimanite-bearing

assemblage from the 1st pelite on an AFM projection. Since tie lines do not cross, the difference in assemblage may be due to a difference in bulk composition rather than in temperature.

Post-metamorphic Igneous rocks

Crosscutting pegmatite dikes are common. Where these are in contact with marble layers, skarn assemblages (including wollastonite, grossular and vesuvianite) may occur. In several localities at the base of the main marble, graphite deposits have developed in vugs within the pegmatites and along joints. This graphite occurrence may be related to mixing of reduced vein fluids with oxidized marble fluids (Rumble and Hoering 1986). Mafic dikes occur, but are less common. Unfoliated Cretaceous plutonic bodies are found throughout the Kigluaiks.

Table 1.1: Abbreviations used in text. Following the convention in Kretz (1983) mineral names are capitalized, whereas mineral component names are not.

Mineral name abbreviations

Aln	allanite	$Ca_2FeAl_2Si_3O_{12}OH$ with rare earth elements added
And	andalusite	Al_2SiO_5
Ap	apatite	$Ca_5(PO_4)_3OH$
Bt	biotite	$K(Mg,Fe)_3AlSi_3O_{10}(OH)_2$
Cal	calcite	$CaCO_3$
Chu	clinohumite	$Mg_9Si_4(OH)_2$
Cpx	clinopyroxene	$Ca(Mg,Fe)Si_2O_6$
Crd	cordierite	$(Mg,Fe)_2Al_4Si_5O_{18} \cdot nH_2O,CO_2$
Di	diopside	$CaMgSi_2O_6$
Do	dolomite	$CaMg(CO_3)_2$
Fo	forsterite	Mg_2SiO_4
Graph	graphite	C
Grt	garnet	$(Ca,Mg,Fe,Mn)_3Al_2Si_3O_{12}$
Hbl	hornblende	$(Na,K)_{0-1}Ca_2(Mg,Fe,Al)_5(Si,Al)_8O_{22}(OH)_2$
Ilm	ilmenite	$FeTiO_3$
Kfs	K-feldspar	$KAlSi_3O_8$
Ky	kyanite	Al_2SiO_5
Ms	muscovite	$KAl_2AlSi_3O_{10}(OH)_2$
Opx	orthopyroxene	$(Mg,Fe)SiO_3$
Phl	phlogopite	$KMg_3AlSi_3O_{10}(OH)_2$
Pl	plagioclase	$CaAl_2Si_2O_8 - NaAlSi_3O_8$
Prg	pargasite	$NaCa_2(Mg,Fe)_5AlSi_7O_{22}(OH)_2$
Qtz	quartz	SiO_2
Rt	rutile	TiO_2
Sil	sillimanite	Al_2SiO_5
Spl	spinel	$MgAl_2O_4$
Sta	staurolite	$Fe_4Al_{18}Si_{7.5}O_{44}(OH)_4$
Tnt	titanite	$CaTiSiO_5$
Tr	tremolite	$Ca_2Mg_5Si_8O_{22}(OH)_2$
Zrn	zircon	$ZrSiO_4$

Table 1.1 continued

Mineral component abbreviations

biotite	ann	annite	$KFe_3AlSi_3O_{10}(OH)_2$
	phl	phlogopite	$KMg_3AlSi_3O_{10}(OH)_2$
feldspar	ab	albite	$NaAlSi_3O_8$
	An	anorthite	$CaAl_2Si_2O_8$
	kfs	K-feldspar	$KAlSi_3O_8$
garnet	alm	almandine	$Fe_3Al_2Si_3O_{12}$
	grs	grossular	$Ca_3Al_2Si_3O_{12}$
	prp	pyrope	$Mg_3Al_2Si_3O_{12}$
pyroxene	di	diopside	$CaMgSi_2O_6$
	en	enstatite	$MgSiO_3$
	fs	ferrosilite	$FeSiO_3$
	hd	hedenbergite	$CaFeSi_2O_6$

Fluid species

H_2O	water, or the supercritical equivalent
CO_2	carbon dioxide, or the supercritical equivalent
CH_4	methane, or the supercritical equivalent
N_2	nitrogen gas, or the supercritical equivalent
H_2	hydrogen gas, or the supercritical equivalent

T_m	temperature of final melting of solid
T_h	temperature of homogenization to one phase
σ	error associated with stable isotope measurement
ϕ	porosity
D	effective diffusion coefficient
D_{fluid}	diffusion coefficient of element in fluid
ρ_f	density of fluid
ρ_s	density of solid
K_d	wt% element in solid/wt% element in fluid
C_o	isotopic composition at edge of marble
C_f	isotopic composition of unaltered marble
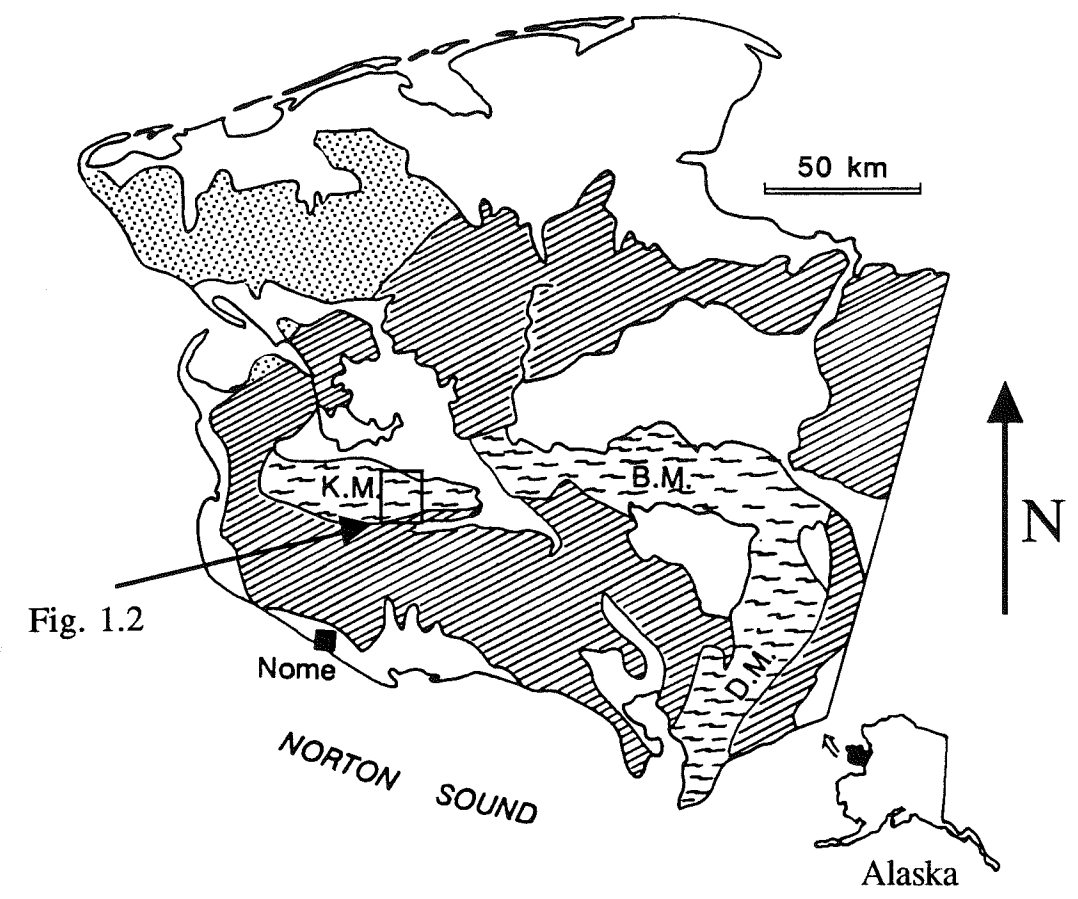
Figure 1.1:   Location map Seward Peninsula, Alaska.   K.M. Kigluaik Mtns., B.M.
Bendeleben Mtns., D.M. Darby Mtns. Diagonal rule is Nome group
blueschist/greenschist; wavy pattern is high grade gneiss complexes and Cretaceous
plutons; stipple is York Mtns, unmetamorphosed sediments; unpatterned is
Quaternary deposits. Modified from Patrick (1987).

Figure 1.2 Lithologic map, Grand Central Valley area, Kigluaik Mtns. Location of outcrops discussed in chapters 2 and 3: A, AB89-41; B, AB89-61; C, AB90-13; D, AB90-27. Lithologic contacts south of Thompson Creek from Lieberman (personal communication).
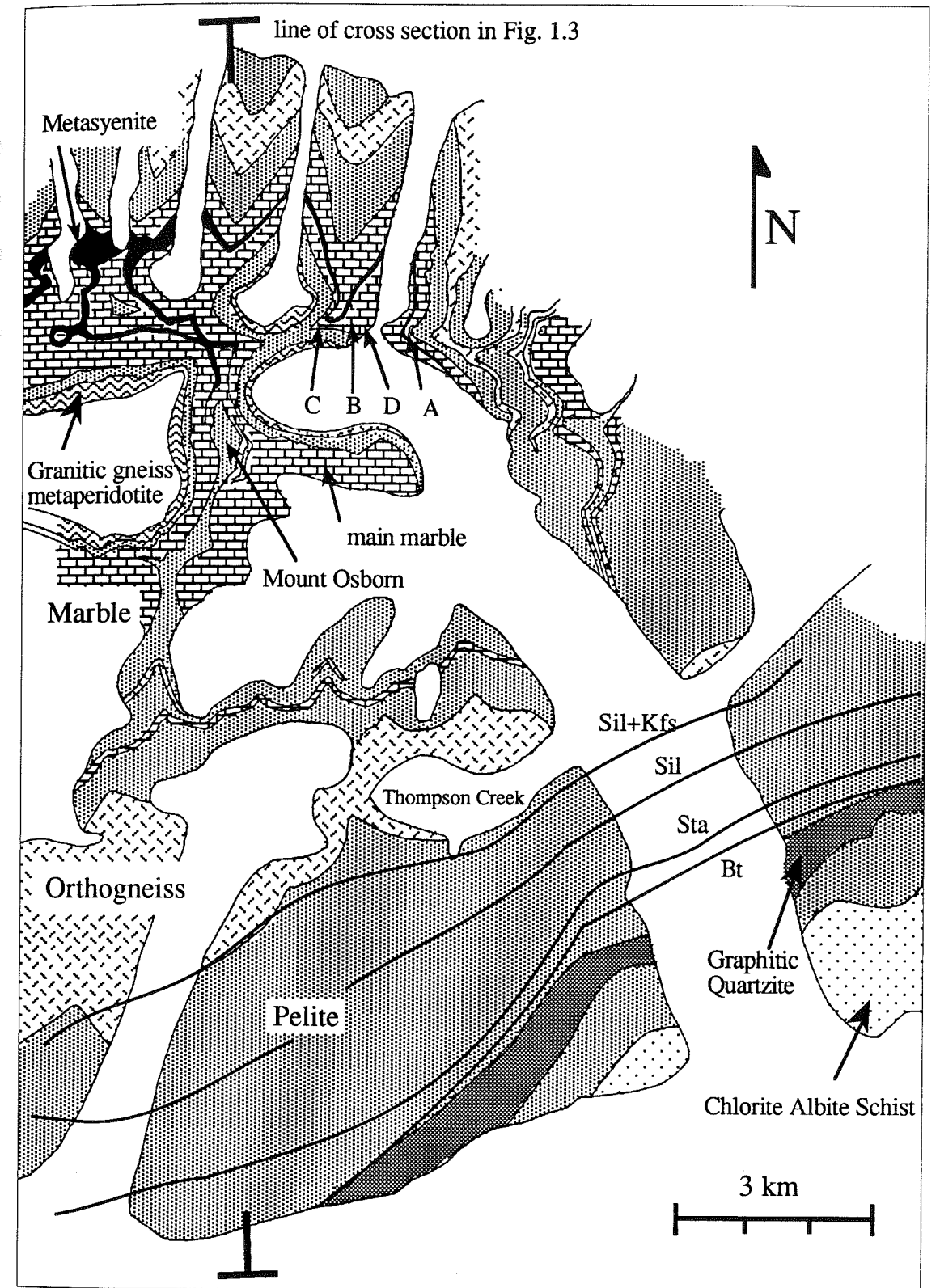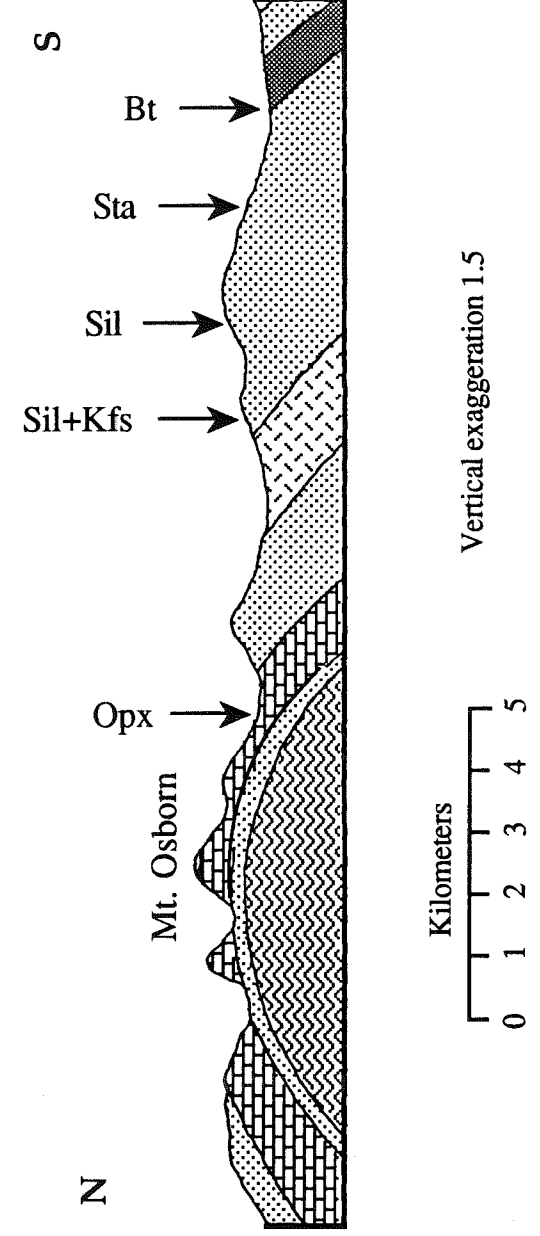
Figure 1.3   N-S cross section through Kigluaik mountain range, showing isograd locations.   Modified from Lieberman (1988).
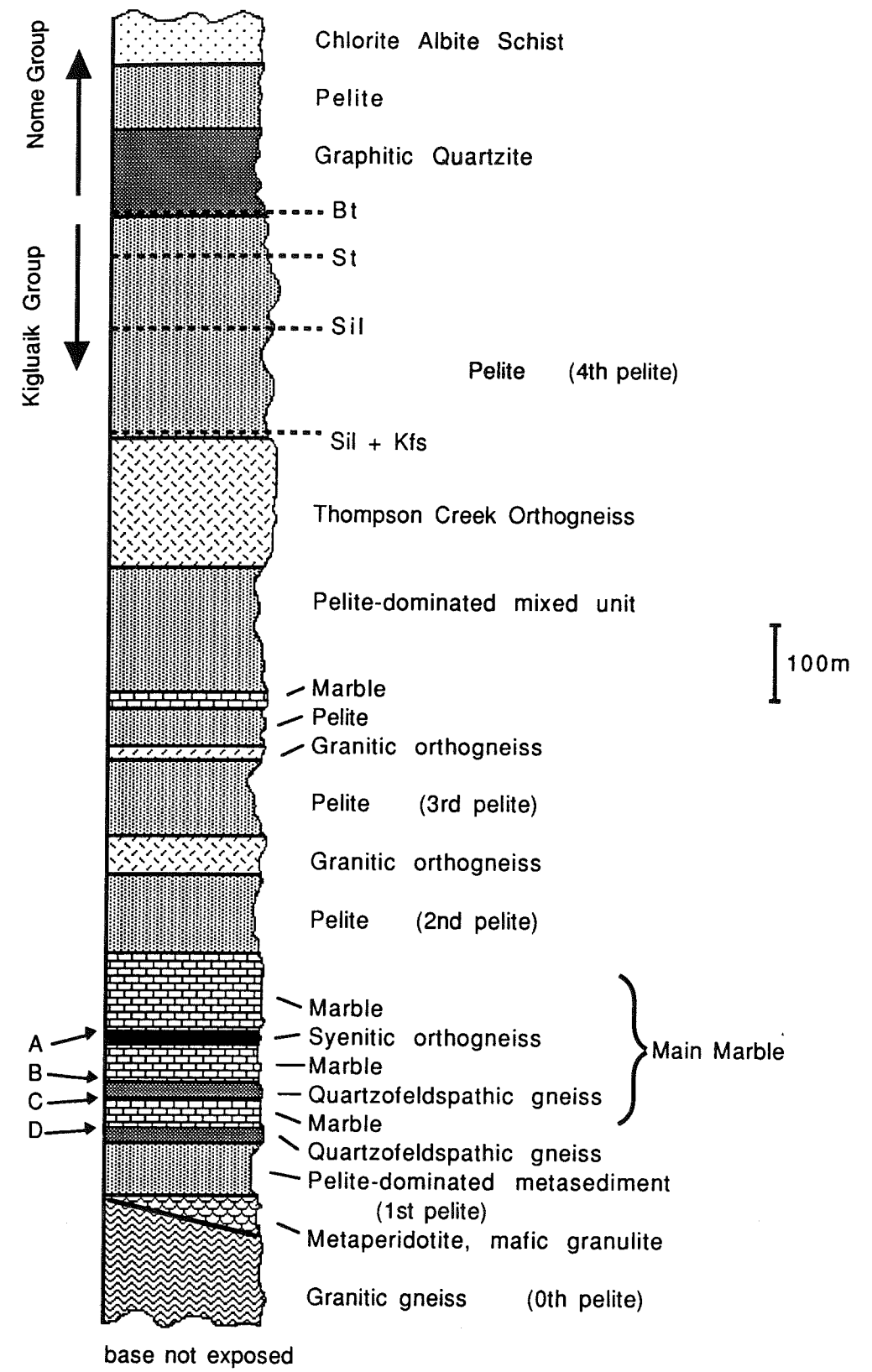
Figure 1.4: Stratigraphic section, Grand Central Valley area. A, B, C and D as in Figure 1.2.
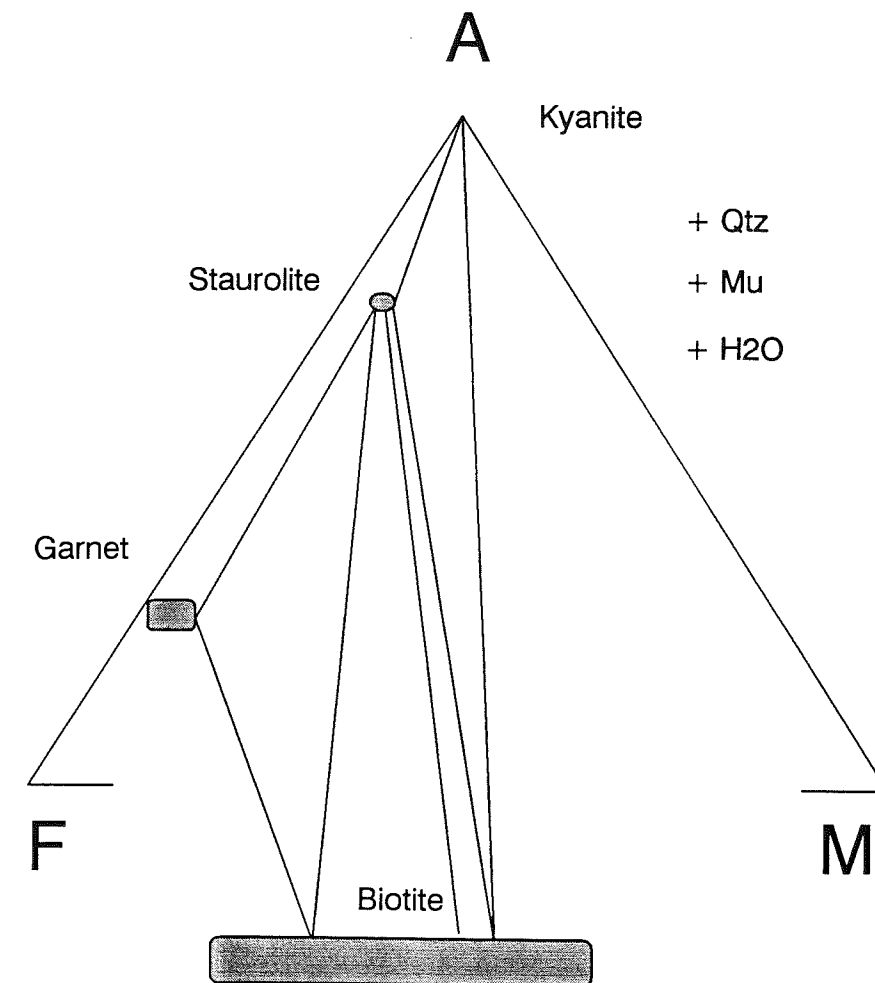
Figure 1.5   AFM projection, staurolite zonepelites.   Grt-bearing AB87-220.1; two-phase AB87-218; Ky-bearing SL81-425.1. Shaded mineral compositions are schematic.
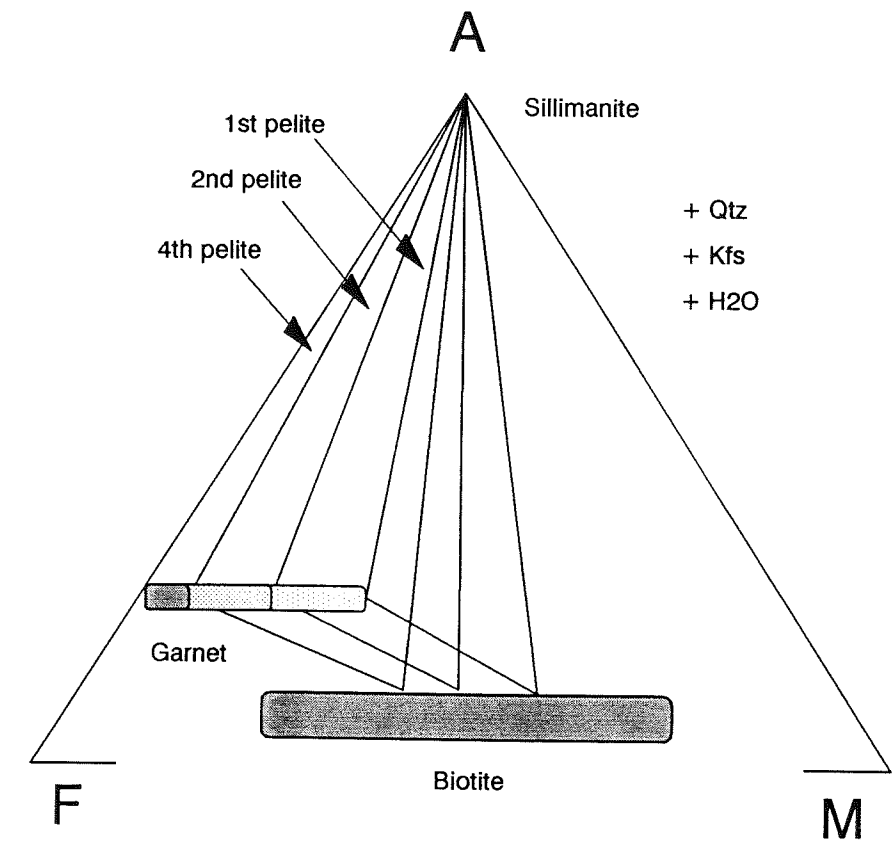
Figure 1.6   AFM projection, Sil+Kfs zone pelites.   1st pelite OS-56; 2nd pelite OS-43; 4th pelite OS-91. Mineral compositions taken from Lieberman (1988). Shaded mineral compositions are schematic.
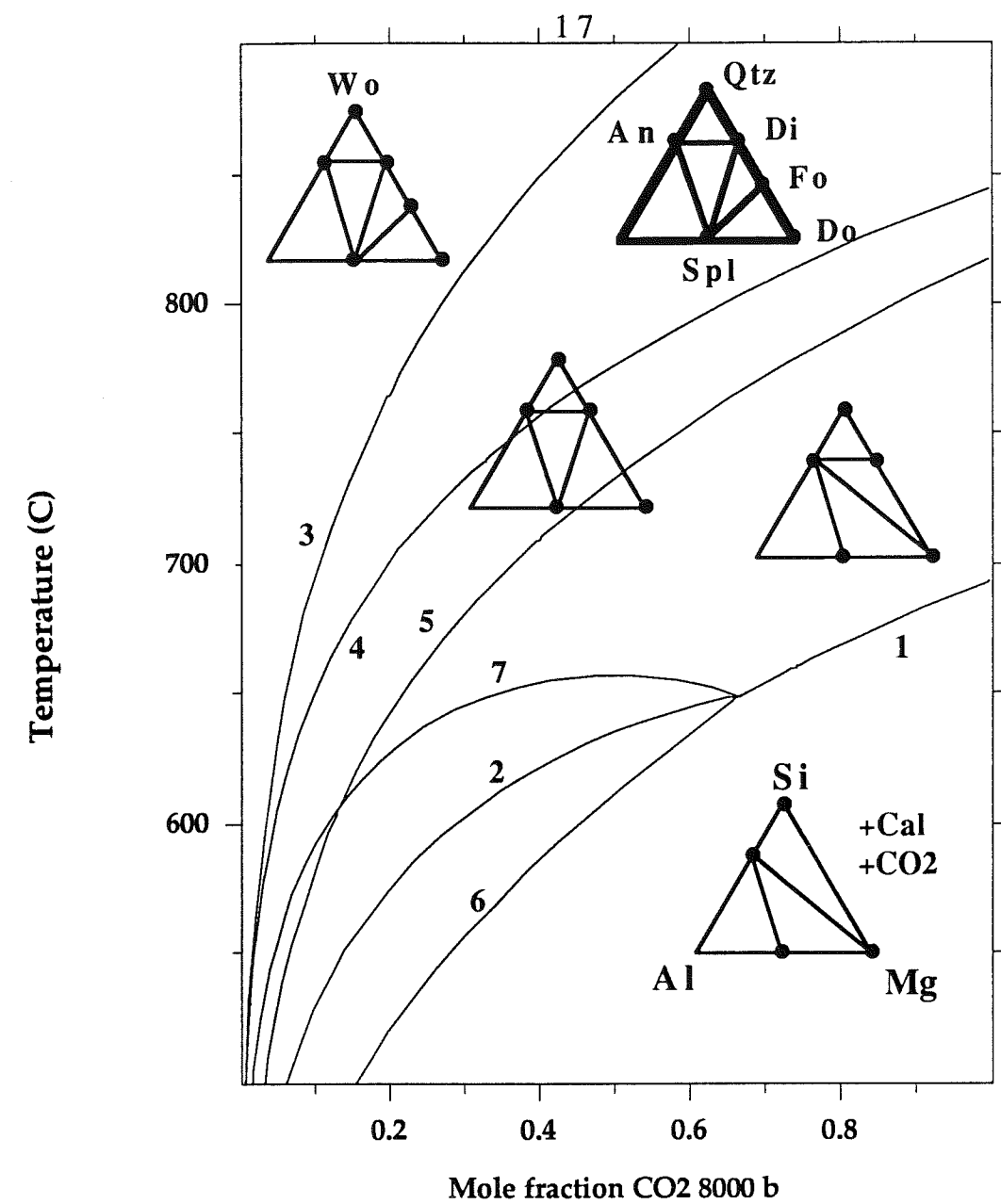
Figure 1.7   T-XCO$_2$ diagram, Kigluaik marbles.   Calculated for the system Ca-Mg-Al-Si-C-O-H projected from calcite. Most peak metamorphic mineral assemblages sampled can be characterized by the bold compatibility triangle. Reaction stoichiometries are as follows:

(A)   Di + 2 CO$_2$ = 2 Qtz + Dol
(B)   H$_2$O + 3 CO$_2$ + 5 Di = 3 Cal + 2 Qtz + Tr
(C)   CO$_2$ + Wo = Cal + Qtz
(D)   4 Cal + 2 Fo + 2 CO$_2$ = 3 Dol + Di
(E)   2 CO$_2$ + Spl + Di + 2 Cal = An + 2 Dol
(F)   7 CO$_2$ + Tr + 3 Cal = 5 Dol + 8 Qtz + H$_2$O
(G)   H$_2$O + CO$_2$ + Dol + 4 Di = 3 Cal + Tr
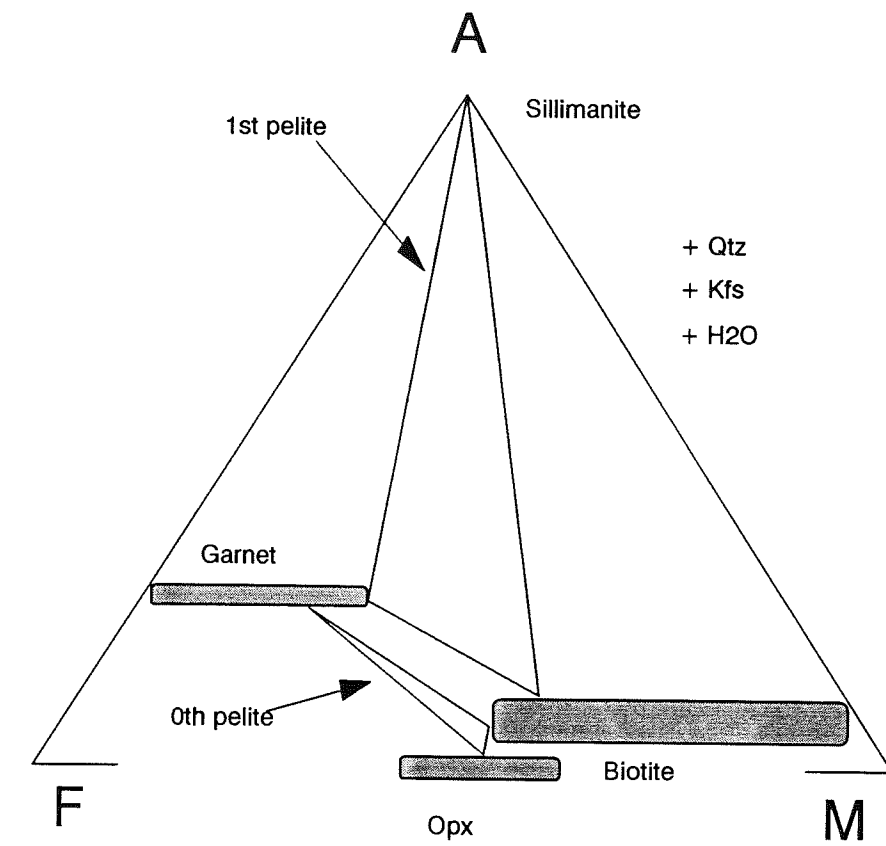
Figure 1.8   AFM projection, granulite grade pelites.   Opx-bearing AB90-19.5; Sil-bearing OS-56. Shaded mineral compositions are schematic.

Chapter 2: Fluid-rock interaction at marble-gneiss contacts

Introduction

Stable isotopes have been used to constrain the fluid histories of metamorphic rocks (see review in Valley 1986). For the last several decades this has been limited to "box model" fluid-rock interaction and effects due to devolatilization. Recent work has applied the mathematical framework of fluid flow through porous media to constrain the flux of fluid through lithologic layers employing stable isotopes as tracers (Baumgartner and Rumble 1988, Bickle and McKenzie 1987, Bickle and Baker 1990a b, Blattner and Lassey 1989). The present work concentrates on using these techniques to quantify and identify the mode of cross-lithology transport of fluid in a well-exposed, amphibolite to granulite grade metamorphic terrane on the Seward Peninsula of Alaska. Here, thick, regionally extensive, flat-lying marble horizons, alternating with metasedimentary and meta-igneous rock types, provide an opportunity to investigate the role of lithology in determining the regional scale of fluid migration.

Analytical procedures

Microprobe analyses of minerals were carried out on a JEOL 733 Superprobe at the University of Washington, Department of Geological Sciences. Stable isotope analyses were carried out on a Finnigan Mat Delta E spectrometer at Department of Geosciences, New Mexico Tech, Socorro, NM. Methods used in collecting and normalizing the data, along with the data, are listed in appendices 2 and 3, respectively.

All thermodynamic calculations were carried out using Ge0calc software (Berman et al. 1987, Lieberman, pers. com.) using the data base of Berman (1988). Provisional data on annite and hedenbergite were also used (Berman, pers. com.) along with data on clinohumite (Rice 1980). Activities of end member mineral components

were calculated by Ge0calc software using the following models: garnet, Berman (1990); feldspars, Fuhrman and Lindsley (1988); biotite, McMullin et al. (1992); calcite in equilibrium with dolomite (Skippen 1974); and ideal multi-site activity models for spinel, forsterite, pyroxenes and clinohumite.

Descriptive and Analytical Data

Closely-spaced samples were collected on five traverses across contacts between the main marble and gneiss units. Sampling was perpendicular to layering, as much as possible. The samples were studied petrographically and subsequently analyzed for oxygen and carbon isotopes. These profiles yielded isotopic gradients sufficiently straight-forward to allow interpretations of fluid transport to be drawn, and have sample numbers AB89-41, AB89-61, AB90-13, AB89-62 and AB90-27 (Appendix 3).

AB89-41

At this contact (A in figures 1.2 and 1.4), a ~100 m thick, dolomitic marble subhorizontally overlies a ~15 m thick metasyenite/metamonzonite unit. The mineral assemblage in the metasyenite is: Hbl + Bt + Cpx + Pl + Kfs ± Ilm ± Grt with abundant and large accessory Ap, Zrn and Aln; Qtz is not present. The metasyenite is granoblastic, coarse-grained and moderately well foliated; it displays minor lithologic layering on the scale of meters. Whole-rock chemical analyses of three metasyenite samples are listed in table 2.1. Except at the contact (see below), the marble above the contact is homogeneous on the scale of cm; it is very coarse-grained (~0.5 cm) and composed of more than 90% Dol with minor Cal + Fo + Phl + Graph + Spl ± Chu ± Cpx. However, the lowermost 1.9 cm of the marble unit consists of more than 90% calcite + forsterite, with minor Dol + Spl + Phl + Graph (table 2.2). Calcite displays exsolution plates and rods of dolomite. Calcite-dolomite thermometry on a reintegrated Cal yields T ~650°C indicating that some whole-grain exsolution of Dol out of the Cal

occurred during retrogressive cooling, a common process in high grade marbles (Essene 1982). Mineral compositions are listed in Appendix 2.

The $\delta^{18}O$ composition of feldspar in the metasyenite ranges from 9.9 to 14.9‰. The marble far from the metasyenite retains sedimentary values of 23.0‰ $\delta^{18}O$ and -0.5‰ $\delta^{13}C$. The calcite-forsterite zone is characterized by O and C isotopic values of 13.0‰ and -2.0‰, respectively. The transition in isotopic composition occurs within the dolomite marble over a distance of little more than 2 cm from the Cal+Fo zone (figures 2.1 and 2.2).

AB89-61

This is another flat-lying contact with marble overlying gneiss (B in figures 1.2 and 1.4). In this case the gneiss is a quartzofeldspathic rock consisting of equal amounts of Bt + Qtz + Pl with lesser amounts of Grt ± Cpx ± Kfs with accessory Ap and Tnt. The marble is compositionally variable on the scale of cm. Most samples consist of Cal, Dol, Cpx and Phl and, in addition, variable combinations of Fo, Spl, Pl and (late) Tr. There is generally much more Cal than Dol; silicates constitute 15-40% of the rock. Calcite displays exsolution lamellae and rods of dolomite.

Quartz $\delta^{18}O$ values are around 16‰, comparable to the composition of quartz near the base of this stratigraphic unit (figure 2.3). $\delta^{18}O$ of Cal varies in a regular fashion from 24.3‰ at about 7 m from the gneiss to 16.2‰ at 2 cm from the contact.

AB90-13

At this locality (C in figures 1.2 and 1.4), a flat-lying calcitic marble is overlain by a thick unit of relatively homogeneous Hbl-bearing quartzofeldspathic gneiss. The gneiss is coarse-grained and displays a moderate foliation defined by oriented mafic minerals. Except within 60 cm of the underlying marble, the assemblage in the gneiss is Hbl + Qtz + Pl + Bt with accessory Ap + Zrn + Aln ± Ilm. Within 60 cm of the marble

Hbl is no longer present; instead, the assemblage is: Cpx + Opx + Kfs ± Grt. Both pyroxenes are fine grained (0.1 mm diameter) and granular. Garnet is embayed and in places surrounded by Pl + Opx symplectite. In the two-pyroxene zone, large plagioclase crystals are antiperthitic. In a narrow transition zone Hbl, Cpx and Opx coexist. Details regarding the mineralogical relationships at this outcrop are covered in chapter 3. The marble is coarse-grained and granoblastic and contains varying amounts of Phl, Cpx, Scp or Pl, Kfs and late Tr.

Figure 2.4 shows $\delta^{18}O$ analyses of calcite in the marble and quartz, hornblende and biotite in the gneiss. Calcite away from the gneiss retains sedimentary values of $\delta^{18}O$ and $\delta^{13}C$. Within 50 cm of the gneiss, $\delta^{18}O$ values of Cal are slightly lowered. In the hornblende zone quartz, hornblende and biotite display constant $\delta^{18}O$ values of 15, 12 and 8‰ respectively. In the two-pyroxene zone quartz values increase slightly to 16.0‰; biotite has a variable isotope composition increasing from 7.0 to 12.0‰ towards the contact with marble, which may be attributed to late alteration due to the ease with which biotite resets (Schwarcz et al. 1970).

AB89-62 and AB90-27

Both of these outcrops are at the base of the Main Marble unit (D in figures 1.2 and 1.4) within 0.5 km of each other. At this horizon, calcitic marble overlies mixed metasedimentary rocks. The metasedimentary rocks consist of graphitic pelite (Qtz + Bt + Pl + Sil + Graph + Grt ± Kfs), biotite schist (Qtz + Bt + Pl ± Graph ± Kfs), and calcsilicate (Cal + Cpx + Ttn + Pl + Qtz ± Scp ± Graph) alternating in layers ranging in thicknesses from a few cm to m. The assemblage in the marble is Cal + Dol + Fo + Phl ± Graph; there is some variability in relative proportions of the minerals. Figure 2.5 compiles data from both outcrops and shows the $\delta^{18}O$ composition of Cal in marble and Qtz in schist as a function of perpendicular distance from the base of the marble (note

that the quartz values represented in the figure have been lowered by 0.33‰ so as to represent calcite which would have been in equilibrium with the quartz at 800°C (Clayton et al. 1989)). The interior of the marble unit retains sedimentary values of 22.6‰ and is isotopically quite homogeneous. Within about 5 m of the contact, $\delta^{18}O$ is lowered more than 3.5‰. The isotopic composition of the quartzofeldspathic rocks is somewhat variable, with $\delta^{18}O$ ranging from 19.0 to 20.2‰.

Interpretation of Data

Baumgartner and Rumble (1988) showed that a change in isotopic composition of a rock caused by diffusive and infiltrative processes results, as time progresses, in distinctive patterns on plots of $\delta^{13}C$ vs $\delta^{18}O$. Diffusion-dominated processes produce a relatively straight-line diagonal trend on plots of $\delta^{13}C$ vs $\delta^{18}O$, relatively independent of the XCO_2 of the fluid. Processes involving advection of material via an H_2O-CO_2 fluid show curved or box-like patterns on plots of $\delta^{13}C$ vs $\delta^{18}O$. Additional complexities can arise if local equilibrium is not maintained (Blattner and Lassey 1989), but, during the time-scale of regional metamorphism, local equilibrium may be assumed. The interior parts of main marble layers in all outcrops show $\delta^{18}O$ in the mid to low 21.4 to 24.3 and $\delta^{13}C$ approximately zero (figure 2.6), appropriate for unaltered high grade marbles (Valley 1986). The convergence of stable isotope ratios from all marble horizons to these values lends support to the conclusion that the interior of marble layers have not been changed since their formation. Both carbon and oxygen isotope compositions are low near contacts with other lithologies. The oxygen isotope composition of fluid in equilibrium with the adjoining lithologies can be presumed to have been somewhere between ~9‰ (igneous) and ~17‰ (pelitic). The marbles show varying amounts of oxygen isotope exchange with such a fluid. Unfortunately, the carbon isotope composition of the interacting fluid is less constrained. The linear variation of $\delta^{18}O$ and

$\delta^{13}C$ suggests principally diffusive interaction rather than combined diffusive-advective interaction between the main marble units and their adjoining lithologies. The oxygen isotope composition toward which marble margins trend is controlled by the composition of the adjacent lithology. In the cases where the adjacent lithology is clearly sedimentary (AB89-62, AB90-27), $\delta^{18}O$ is lowered less than in the case where the adjacent lithology is clearly igneous (AB89-41). Infiltration of an external pervasive fluid would have homogenized isotopic compositions in gneissic units. But gneisses retain the protolith signature of oxygen isotopic composition indicating that a pervasive fluid did not homogenize the isotopic composition of the rocks.

AB89-41

The uniform, SiO_2-poor mineralogic composition of the marble beyond the thin Cal+Fo zone at this contact suggests that the Cal+Fo zone was formed by chemical interaction between the metadolomite and the metasyenite. By influx of silica, calcite and forsterite can be produced from dolomite by the reaction:

$$2 \text{ Dol} + SiO_2 \text{ (dissolved)} \rightarrow 2 \text{ Cal} + \text{Fo} + 2 CO_2. \tag{1}$$
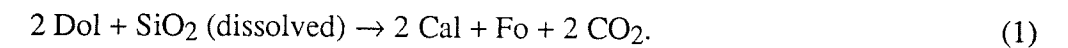
The growth of the Cal+Fo zone through the introduction of SiO_2 is strongly supported by the results of modal analyses; calcite and forsterite are present almost exactly in the required molar ratio 2:1 (table 2.2). In reaction (1), SiO_2 is added to the metadolomite via a fluid and the activity of silica is necessarily less than 1 (quartz standard state). Depending on silica activity, reaction (1) is not stable under all fluid compositions (figure 2.7). The reaction from dolomite to calcite + forsterite *could* have been driven by an increase in silica activity and/or a decrease in CO_2 activity, presumably by dilution with H_2O (or CH_4?). Reaction (1) is univariant at constant P and T and puts limits on either $aSiO_2$ or aCO_2. Since about 15 wt% silica was added to the metadolomite to form forsterite and because $aSiO_2$ in the syenite was much greater than $aSiO_2$ in the

metadolomite (see below), it is reasonable to infer that the reaction was not only accompanied by SiO_2 influx, but actually driven by an increase in $aSiO_2$. The proposed path followed by fluid in the Cal+Fo zone is indicated on the diagram. The metadolomite started at a low value of $aSiO_2$, in equilibrium with Fo, Cal and Chu. With an increase in silica activity, CO_2 was produced, increasing the activity of CO_2. The fluid was buffered along the reaction curve until the fluid was pure CO_2. The system remained at these conditions until all the Dol was exhausted by reaction with silica. Then $aSiO_2$ could increase into the Cal+Fo field. The activity of SiO_2 never reached the diopside-forming reaction (except in one late cross-cutting vein).

Although the metasyenite was undersaturated in silica (no quartz is present in the gneiss), the phases present in the rock define a silica activity. As long as the silica activity was higher in the metasyenite than in the metadolomite, silica would move down its chemical potential gradient from the gneiss into the marble. The silica activity in the metasyenite can be defined by the reaction:

$$3 \text{ an} + 3 \text{ di} = \text{prp} + 2 \text{ grs} + 3 \text{ SiO}_2 \tag{2}$$

and the equivalent Fe end member reaction:

$$3 \text{ an} + 3 \text{ hd} = \text{alm} + 2 \text{ grs} + 3 \text{ SiO}_2. \tag{3}$$

These reactions are shown in P-T space in figure 2.8, adjusted for the mineral compositions in a sample 33 cm from the contact. The intersection of reactions (2) and (3) defines a Grt-Cpx Fe-Mg exchange equilibration temperature, 825°C, which agrees satisfactorily with previous estimates from this area (Lieberman 1988; Lieberman and Petrakakis 1992). For pressures of 7.5 to 8 kbar, the silica activity is about 0.8; this is higher than in any Dol-bearing assemblage (see figure 2.7). Therefore silica would move from the gneiss into the marble. Even though all the silica in reaction (1) was added to the system via a fluid, there was still an 8% volume decrease of solids, due to a

density increase and loss of CO_2. Therefore, the reaction was not inhibited by volume constraints.

The data indicate extensive stable isotope interaction between the Cal+Fo zone and the metasyenite. Rayleigh distillation during decarbonation according to reaction (1) can account for the carbon isotope depletion, and some, but not all, of the observed oxygen isotope depletion (figure 2.9). The remaining oxygen isotope depletion can be attributed to interaction with the gneiss. The vehicle of such interaction can be ascribed to a fluid. The composition of this fluid can be examined using mineral equilibria. The H_2O activity in the syenite as defined by biotite dehydration reactions was about 0.2 (figure 2.10). At these high temperatures, fluids mix almost ideally, so, if a fluid was present, $XH_2O = 0.2$. The other constituents of the fluid would presumably have been either CO_2 or CH_4. However, the carbon isotopic composition of the Cal+Fo zone was not changed beyond that attributed to Rayleigh distillation. Therefore, it is unlikely that any upward infiltrating fluid was carbon-bearing, except in the unlikely case that the $\delta^{13}C$ composition of the fluid was in exact equilibrium with the calcite of the Cal+Fo zone. A more reasonable interpretation is that the pore spaces of the metasyenite were unsaturated in fluid and that isotopic interaction between the metasyenite and the Cal+Fo zone occurred through the CO_2 that was forced downwards, away from the Cal+Fo reaction front. In a similar manner, silica was transported from the metasyenite to the Cal+Fo reaction front by diffusion against the flow of CO_2 evolving from the reaction. Unfortunately, little is known about the diffusion rate of silica in C-O-H fluids of any composition. Silica has a very low solubility in CO_2 fluid (Walther and Orville 1983). This may have been the cause of the very limited (2 cm) extent of silica influx into the metadolomite. A flux of less than 1 g SiO_2/cm^2 from the gneiss into the marble occurred during the course of the entire metamorphic cycle.

The metadolomite at 2-4 cm from the syenite contact contains 99% carbonate + graphite (table 2.2). Therefore, the depletion of $\delta^{18}O$ and $\delta^{13}C$ in this zone could not be the result of devolatilization. The isotopic change most likely occurred by advective-diffusive transport. Since the Cal+Fo zone shows, within error, no gradient in $\delta^{18}O$ or $\delta^{13}C$, it is assumed that interaction with the metasyenite kept the isotopic composition of calcite in the Cal+Fo zone at 13‰ and -2.2‰, respectively. The equations developed by Bickle and McKenzie (1987) for one-dimensional, combined advective-diffusive transport can be employed to quantitatively estimate the extent of fluid advection up into (or away from) the metadolomite. A moving reference frame is adopted here, where the origin is set at the interface between the Dol zone and the Cal+Fo zone; the positive direction is up. In this convention, as the Cal+Fo reaction progresses into the metadolomite the rock body is moving down with respect to the coordinate system, and hence has a negative velocity. The fits to the $\delta^{18}O$ and $\delta^{13}C$ data (figure 2.2) were determined by minimizing the quantity $\Sigma((p-x)/\sigma)^2$ (Bickle and Baker 1990a); p is the predicted value of isotope composition, x is the measured value and σ is the error of the measurement. For this data set, the best fit is obtained when downward directed velocity is used. The isotopic composition of Cal was adjusted to represent Dol in equilibrium with the measured Cal at 800°C; 0.2 was added to $\delta^{18}O$ values of Cal (Sheppard and Schwarcz 1970; Northrop and Clayton 1966), and 0.33 was added to $\delta^{13}C$ values of Cal (Sheppard and Schwarcz 1970).

Equation (26) from Bickle and McKenzie (1987) calculates the change in isotopic composition in terms of the Peclet number, non-dimensional time, composition at the boundary (C_f), and the original composition of the lithology (C_o). The Peclet number is defined as $w\phi L/D$, and is a measure of the relative importance of advection vs. diffusion in transporting the material; w is the vertical velocity of the fluid, L is a

characteristic length scale, D is the effective diffusion coefficient of the isotope, and ϕ is porosity. For transport by a fluid in a porous medium D is taken as ϕD_{fluid}. D_{fluid} is assumed to be 10^{-8} $m^2 s^{-1}$, independent of temperature (Rubie 1986; Bickle and McKenzie 1987). Non-dimensional time is approximately $(Dt / L^2)(\rho_f / \rho_s K_d)$; t is time, ρ_f is the density of the fluid (~1 g/cm^3 at 800°C, 8 kbar), ρ_s is the density of the solid (~2.8 g/cm^3), and K_d is the solid-fluid partition coefficient (0.55, Cartwright and Valley 1991). For this outcrop, C_o=-1.9, C_f=-0.3 for $\delta^{13}C$; C_o=13.2, C_f=23.2 for $\delta^{18}O$; L=1 m.

The fits to the data are listed in table 2.3. The fact that a downward directed velocity best fits the data indicates that the Cal+Fo reaction encroached into the metadolomite faster than O and C *advected* into the metadolomite. The fit for non-dimensional time can be rearranged to yield an estimate of porosity (Bickle and Baker 1990a). For time scales >1 Ma the derived porosities are around 10^{-10} or less, questionably low to have sustained transport of stable isotopes over millions of years. A more likely possibility is that no fluid was present in the dolomite zone and that isotope transport occurred by lattice diffusion through the Dol crystals. In this case the $(\rho_f / \rho_s K_d)$ term of non-dimensional time is unity. For the same time scale as above, the derived diffusion coefficients for oxygen and carbon isotopes in Dol must be < 3 X 10^{-18} $m^2 s^{-1}$ and < 1 X 10^{-18} $m^2 s^{-1}$, respectively. These estimates agree very well with those measured on Dol by Anderson (1972) under dry conditions at 800°C. The presence of fluid is known to enhance crystalline diffusion rates (Sharp 1991). Measurements of oxygen diffusion rates in calcite increase 2 to 3 orders of magnitude under vapor saturated compared to dry conditions (Anderson 1969; Kronenberg et al. 1984). The fact that diffusion rates in the dolomite zone were no more than 10^{-18} $m^2 s^{-1}$ further supports the conclusion that there was no fluid present in the dolomite zone.

Similar arguments were used by Baker (1990) to imply the absence of grain-boundary fluids for extended time periods during the metamorphism of lower crustal rock in the Ivrea Zone, Italy.

Bickle and Baker (1990a) showed that an estimate of time-integrated flux can be calculated from the derived values of Peclet number and non-dimensional time. For this outcrop, where no fluid is present, flux represents the downward movement of the metadolomite towards the Cal+Fo reaction boundary, or can be thought of as the amount of dolomite that reacted to form Cal+Fo. The measured thickness of the Cal+Fo zone is 1.9 cm. Accounting for the 8% volume loss of the reaction, 2.0 cm of metadolomite have been converted to Cal+Fo. The flux calculations derived from oxygen and carbon isotope data are 0.0065 and 0.0026 m^3/m^2, respectively, or 0.65 and 0.26 cm of metadolomite consumed; these estimates are consistent within an order of magnitude of the observed 2.0 cm metadolomite consumed.

AB89-61

At outcrop AB89-61 the zone of isotopic lowering in the marble is more than two orders of magnitude wider than at AB89-41 (compare figures 2.2 and 2.3). Since pressure, temperature and time of metamorphism were the same for both outcrops, clearly there must have been a significant difference in fluid conditions between the two. In order to fit an infiltration model to the data as previously described, 0.33 was subtracted from the measured quartz values of $\delta^{18}O$ to represent calcite that would have been in equilibrium with the quartz at 800°C (Clayton et al. 1989). For this outcrop the pinned boundary equation of Bickle and Baker (1990a) is used, with the boundary fixed at the marble-gneiss contact. For this outcrop, L=1000 m, C_o=15.8, C_f=24.1. The results of the fit are given in table 2.3 and shown in figure 2.3. As with AB89-41, the best fit is obtained when a downward directed velocity is used. The boundary at this

outcrop is not moving relative to the rock body, therefore the parameter fits indicate downward movement of fluid. The quantity of fluid calculated as the time integrated flux is -.0085 m^3/m^2, i.e. about 1 cm of fluid per cm^2 was forced out the bottom of the marble. The porosity estimate for a time scale >1 Ma is < 5.4 X 10^{-6}. If the interior part of a thick marble layer is essentially impermeable, then it is not unreasonable to conclude that any fluid generated internally near the bottom of the marble would be forced down, out of the marble.

AB90-13

At this outcrop there are indications of interaction on both sides of the lithologic contact. Analysis by singular value decomposition (Fisher 1989) indicates that the two pyroxene zone was formed by dehydration of the amphibole-bearing gneiss (more details in chapter 3). Since no significant pressure or temperature gradients could have existed during this process, the reaction must have been driven by a change in fluid composition to lower aH$_2$O, presumably by dilution with CO_2 from the underlying marble. The length-scale of this fluid interaction into the gneiss is 60 cm. The inflection point in the steep stable isotope gradient between gneiss and marble occurs at the lithologic contact. This observation indicates that transport was dominated by diffusion, otherwise this inflection point would have been moved into the downstream rock by the advecting fluid (Ganor et al. 1989). The oxygen isotope length-scale of interaction in the marble is about 50 cm. Since length-scales of interaction are almost identical on both sides of the boundary, transport dominated by diffusion, not advection, is indicated (Bickle and McKenzie 1987).

AB89-62 and AB90-27

The lithologic variation at this stratigraphic level (base of the main marble) is more extensive in the vicinity of the marble contact than at other outcrops described

here, making modeling of isotopic variation more complex. However, the interior of the marble unit retains sedimentary $\delta^{18}O$ and $\delta^{13}C$ compositions, indicating little interaction with external fluids. As at AB90-13, a steep isotopic gradient exists at the lithologic boundary, indicating a diffusion-dominated transport process at the lower contact of the marble. The extent of isotopic depletion in the marble is similar to that at AB89-61.

Conclusions

The steep isotopic gradients found at all lithologic contacts described in this chapter preclude the infiltration of large quantities of fluid across the main marble, otherwise the isotopic step in composition would have been propagated into the downstream lithology (Ganor et al. 1989). The main marble acted as an effective aquitard to cross lithology fluid flow, as has been found for marbles in other terranes (Rye et al. 1976, Nabelek et al. 1984, Ferry 1989). The gradient is so steep at AB89-41 that a pervasive, interconnected fluid must never have been present. The isotopic interaction between lithologic layers is dominated by diffusive processes. The amount of this diffusive interaction is related to the bulk composition of the marble. Pure carbonate marbles underwent little devolatilization, and therefore developed no porosity through which interaction could have occurred. Impure marbles underwent devolatilization reactions during the development of silicate minerals such as diopside and forsterite. This lead to the development of interconnected porosity, allowing isotopic interaction via a fluid. The implications of this study are that fluid was only present in marbles during transient devolatilization events. In addition, the lack of isotopic homogeneity between different gneissic units indicates that large amounts of fluid have not interacted with these layers.

Table 2.1   Whole-rock composition of metasyenites

	AB90-3.1	AB90-40.2	AB90-40.3
SiO_2	53.75	56.66	55.94
TiO_2	0.89	0.40	0.26
Al_2O_3	18.88	18.56	17.08
Cr_2O_3	0.02	0.03	0.02
Fe_2O_3	7.65	7.60	9.27
MnO	0.11	0.24	0.50
MgO	2.00	1.01	1.00
CaO	4.44	3.31	3.56
BaO	0.17	0.04	0.03
SrO	0.09	0.03	0.03
Na_2O	3.40	3.51	1.94
K_2O	6.83	7.51	8.42
P_2O_5	1	1	1
LOI	0.29	0.32	0.22
Sum	99.52	100.22	99.27

Table 2.2   Modal analyses of marbles

	Cal	Dol	Fo	Chu	Spl	Phl	Graph	Di	points
AB89-41	Mole%								
Cal+Fo	65.1	5.9	28.8	0.0	0.2	0.0	0.0	0.0	3193
Dol	5.8	90.4	0.0	0.1	0.5	0.3	2.9	0.0	3340

AB89-61	Approximate Area%								
cm									
2.5	75							25	
9	75					5		25	
11	55	10	35						
15	65	5				10		20	
33	5	90				5			
41	55	20	20			5			
53	80							20	
71	60					5		35	
94	65	10	20			5			
102	50	10	30			10			
107	60	10	5			10		15	
135	100								
366	50	35	5			5		5	
671	85	5						10	

Table 2.3   Fit parameters for stable isotope gradients

	C_o	C_f	Pec	t'	L(m)
AB89-41 ^{18}O	13.2	23.2	66	9.9×10^{-5}	1
AB89-41 ^{13}C	-1.9	-0.3	62	4.2×10^{-5}	1
AB89-61 ^{18}O	15.8	24.1	5	1.1×10^{-6}	1000
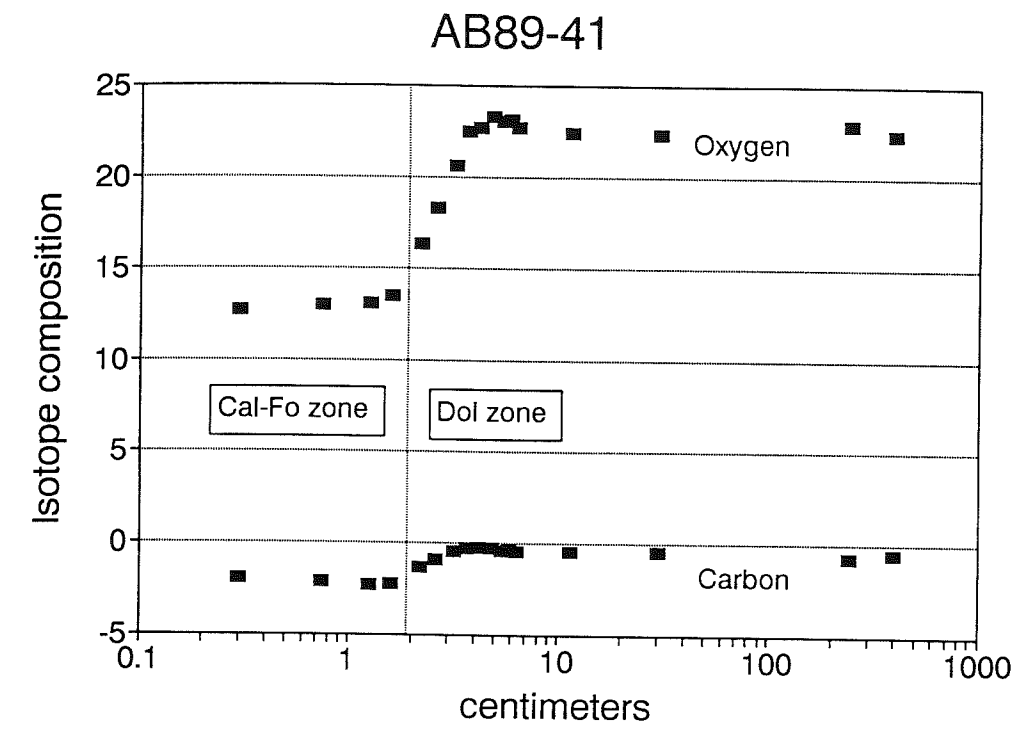
AB89-41

Figure 2.1 Stable isotope composition, AB89-41 marble. Metasyenite contact is at 0.0 cm; note logarithmic scale for horizontal axis.

A

AB89-41

B
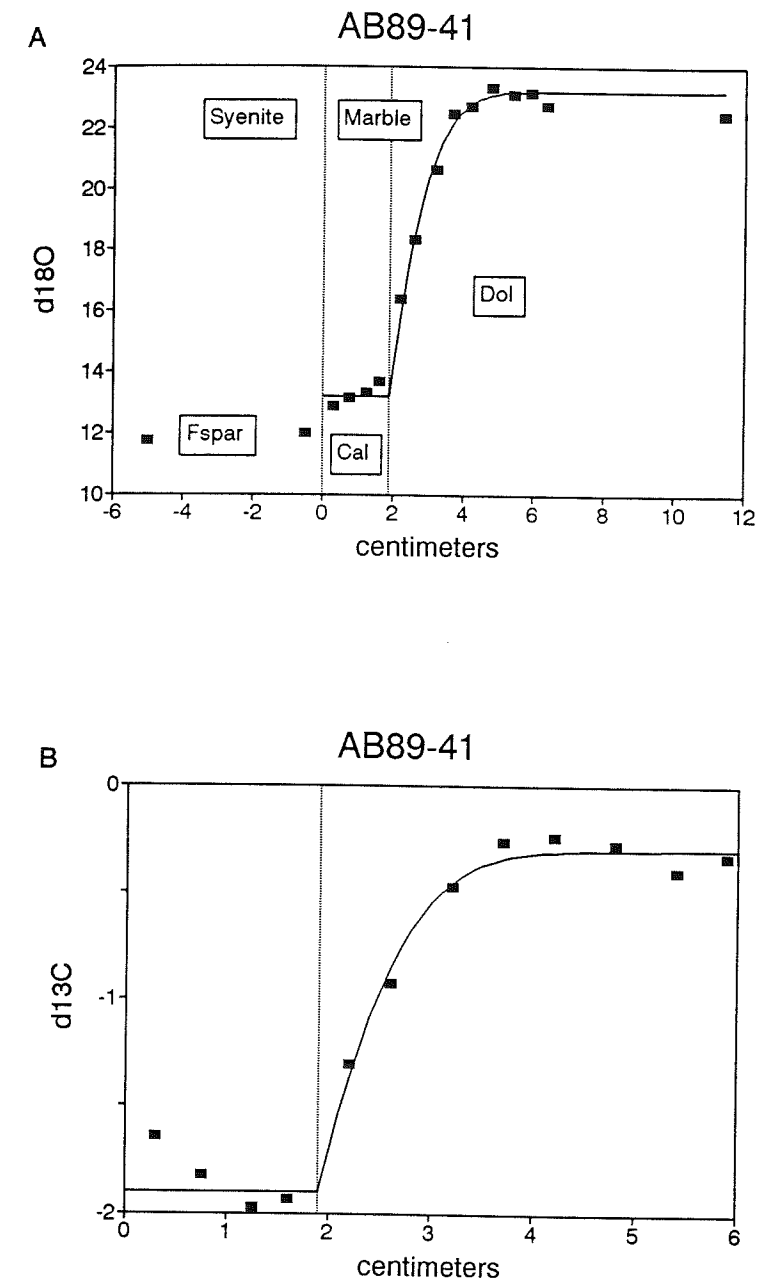
AB89-41

Figure 2.2   Fit through stable isotope data, AB89-41.   Calcite and feldspar compositions have been adjusted to represent the composition dolomite would have in equilibrium with the measured value at 800°C.
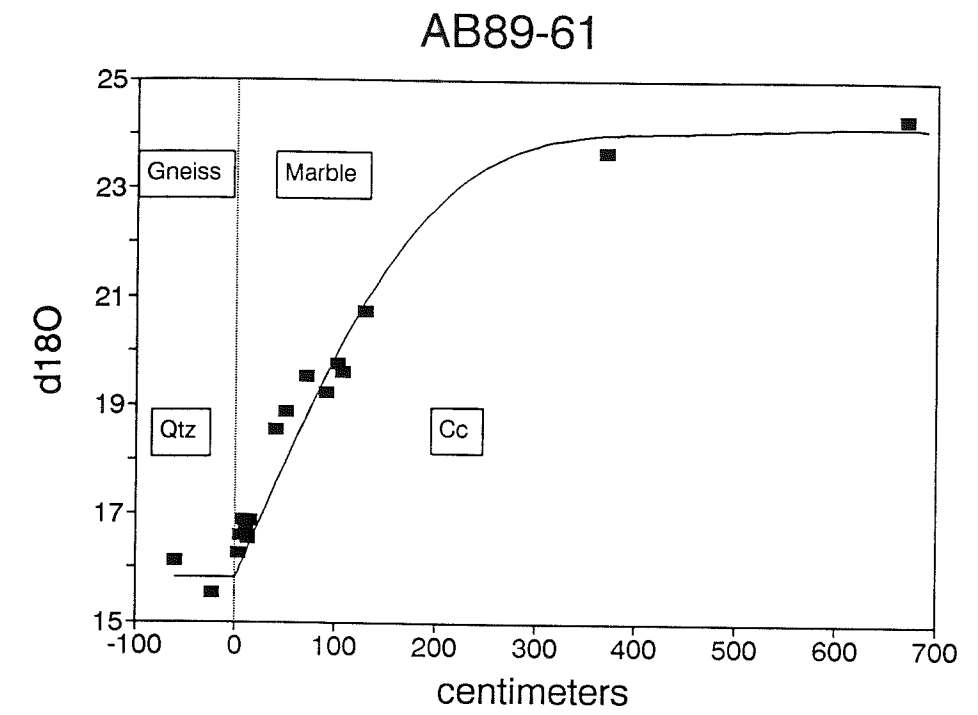
AB89-61

Figure 2.3   Fit through oxygen isotope data, AB89-61.   Qtz values have been
adjusted to represent Cal in equilibrium with the measured Qtz values at 800°C.
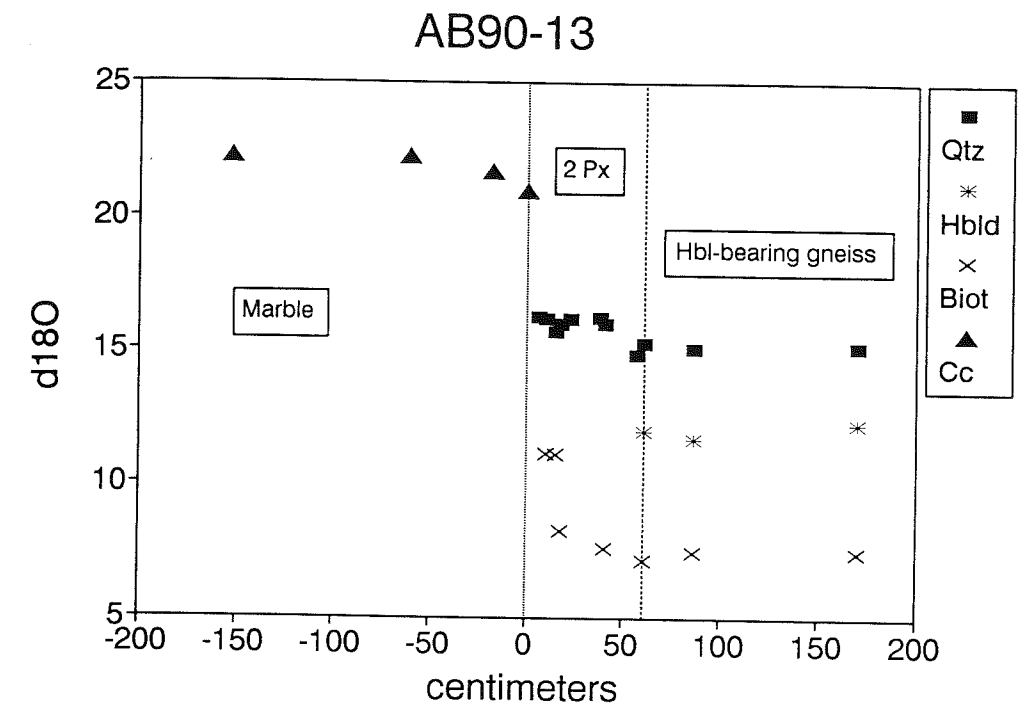
Figure 2.4   Stable isotope data, AB90-13.

AB89-62 and AB90-27

Legend:
- ▲ AB90-27 calcite
- ■ AB89-62 calcite
- □ AB89-62 adjusted qtz

Axis labels: d18O (vertical), centimeters (horizontal)

Region labels: Schist, Marble
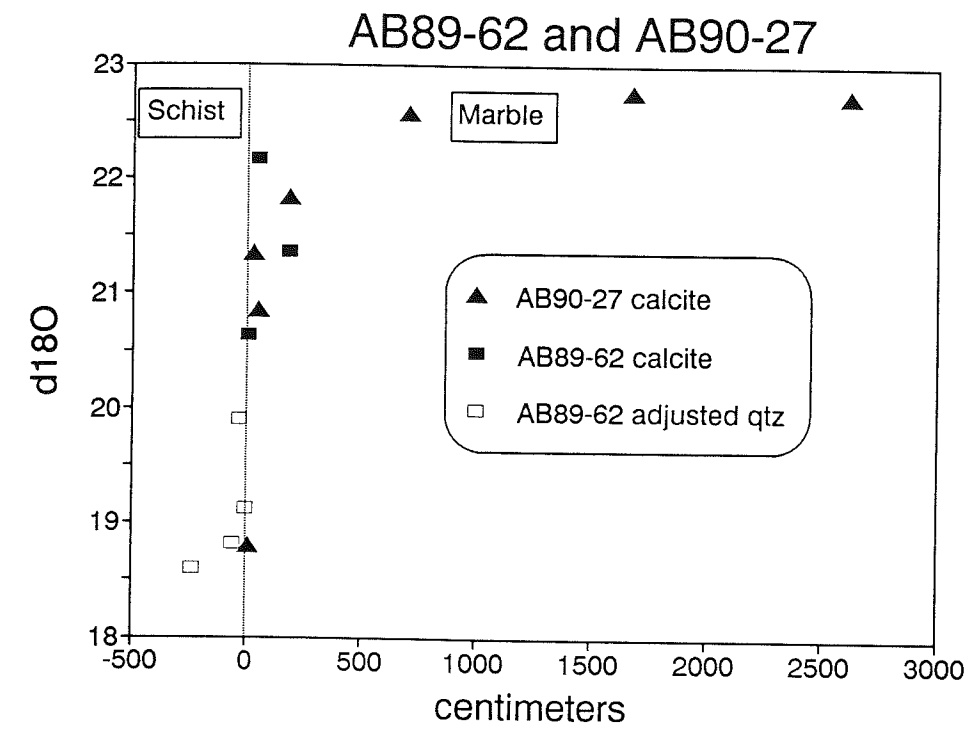
Figure 2.5   Stable isotope data, AB89-62 and AB90-27.   Qtz values have been adjusted to represent Cal in equilibrium with the measured Qtz values at 800°C.
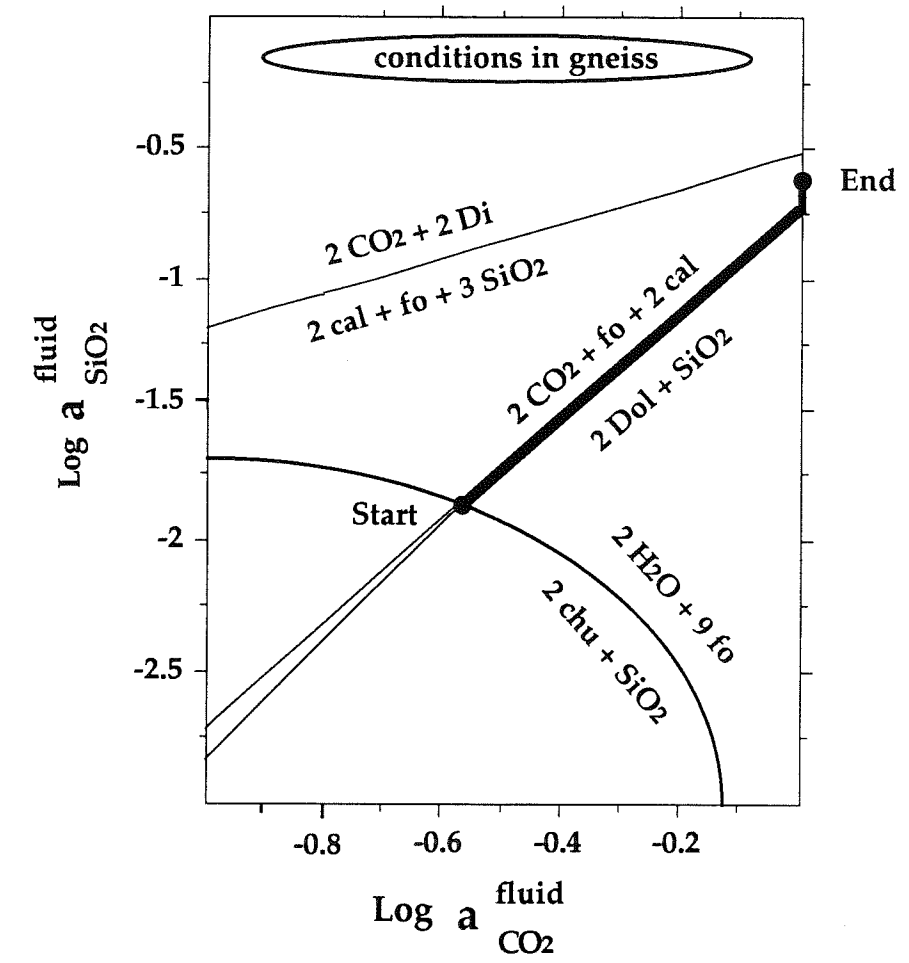
Figure 2.7   Log aSiO$_2$ vs. log aCO$_2$, AB89-41 marble.   Thick line shows
proposed buffering path followed by fluid in Cal+Fo zone. See text for details.
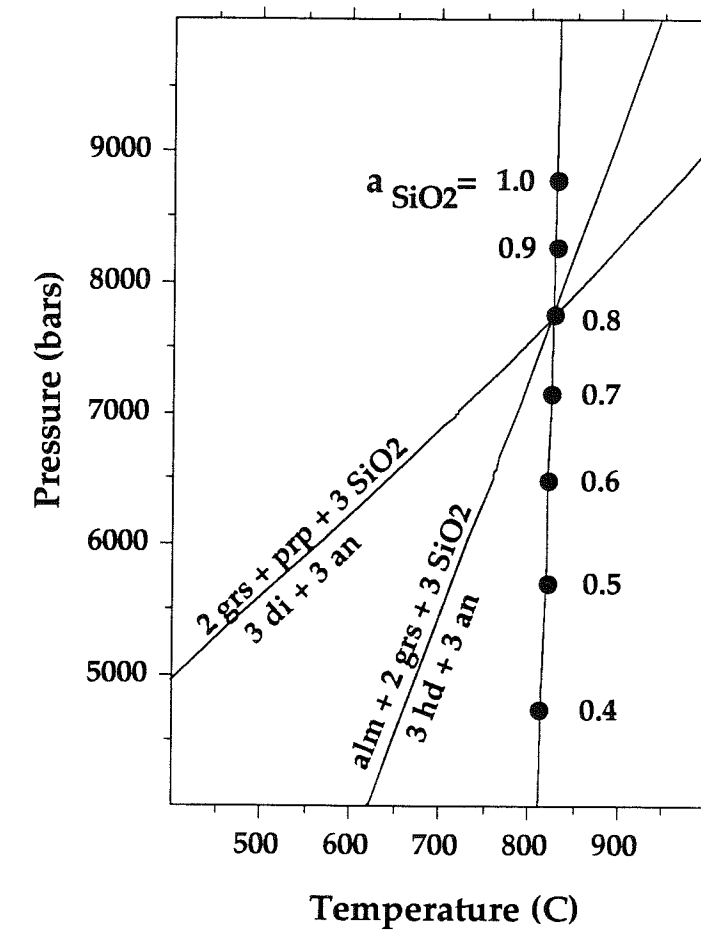
Figure 2.8   Activity of SiO_2, AB89-41 metasyenite.   Equilibria involving Grt,
Cpx, Pl for a sample 33 cm below the marble. The vertical line represents the
reaction: alm + 3 di = prp + 3 hd. The intersection near 8000 bars is obtained when
$aSiO_2$ is set to 0.8.   The large dots show the location of the intersection at other
values of silica activity.

AB89-41
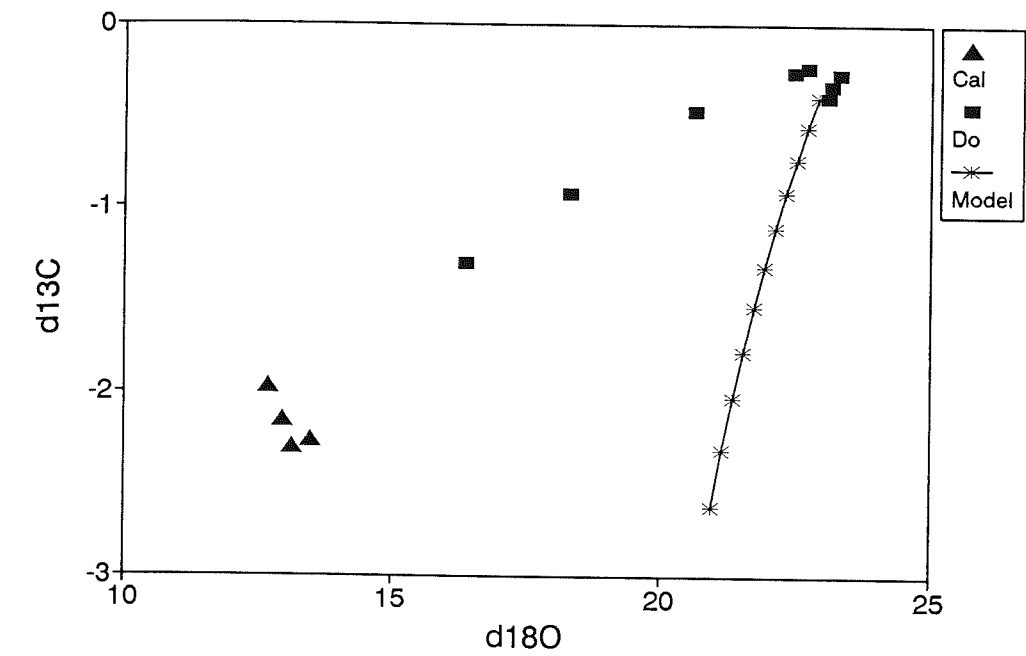
Figure 2.9 δ^{13}C vs. δ^{18}O, AB89-41.   Thick line shows the path followed by calcite during the reaction $2Dol + SiO_2 = 2Cal + Fo + 2CO_2$ following the method of Rumble (1982). For calculation, Dol starts at -0.2‰ δ^{13}C and 23‰ δ^{18}O, SiO_2 is 12‰ δ^{18}O. Fractionation factors taken from Sheppard and Schwarcz (1970) and Northrop and Clayton (1966). Tick marks indicate 10% reaction toward completion.
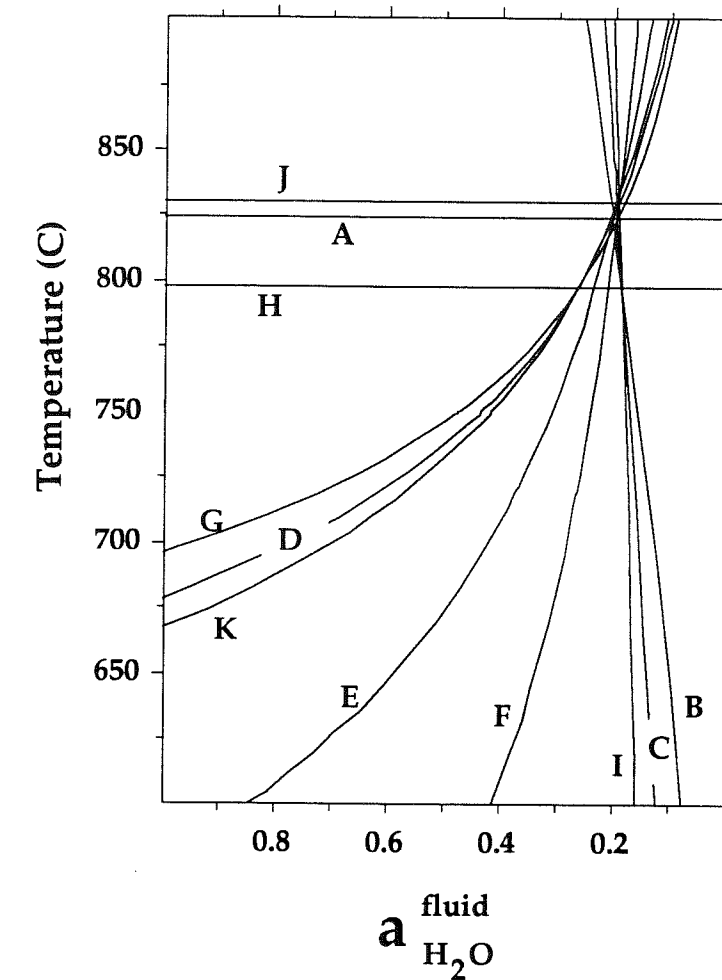
Figure 2.10   T-aH_2O, AB89-41 metasyenite.   Diagram calculated at 8 kbar for equilibria involving Grt, Cpx, Bt, Pl and Kfs indicating H_2O activity ~0.2. Qtz is not involved in any reaction. It can be noted that reactions D, E, F, G and K are prograde hydration reactions.

(A)   prp + 3 hd = alm + 3 di
(B)   2 H_2O + 3 prp + 2 kfs + 6 hd + 3 grs = 2 ann + 6 an + 9 di
(C)   2 H_2O + 3 prp + 2 kfs + 3 grs = 6 an + 3 di + 2 phl
(D)   2 ann + 6 an + 3 hd = 2 H_2O + 2 kfs + 3 grs + 3 alm
(E)   2 ann + 6 an + 3 di = 2 H_2O + prp + 2 kfs + 3 grs + 2 alm
(F)   6 an + 3 hd + 2 phl = 2 H_2O + 2 prp + 2 kfs + 3 grs + alm
(G)   6 an + 9 hd + 2 phl = 2 H_2O + 2 kfs + 3 grs + 6 di + 3 alm
(H)   phl + 3 hd = ann + 3 di
(I)   2 H_2O + 3 prp + 2 kfs + 3 grs + ann = 6 an + 3 hd + 3 phl
(J)   prp + ann = alm + phl
(K)   3 ann + 6 an + 3 di = 2 H_2O + 2 kfs + phl + 3 grs + 3 alm

Chapter 3: Localized fluid-controlled granulite grade assemblage

Introduction

One of the characteristic changes in mineral paragenesis from amphibolite to granulite grade metamorphic rocks is the disappearance or decline of hornblende coincident with the appearance of orthopyroxene alongside clinopyroxene in mafic rocks. Where this occurs, it has in many cases been ascribed to a reduction in H_2O activity due to dilution with CO_2 (Touret 1985, Hansen 1984, Bradshaw 1989, Harris and Bickle 1989, Santosh et al. 1990, Pattison 1991). Among possible sources of CO_2 is one that has received little attention, namely CO_2 evolved from carbonate metasediments (Glassley 1983, Glassley et al. 1989). This is because many granulite terranes contain little carbonate material. In this chapter I present a field example which clearly shows the association of a CO_2-evolving marble and localized progress of amphibolite to granulite dehydration reactions. It is a local phenomenon superimposed on the temperature rise which is responsible for the regional granulite facies assemblages found in the Kigluaik Mountains.

Outcrop Description

The lowermost member of the main marble unit consists mostly of a calcite and forsterite dominated marble, but has some variability, especially towards the top, where it is a calcite-diopside marble. It is overlain by a 100 m thick unit of relatively homogeneous Hbl-bearing quartzofeldspathic gneiss. Detailed sampling of the marble-gneiss contact has revealed that the lowermost 60 cm of the gneiss, instead of containing hornblende, contains orthopyroxene and clinopyroxene (figure 3.1). The outcrop described in this paper is located in the north wall of the east cirque of Mount Osborn (C in figure 2.1).

Diopside and phlogopite are the major silicate phases in the coarse-grained (0.5 mm) granoblastic marble near the gneiss contact; plagioclase, scapolite and orthoclase are also present in small quantities. Dolomite is rare or absent, and when present is fine grained and interstitial which suggests it may represent exsolution from calcite upon cooling. Late tremolite formed at the expense of diopside in some samples. The gneiss is coarse-grained (0.5 mm) and displays a moderate foliation defined by oriented mafic minerals. The typical gneiss is composed of 35% plagioclase, 30% hornblende, 20% quartz, 15% biotite (figure 3.1) and accessory apatite, zircon, allanite. Its homogeneity on the outcrop scale suggests that the protolith might have been an igneous rock.

Within 60 cm of the underlying marble, hornblende is no longer present. Instead the gneiss contains 40% feldspar (mostly plagioclase), 25% quartz, 20% biotite and 15% pyroxenes, with ilmenite as an additional accessory phase. In one sample (17 cm from the marble), garnet is present and clinopyroxene is absent. Both pyroxenes are fine grained (0.1 mm diameter) and granular and do not clearly form pseudomorphs after Hbl (mineral abbreviations in table 1.1). Garnet is embayed and in some cases is surrounded by Pl + Opx symplectite. Plagioclase crystals display a range of grain sizes from 0.1 to 1.0 mm; some of the large crystals are antiperthitic. In a narrow transition zone Hbl, Cpx and Opx coexist.

Mineral Compositions

The following section describes the compositions of minerals in selected samples from the Hbl-bearing gneiss, Hbl-free gneiss, and the transition between the two. Mineral compositions are listed in appendix 2.

Hornblende

The amphibole in the Hbl-bearing gneiss is green and pleochroic (X pale green, Y green, Z dark brown-green). Its composition falls in the range of ferroan pargasitic

hornblende, bordering on ferroan ferri-pargasitic hornblende (names from Leake, 1978); amounts of exchange components are (Thompson 1982a, Dymek 1983): X_{tk} ($Mg_{-1}Si_{-1}$ $AlAl$) ≈ 1.13, X_{ed} ($\square_{-1}Si_{-1}$ $NaAl$) ≈ 0.54, X_{tispl} (Al_{-2} $MgTi$) ≈ 0.17, X_{ab} ($Ca_{-1}Al_{-1}$ $NaSi$) ≈ 0.10. No compositional zoning is observed within individual grains, and there is little inter-sample variation (figure 3.2). In a sample from the transition zone, the amphibole composition is more variable and less aluminous than that of the Hbl-bearing gneiss, ranging through edenitic hornblende to magnesio-hornblende (figure 3.2); $X_{tk} = 0.77$, $X_{ed} = 0.25$, $X_{tispl} = 0.07$, $X_{ab} = 0.12$. In one sample from the Hbl-free gneiss (15 cm from the marble) a small brown amphibole grain was found. It is not an inclusion, but occurs between a quartz and feldspar grain. The composition of this amphibole overlaps with that of the Hbl-bearing gneiss when plotted on figure 3.2, but differs significantly in Ti content (see appendix 2); $X_{tk} = 1.13$, $X_{ed} = 0.55$, $X_{tispl} = 0.42$, $X_{ab} = 0.16$. The appropriate name is titanian ferroan pargasitic hornblende.

Feldspars

In the Hbl-bearing gneiss plagioclase is not zoned, but varies from An_{42} to An_{49} from sample to sample. The orthoclase component is always less than 3% and no antiperthite is visible microscopically. In the Hbl-free gneiss feldspar compositions are more complex, with plagioclase ranging in composition from An48 to An76 (figure 3.3). The gap in feldspar composition from An_{59} to An_{65} is an artifact of sampling. Orthoclase component remains below 3%. None of the more anorthitic feldspars are antiperthitic and they are commonly no more than 0.1 mm in diameter. They are typically found in a mass of biotite and pyroxene grains. Some large (1 mm) more albitic plagioclase grains are antiperthitic.

In the Hbl-free gneiss Kfs is present in three forms: (i) as rims separating quartz from plagioclase (figure 3.4a); (ii) as separate grains; (iii) in antiperthite (figure 3.4b, c,

d). Only large plagioclase grains, but not all of them, are antiperthitic. The host composition is usually about An_{52}, slightly more anorthitic than Pl in the Hbl-bearing gneiss. The Kfs guest composition is ~Or_{90}-Ab_9-An_1. Results of two-feldspar thermometry on host and guest compositions using MTHERM3 (Fuhrman and Lindsley 1988) yield T=~600°C, indicating that the host and lamellae reequilibrated upon cooling. A microprobe linescan across several Kfs guests within a Pl host shows no consistent enrichment or depletion of plagioclase components adjacent to the Kfs blebs (figure 3.5). An increase in anorthite component approaching a Kfs bleb has been taken to indicate formation of antiperthite from a previously homogeneous feldspar (Kay, 1977). However, the spacing of Kfs lamellae in the present case (~20 μm) may be too small to manifest the build-up. The reintegrated composition of one typical antiperthite grain (25% Or, 34% Ab, 41% An; figures 3.4d and 3.6) lies well within the two-feldspar field at 800°C. This indicates that antiperthite formation was not caused by exsolution from a previously homogeneous feldspar, but must have occurred by some sort of replacement process (e.g. Griffin 1968). The geometry of some Kfs blebs within plagioclases, such as figure 3.4d, rules out Kfs growth along cracks, fractures or cleavages.

Other Mafic Minerals

Biotite Mg# varies from sample to sample from 0.53 to 0.65 in an unsystematic way. In vector component notation (Thompson, 1982a; Dymek, 1983) X_{tk} remains constant at about 0.25 as does X_{tlc} ($K_{-1}Al_{-1}$ □Si) at about 0.05, but X_{tispl} and X_{dioct} (Mg_{-3} Al_2□) increase somewhat from the Hbl-bearing gneiss to the Hbl-free gneiss (0.20 to 0.41 and 0.10 to 0.25, respectively). X_{tispl} and X_{dioct} are highly positively correlated among the 6 analyses, suggesting that the Ti substitution occurring in these

biotites may be Mg_{-2} $Ti\square$. Fluorine contents are low and show no variation with distance from the marble.

Mineral analyses of pyroxenes and garnet are listed in appendix 2. The low Ca content of Opx from 18 cm is due to the fact that it does not coexist with Cpx; instead, garnet is present. The garnet composition is: $X_{alm} = 0.55$, $X_{prp} = 0.25$, $X_{sps} = 0.05$, $X_{grs} = 0.15$. For the two samples analyzed where Opx and Cpx coexist, the two-pyroxene solvus thermometer (Lindsley 1983) yields approximately 800°C, in agreement with previous estimates from the field area (Lieberman 1988, Lieberman and Petrakakis 1992).

Mineral reactions

The two mineral assemblages present in the gneiss, $Hbl + An_{50} + Qtz + Bt$ and $Opx + Cpx + $ (up to) $An_{76} + Qtz + Kfs + Bt$, could be the result of similar environmental conditions (P, T, aH_2O) affecting slightly different bulk rock compositions, or the metamorphism of the same bulk composition under differing environmental conditions. In order to distinguish between these two possibilities (Greenwood, 1967) the mineral assemblages were analyzed by matrix methods.

The programs written by Fisher (1989) utilizing singular value decomposition were employed in order to look for possible reaction relationships between the two assemblages. The sample from 86 cm represents the Hbl-bearing assemblage, whereas the 15 cm sample represents the Hbl-free assemblage with the exception of biotite. A single composition of biotite was used in the analysis.

The data input and output for the analysis are listed in table 3.1. Ilmenite is a minor phase and has not been quantitatively analyzed; it is listed as a pure Fe-endmember component. Although An_{76} is the most extreme composition found in the thin section analyzed, more anorthitic plagioclase may exist. In order to account for the

anorthitic plagioclase in the Hbl-free gneiss, end-member anorthite is listed as a phase. Orthoclase is also listed as the pure end-member phase. As recommended by Fisher, Si and H were omitted from the calculation because they can be balanced later by quartz and water. Goodness of fit as evaluated by examining the ratio {(data minus model) / error}, ideally less than one, is acceptably small in most cases. Although 11 (19%) of the residuals are greater than one, seven of them are minor components in the mineral and therefore not critical.

Two reaction relationships were found among the minerals present in the two assemblages (table 3.1). Since the most obvious feature of this outcrop is the appearance of pyroxenes, the equations were normalized to produce one mole of Opx. Quartz and H_2O stoichiometries were calculated using the original mineral compositions.

Discussion

Reaction (B) listed in table 3.1 is consistent with modal changes at this outcrop. It consumes Bt, Hbl and Qtz and produces feldspars and both pyroxenes. In contrast, reaction (A) consumes Cpx and anorthite component and produces Hbl along with Opx! However, these reactions can be linearly combined in order to isolate a reaction that consumes Hbl and one that consumes Bt. These are:

Hbl + 1.96 Qtz =

$$1.22 \text{ Cpx} + 1.47 \text{ Opx} + 1.01 \text{ An}_{63} + 0.26 \text{ Kfs} + 0.26 \text{ Ilm} + H_2O \qquad (1)$$

Bt + 2.59 Qtz + 0.18 Cpx =

$$1.32 \text{ Opx} + 0.16 \text{ An}_{89} + 0.93 \text{ Kfs} + 0.20 \text{ Ilm} + H_2O. \qquad (2)$$
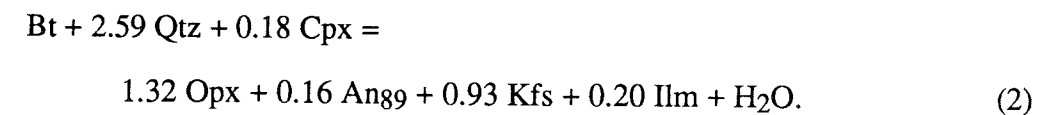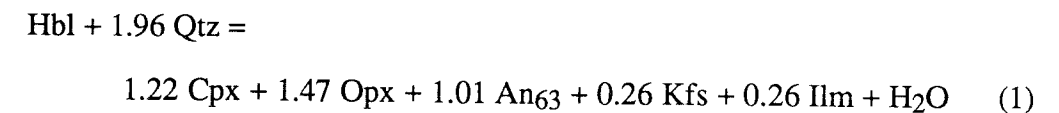
For each reaction, the two plagioclases have been combined and expressed as the appropriate intermediate plagioclase. Cast in these terms the reactions are recognizable as a Hbl breakdown reaction (1) and a biotite breakdown reaction (2). These reactions are depicted graphically in figure 3.7, a form of reaction space (Thompson 1982b). The

horizontal and vertical axes represent reaction (1) and (2), respectively. The tick marks indicate progress of the reactions as written per liter of rock. For the measured modal amounts of minerals in the Hbl-bearing gneiss, eventually a reactant will be exhausted for either reaction. These limits are shown by the dashed lines and labeled with the mineral which is exhausted. The light lines represent the direction of reaction progress that neither produces nor consumes the mineral which labels the line. The plus and minus signs indicate whether the mineral is produced or consumed if the direction of reaction falls to one side or the other of the line.

Modal composition data constrain the direction of reaction progress to be dominated by reaction (1), sub-horizontal to the right in figure 3.7. Biotite is abundant in the Hbl-free gneiss. Therefore the reaction direction must reach the limit of hornblende well below the point where the limit of biotite and the limit of hornblende intersect. The lower limit of reaction direction comes from the Kfs line; Kfs component has been produced in the Hbl-free gneiss. This circumstance even allows for the possibility that the biotite reaction ran backwards, producing biotite from Kfs and Opx.

A combination of reaction (1) and (2), dominated by (1) adequately explains all the mineralogic differences between the Hbl-bearing and Hbl-free gneiss: Hbl is exhausted; Cpx, Opx, Kfs and An component are produced. The fact that these reaction relationships exist between the minerals in the two assemblages indicates that the assemblages must have equilibrated under different environmental conditions, and their differences cannot be attributed solely to variations in bulk composition (Greenwood, 1967). Since, during regional metamorphism a temperature or pressure gradient cannot be maintained over just 60 cm, the only environmental condition left is fluid composition.

Fluid Composition

Both (1) and (2) are dehydration reactions, and therefore could have been driven by a decrease in water activity. Dilution with CO_2, presumably from the underlying marble, is a mechanism capable of lowering water activities. This idea can be tested by examining fluid composition in the gneiss as a function of distance from the marble. Figure 3.8 is an isobaric T-aH_2O diagram for equilibrium among the components:

$$phl + 3\ Qtz = 3\ en + Kfs + H_2O \tag{3}$$

for three different rocks in the Hbl-free gneiss. The three lines are labeled with distance in cm from the contact with marble. At 800°C, the calculated water activity decreases from 0.24 at 61 cm to 0.20 at 15 cm, indicating a trend toward more H_2O-poor conditions near the marble. The absolute value of the calculated aH_2O could change by choosing different solid solution models for the phases involved or different P or T conditions, but the trend toward more water-poor conditions is still valid.

The mineral assemblage in the marble indicates that it could be a source of high XCO_2 fluid. Figure 3.9 is an isobaric T-XCO_2 diagram appropriate for bulk compositions of marbles like this one, namely relatively high in K and Al. This diagram is projected from calcite and anorthite in the KCMASCH system. For bulk compositions that lie near the Di-Phl tie line, fluid composition was probably buffered along the path shown (Greenwood 1975). For a marble originally composed of Cal + Dol + Qtz + Ms at some arbitrary low value of XCO_2, the first reaction encountered upon heating was:

$$5\ Dol + 8\ Qtz + H_2O \rightarrow Tr + 3\ Cal + 7\ CO_2. \tag{4}$$
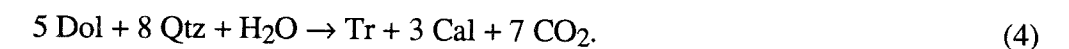
As temperature rose, fluid composition buffered to invariant point (I). At this point, the net mineral reaction which proceeded (Rice and Ferry 1982) at $XCO_2 = 0.4$ was:

$$0.9 \text{ Dol} + 2.3 \text{ Ms} + 1.2 \text{ Tr} \rightarrow$$

$$\text{Cal} + 5.1 \text{ Qtz} + 2.3 \text{ An} + 2.3 \text{ Phl} + 0.8 \text{ CO}_2 + 1.2 \text{ H}_2\text{O}. \quad (5)$$
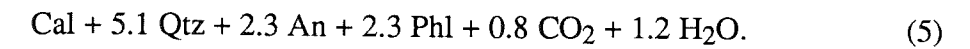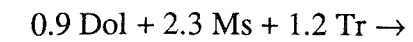
Since the only tremolite in the marble was produced while buffering along reaction (4), tremolite was most likely the first reactant exhausted (Rice and Ferry 1982). Upon further heating, fluid composition buffered along:

$$\text{Dol} + \text{Ms} + 2 \text{ Qtz} + \text{H}_2\text{O} \rightarrow \text{Cal} + \text{Phl} + \text{CO}_2 \quad (6)$$
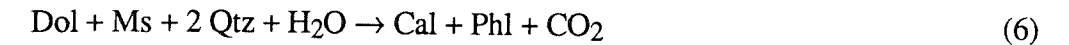
until invariant point (II) was reached. With additional heat, Kfs appeared and Ms was exhausted by the net reaction at $XCO_2 = 0.55$:

$$3 \text{ Dol} + 16 \text{ Cal} + 38 \text{ Qtz} + 19 \text{ Ms} \rightarrow$$

$$19 \text{ An} + 18 \text{ Kfs} + \text{Phl} + 18 \text{ H}_2\text{O} + 22 \text{ CO}_2. \quad (7)$$
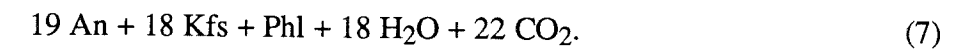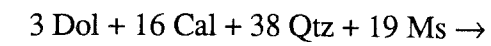
As heating continued, fluid composition buffered to invariant point (III) along:

$$3 \text{ Dol} + \text{Kfs} + \text{H}_2\text{O} \rightarrow 3 \text{ Cal} + \text{Phl} + 3 \text{ CO}_2. \quad (8)$$
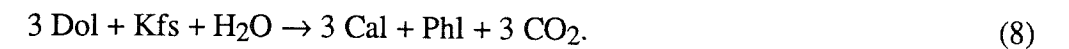
At invariant point (III) the net reaction was:

$$16 \text{ Qtz} + 3 \text{ Phl} + 9 \text{ Cal} \rightarrow 8 \text{ Di} + \text{Dol} + 3 \text{ Kfs} + 3 \text{ H}_2\text{O} + 7 \text{ CO}_2. \quad (9)$$
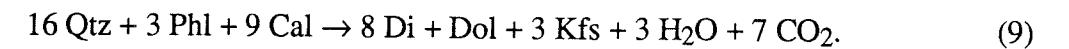
Depending on bulk composition, either quartz or phlogopite was exhausted. In the marble from this locality, quartz was exhausted, leading to continued buffering along reaction (8) as temperature rose until Dol or Kfs was exhausted. The resulting assemblage is Cal + Di + Phl + An + (Kfs or Dol).

Much of the marble unit well below this outcrop consists of Cal + Dol + Fo + Phl ± Spl. Fluid in marbles of this bulk composition are buffered to high XCO_2 along reactions such as:

$$\text{Dol} + 2 \text{ Qtz} \rightarrow \text{Di} + 2\text{CO}_2 \quad (10)$$

$$2 \text{ Dol} + \text{An} \rightarrow 2 \text{ Cal} + \text{Di} + \text{Spl} + 2 \text{ CO}_2 \quad (11)$$

$$3 \text{ Dol} + \text{Di} \rightarrow 4 \text{ Cal} + 2 \text{ Fo} + 2 \text{ CO}_2 \quad (12)$$
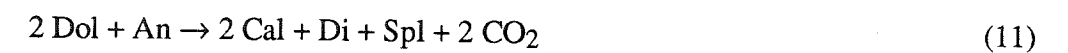
(reactions A, E and D, respectively, in figure 1.7). Therefore, the observed mineral assemblages indicate that this marble was a viable source of CO_2-rich fluids with which to dilute fluids in the overlying gneiss. It is interesting to note that high XCO_2 fluids from marbles were only possible if fluid composition was internally buffered. If the equilibrium pore fluid composition was dominated by an infiltrating fluid, the bulk of reaction progress would have produced the observed mineral assemblages in the presence of fluids of much lower CO_2 content.

Conclusions

The change from amphibolite to granulite facies paragenesis at this outcrop is not a manifestation of a difference in bulk composition, but a consequence of a difference in pore fluid composition during metamorphism. The difference in fluid composition was caused by CO_2 evolved from the underlying marble. Mineral assemblages in the marble are consistent with the marble being a source of CO_2-rich fluids. The decrease in H_2O activity of fluid in the gneiss drove dehydration reactions which consumed hornblende and quartz $\pm$ biotite, and produced orthopyroxene, clinopyroxene, anorthite-rich plagioclase, orthoclase (sometimes as antiperthite) and ilmenite. This reaction was restricted to within 60 cm of the marble, indicating the limited role of fluid movement in controlling mineral parageneses in this terrane. Since no graphite was precipitated during the introduction of CO_2-rich fluids, oxygen fugacity during metamorphism must have been above graphite stability (Lamb and Valley 1985). Pervasive influx of H_2O-rich fluids into the marbles can be ruled out because this would have lead to marble-derived fluids that were more H_2O-rich than the observed $aH_2O=0.2$ in the gneiss. Pervasive influx of CO_2-rich fluids into the gneissic units can be ruled out because the dehydrated mineral assemblage is spatially associated with the marble.

Table 3.1   Singular value decomposition

	Hbl	Pl	Bt	Ilm	Opx	Cpx	An	Kfs
Si	6.465	2.544	2.789	0	1.957	1.945	2	3
Ti	0.183	0	0.235	1	0.003	0.006	0	0
Al	2.014	1.456	1.289	0	0.035	0.069	2	1
Fe	2.197	0	1.205	1	0.900	0.341	0	0
Mn	0.052	0	0.012	0	0.016	0.007	0	0
Mg	2.282	0	1.349	0	1.058	0.728	0	0
Ca	1.806	0.462	0.000	0	0.031	0.884	1	0
Na	0.386	0.511	0.009	0	0.001	0.020	0	0
K	0.285	0.014	0.956	0	0	0	0	1
H	2	0	2	0	0	0	0	0

estimated errors

Ti	0.050	0.005	0.070	0.005	0.005	0.005	0.005	0.005
Al	0.100	0.080	0.070	0.005	0.010	0.010	0.005	0.005
Fe	0.100	0.005	0.070	0.005	0.100	0.050	0.005	0.005
Mn	0.010	0.005	0.010	0.005	0.010	0.010	0.005	0.005
Mg	0.100	0.005	0.070	0.005	0.100	0.070	0.005	0.005
Ca	0.100	0.080	0.010	0.005	0.008	0.050	0.005	0.005
Na	0.020	0.080	0.005	0.005	0.005	0.010	0.005	0.005
K	0.020	0.010	0.050	0.005	0.005	0.005	0.005	0.005

Model matrix

Ti	0.261	-0.004	0.208	1.000	0.007	-0.008	-0.000	0.003
Al	2.035	1.455	1.278	0.000	0.036	0.065	2.000	1.001
Fe	2.032	0.008	1.295	1.000	0.891	0.371	0.000	-0.005
Mn	0.036	0.001	0.019	0.000	0.016	0.010	0.000	-0.000
Mg	2.422	-0.007	1.276	0.000	1.065	0.703	-0.000	0.005
Ca	1.768	0.464	0.019	-0.000	0.029	0.891	1.000	-0.001
Na	0.378	0.511	0.014	-0.000	0.001	0.021	0.000	-0.000
K	0.273	0.015	0.929	-0.000	-0.001	0.002	0.000	1.000

(Data-Model)/error

Ti	-1.57	0.76	0.39	-0.02	-0.81	2.84	0.04	-0.52
Al	-0.21	0.01	0.15	-0.01	-0.11	0.37	0.01	-0.14
Fe	1.65	-1.61	-1.28	0.05	0.09	-0.60	-0.09	1.10
Mn	1.64	-0.16	-0.66	-0.00	0.03	-0.28	-0.01	0.08
Mg	-1.40	1.36	1.04	-0.04	-0.07	0.36	0.08	-0.93
Ca	0.38	-0.02	-1.94	0.01	0.24	-0.14	-0.02	0.25
Na	0.38	-0.00	-0.98	0.00	0.08	-0.14	-0.00	0.05
K	0.58	-0.06	0.54	0.00	0.12	-0.42	-0.01	0.08

Reactions

	Hbl	Pl	Bt	Ilm	Opx	Cpx	An	Kfs	Qtz	Water
A	1.47	-0.93	-2.41	0.08	1.00	-2.24	-0.15	1.85	-3.28	0.47
B	-0.26	0.19	-0.47	0.16	1.00	0.23	0.14	0.51	-1.72	0.36

AB90-13

Hbl

Pl

Bt

Qtz

Hbl

Pl

Px

Bt

Qtz

Hbl zone

2 Px zone

Px

Pl + Kfs

Bt

Qtz

60 cm

Marble
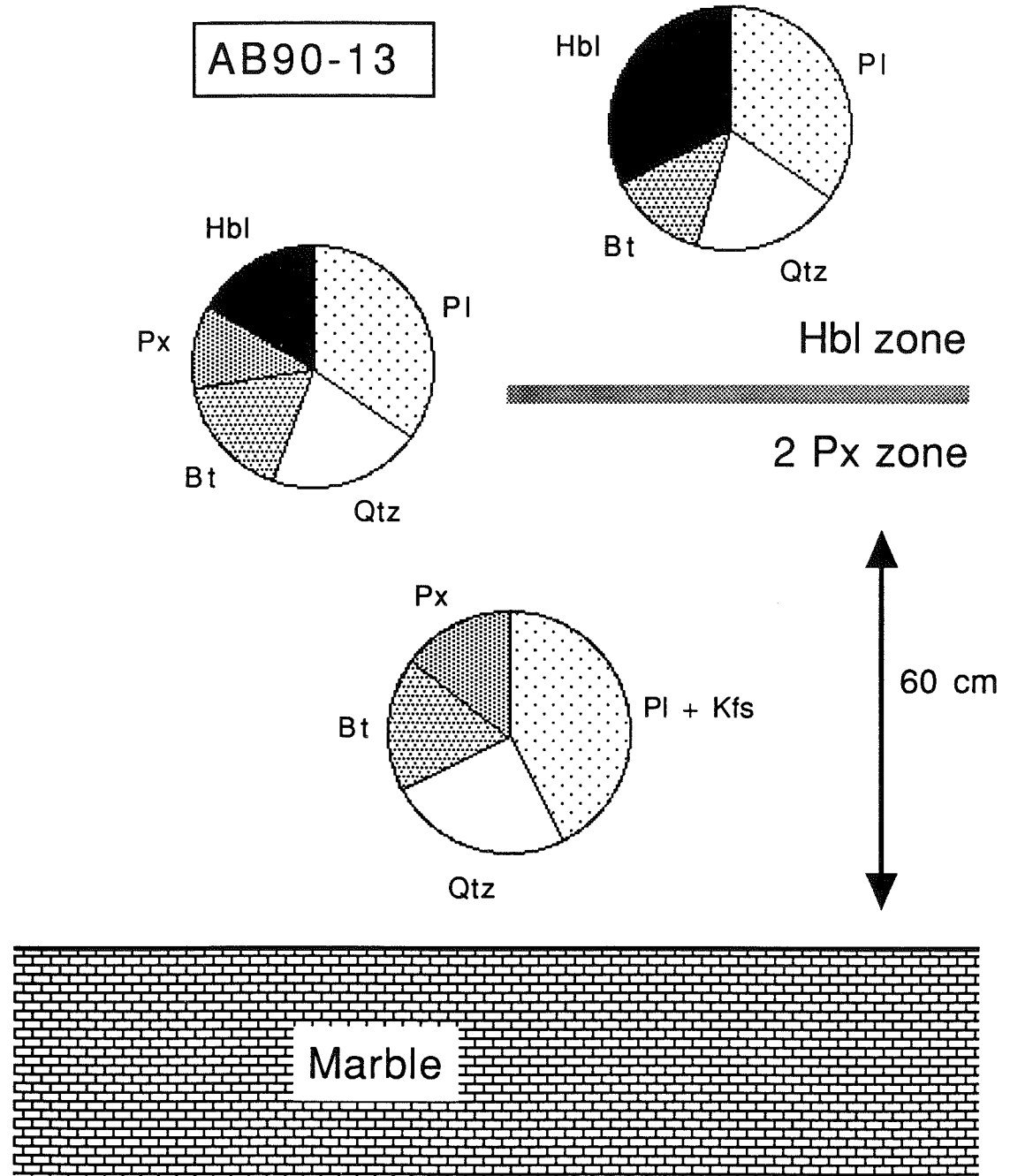
Figure 3.1   Cartoon cross section of outcrop AB90-13.   Shows change in modal
mineralogy from the Hbl-bearing gneiss to the Hbl-free gneiss.
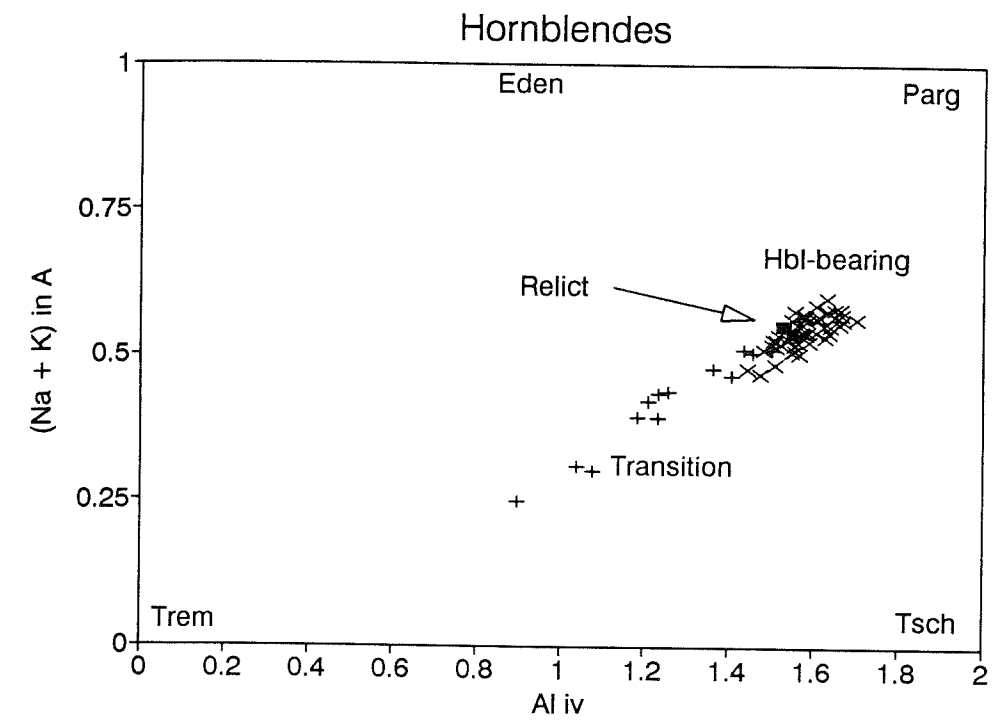
Figure 3.2 $(Na+K)^A$ vs. Al^{iv} for Hbl.   X are compositions in three different samples from the Hbl-bearing gneiss (86, 244 and 594 cm). Crosses are compositions in one thin section from the transition zone (61 cm). Filled square is the composition of the one relict amphibole grain in the Hbl-free gneiss (15 cm).

An

AB90-13 +18 cm

Ab   Or
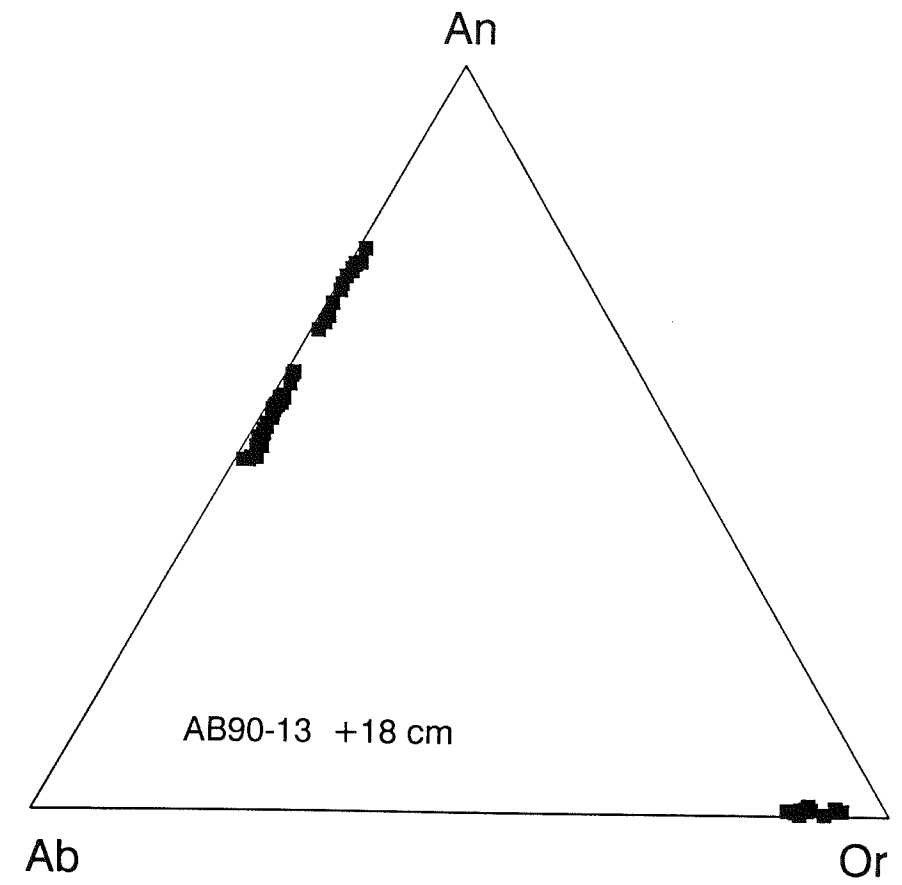
Figure 3.3   Feldspar ternary diagram, Hbl-free gneiss.   Shows compositions of
feldspars in one thin section from the Hbl-free gneiss (18 cm).
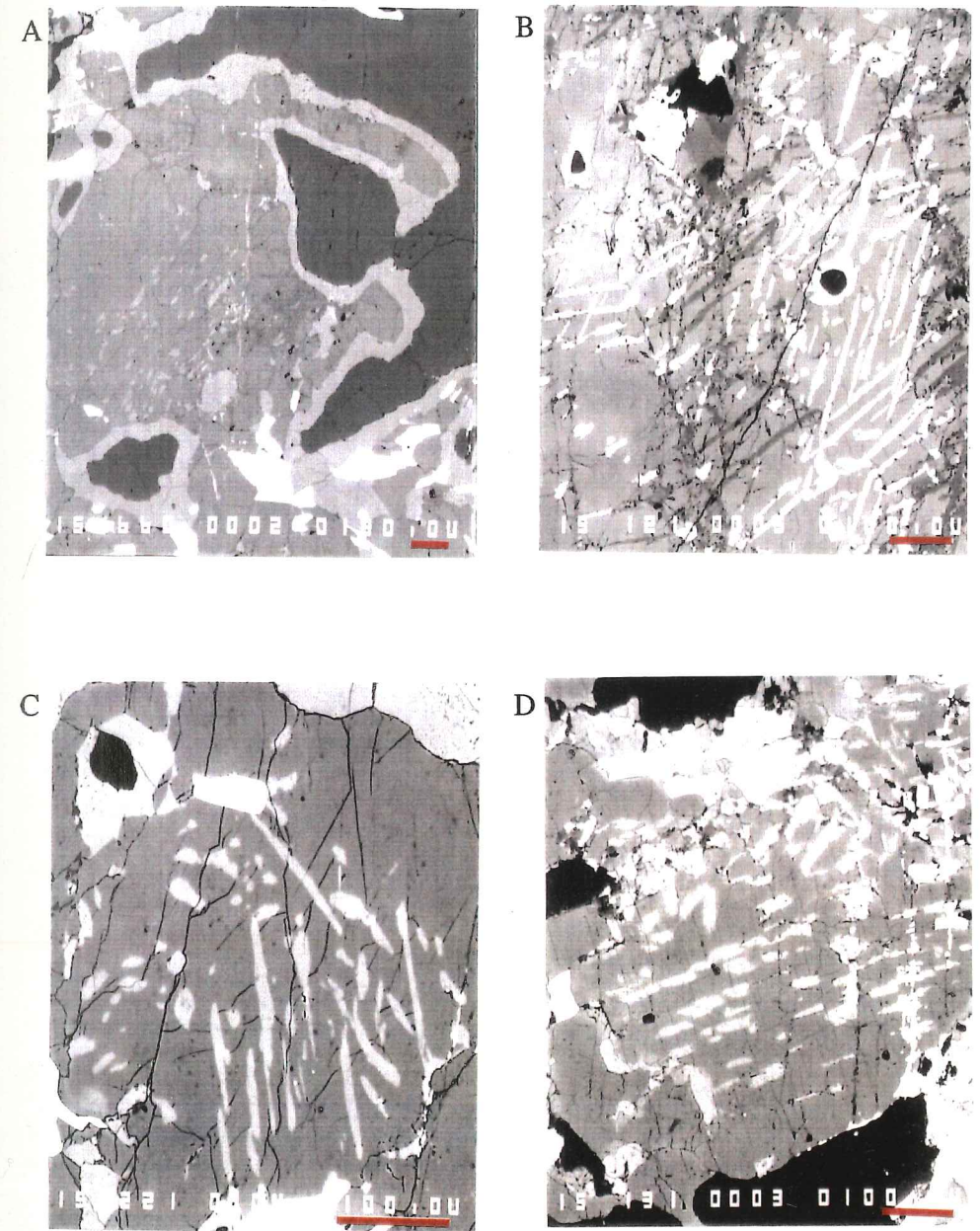
Figure 3.4   Backscatter photomicrographs of Kfs in Hbl-free Gneiss.
a) - Kfs (light) forming rims separating Qtz (dark) from Pl (medium).
b) - Antiperthite with up to 3 orientations of Kfs lamellae (light) in Pl
host (medium); dark is sericitic alteration of Kfs. c) - Antiperthite.
d) - Antiperthite showing blocky-shaped Kfs blebs (light) in Pl host
(medium). All from 18 cm. All scale bars are 100 μm.
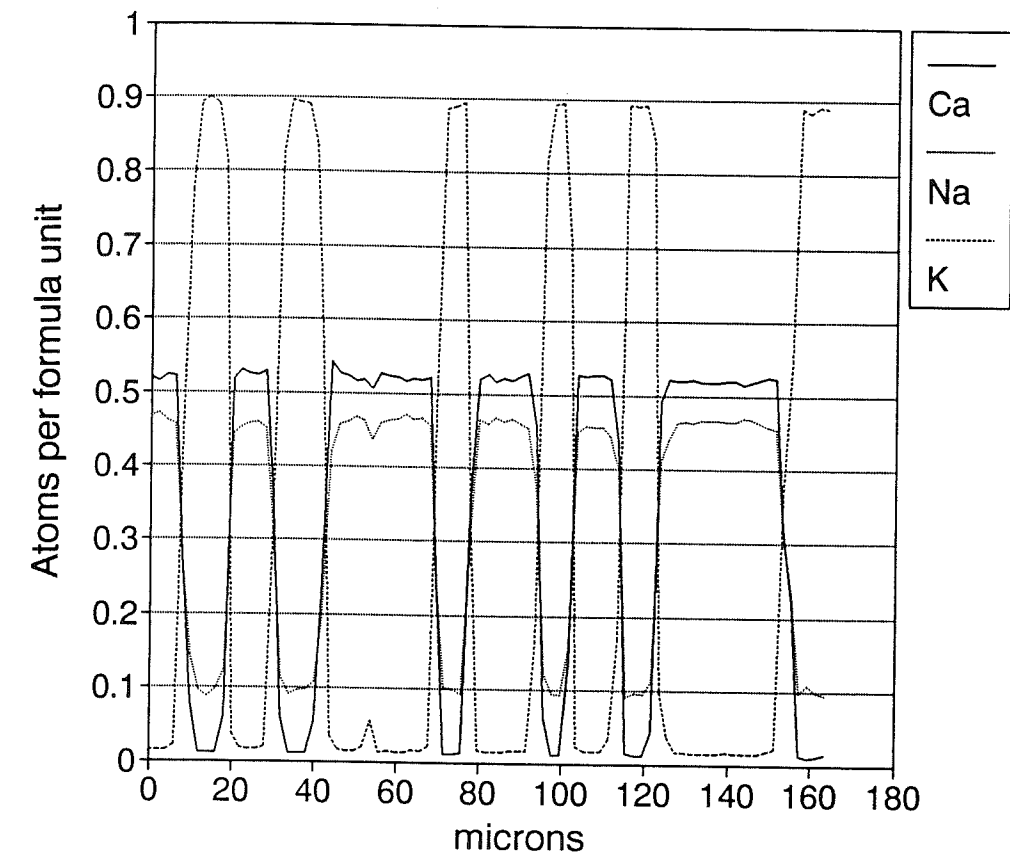
Figure 3.5   Microprobe traverse across antiperthite lamellae.   Traverse taken from
grain shown in figure 3.4b. Note that there is no consistent increase or decrease of
plagioclase components near Kfs lamellae.
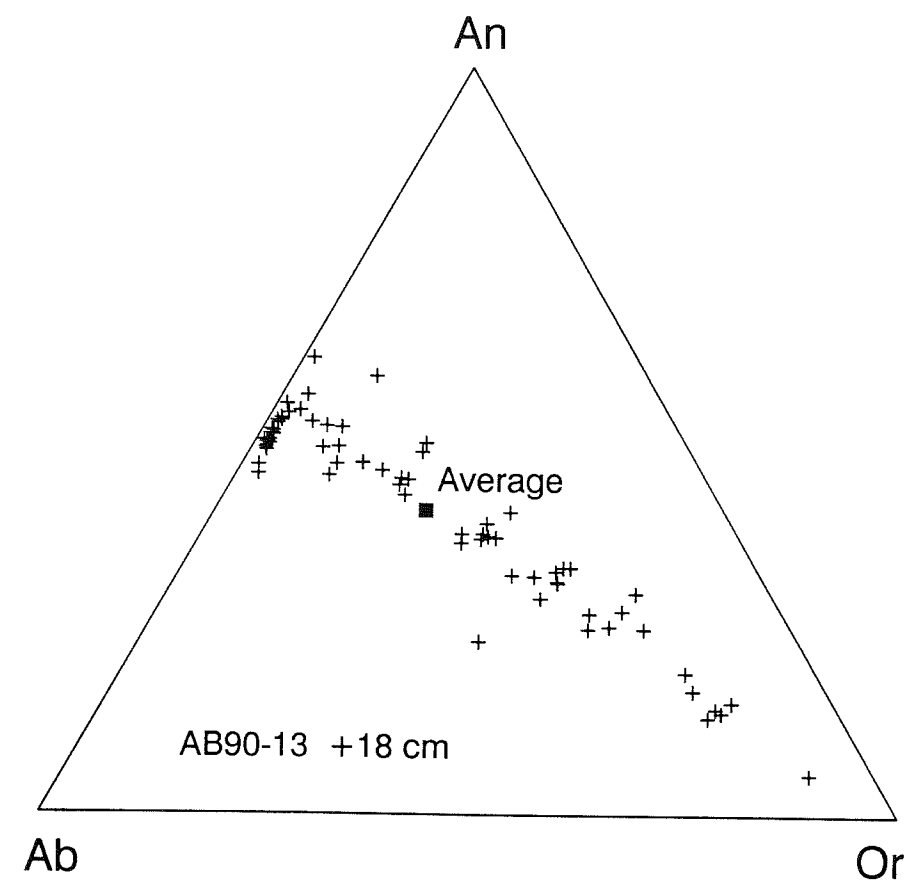
Figure 3.6   Feldspar ternary diagram of reintegrated antiperthite.   Grain chosen is shown in Fig 16d. Crosses are individual 30 μm diameter spots. Filled square is integrated average.

$$\text{Hbl:} \quad \text{Hbl} + 1.96 \text{ Qtz} \quad = 1.22 \text{ Cpx} + 1.47 \text{ Opx} + 1.01 \text{ An}_{63} + .26 \text{ Kfs} + .26 \text{ Ilm}$$

$$\text{Bt:} \quad \text{Bt} + 2.59 \text{ Qtz} + .18 \text{ Cpx} \quad = 1.32 \text{ Opx} + .16 \text{ An}_{89} + .93 \text{ Kfs} + .20 \text{ Ilm}$$
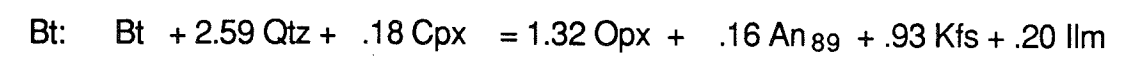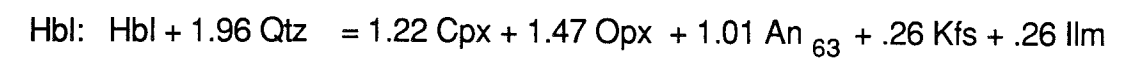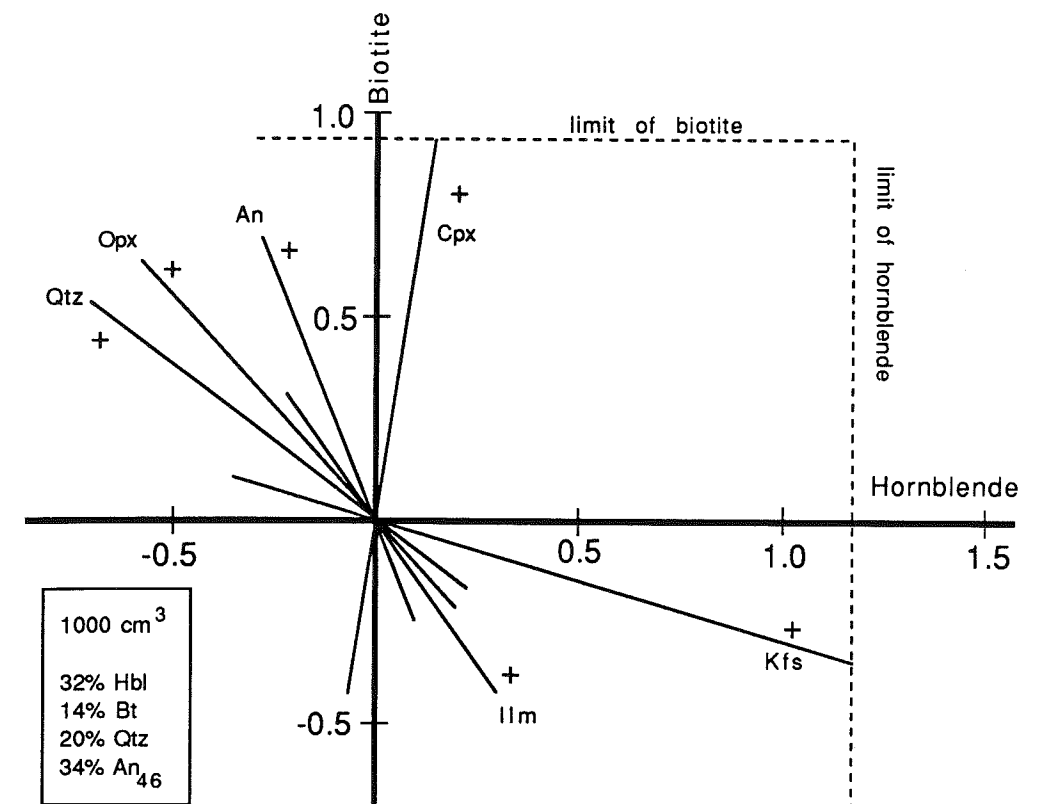
Figure 3.7   Reaction space for Hbl-bearing to Hbl-free transition.   See text for details.
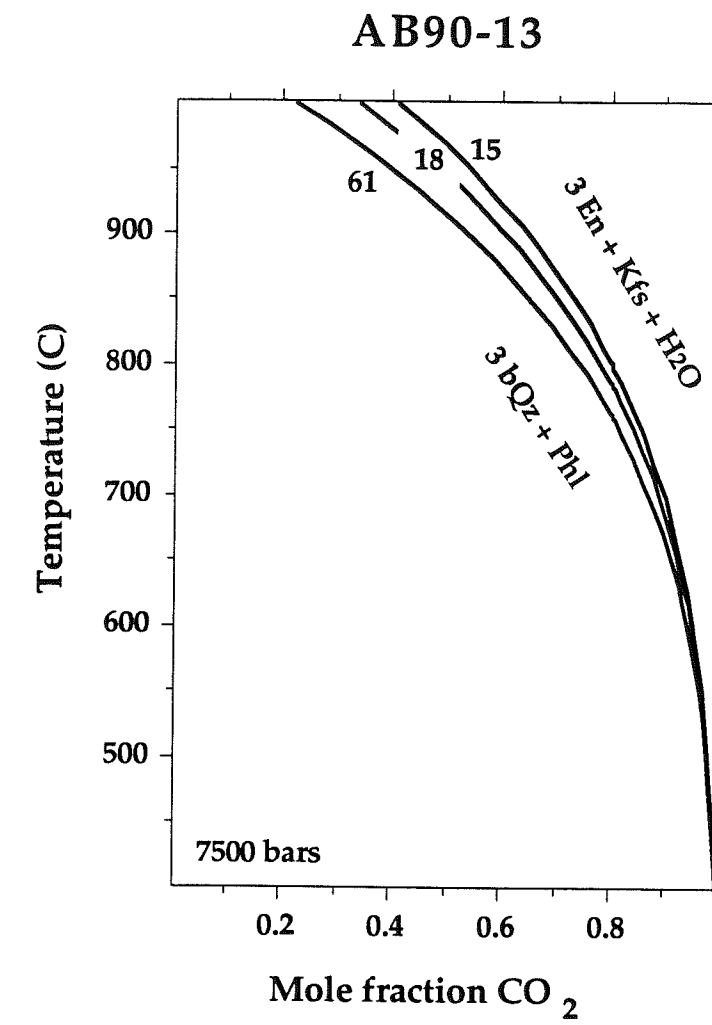
AB90-13

Figure 3.8   T-XCO$_2$ diagram, Hbl-free gneiss.   Calculated for rocks from the transition zone (61) and the Hbl-free gneiss (18 and 15); lines labeled with distance (cm) from the marble. Water activities are lower near the marble.

Temperature (C)

Mole fraction CO2

Figure 3.9 T-XCO$_2$ diagram, AB90-13 marble. Calculated for 8 kbar projected from Cal and An for marbles of bulk composition similar to the marble at AB90-13 in the system KCMASCH for a binary H$_2$O - CO$_2$ fluid. Some reactions have been omitted for clarity. The numbered reactions on the figure correspond to the ones in the text. The bold line shows the buffering path described in the text.

(4)   7 CO$_2$ + Tr + 3 Cal = 5 Dol + 8 Qtz + H$_2$O
(6)   4 CO$_2$ + Phl + 2 Cal + An = 3 Dol + Ms + 2 Qtz
(8)   3 Cal + Phl + 3 CO$_2$ = H$_2$O + Kfs + 3 Dol
(A)   H$_2$O + CO$_2$ + Dol + 4 Di = 3 Cal + Tr
(B)   2 H$_2$O + 2 Kfs + Phl + 3 An = 3 Di + 3 Ms
(C)   H$_2$O + 3 CO$_2$ + Kfs + 3 Di = 3 Cal + Phl + 6 Qtz
(D)   5 An + Cal + 5 Phl + 14 Qtz + 3 H$_2$O = CO$_2$ + 3 Tr + 5 Ms
(E)   H$_2$O + 9 CO$_2$ + 4 Phl + 5 Cal + 4 An = 7 Dol + 4 Ms + Tr
(F)   5 Di + 3 CO$_2$ + H$_2$O = Tr + 2 Qtz + 3 Cal
(G)   2 H$_2$O + 4 CO$_2$ + Phl + 7 Di + An = 4 Cal + Ms + 2 Tr
(H)   Di + 2 CO$_2$ = 2 Qtz + Dol
(J)   H$_2$O + CO$_2$ + Kfs + An = Cal + Ms + 2 Qtz
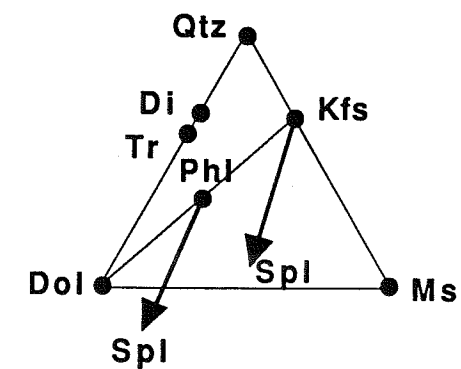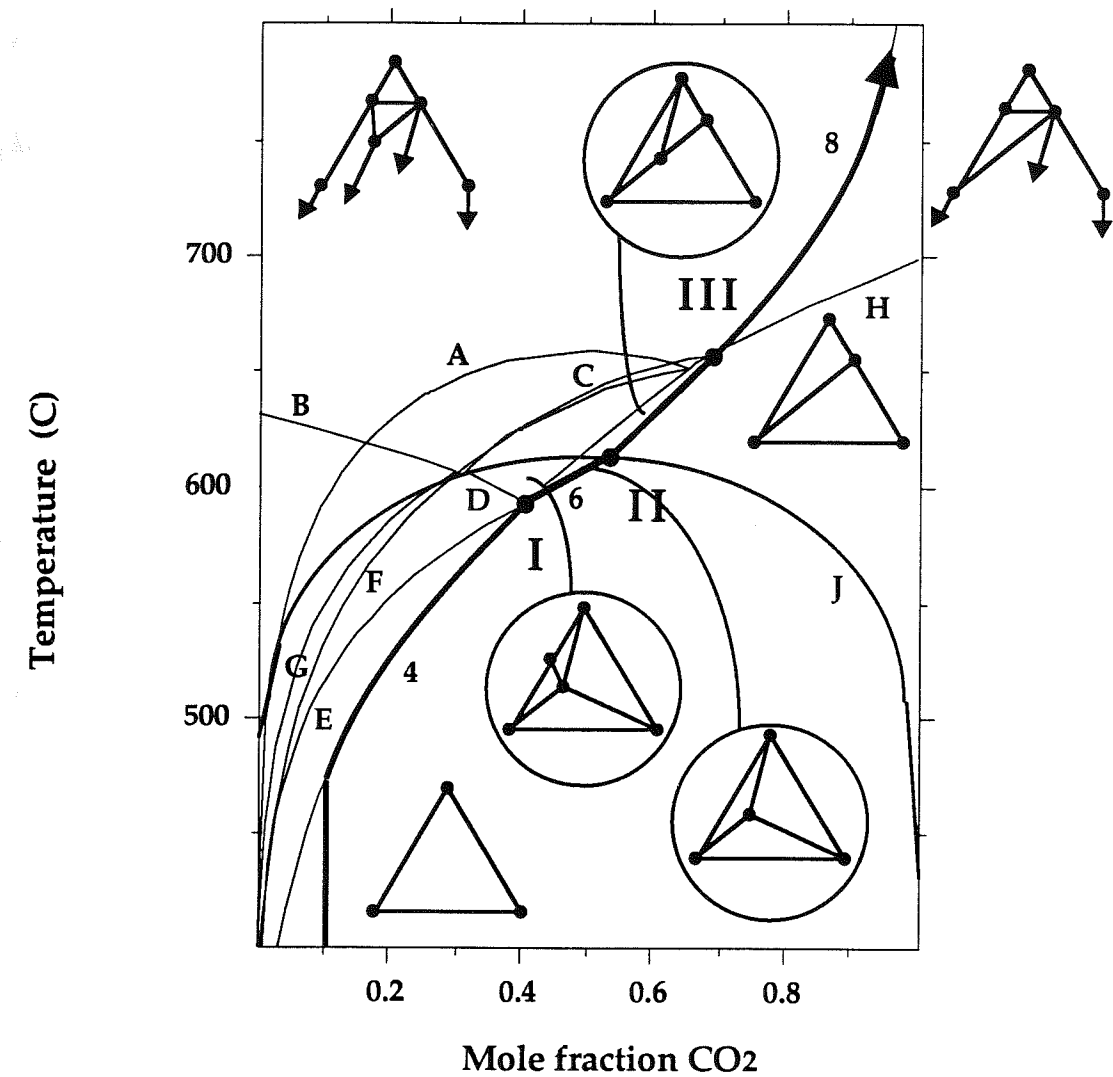
Chapter 4: Fluid inclusions

Introduction

The study of fluid inclusions in metamorphic rocks provides information about the composition of the fluid phase present during the metamorphism, its evolution during metamorphic mineral growth, and the pressure and temperature conditions of metamorphism. Fluid inclusions also form from fluids either generated in the rock or introduced after the peak of metamorphism, during cooling and uplift. Interpretation of the properties of the several generations of fluid inclusions commonly preserved in metamorphic minerals may give evidence on the uplift history of the metamorphic terrane or about specific recrystallization or deformational events affecting the fluid inclusion-bearing phase.

M.L. Crawford (1981, p. 157)

Fluid inclusions are small quantities of fluid encased in mineral grains. In metamorphic rocks these inclusions vary widely in size, but are frequently less than 30 μm in diameter. Fluid can be trapped in inclusions during growth of the mineral (primary) or along healed fractures in existing minerals (pseudosecondary and secondary). The fluid in inclusions is generally considered to have been trapped at or after the peak of metamorphism because most prograde P-T paths are such that the internal pressure of the inclusion would increase to the point that it would burst (decrepitate) along this path.

Concerted fluid inclusion work in high grade rocks was inspired by the discovery of a profound change in fluid inclusion composition from H_2O to CO_2 at the amphibolite to granulite facies transition in Norway (Touret 1971). Since granulite facies assemblages are characterized by a lower activity of H_2O than their amphibolite counterparts, the CO_2 in the inclusions may represent the H_2O-poor, peak metamorphic fluid (Touret 1985). This has lead to theories of granulite facies paragenesis development due to CO_2 streaming from some deeper source (Newton et al. 1980). However, the idea that CO_2-rich inclusions contain peak metamorphic fluids has been called into question by Lamb et al. (1987) on the grounds that carbonic inclusions have been found in granulite grade rocks for which mineral assemblage information indicates H_2O-rich peak metamorphic fluids.

In this chapter the results of fluid inclusion analysis across the blueschist to amphibolite and amphibolite to granulite facies transitions is examined in order to assess the composition of fluid trapped during the metamorphic cycle and the timing of entrapment.

Sample locations

Two suites of samples were analyzed for fluid inclusion composition and density. One suite consists of nine pelitic quartzofeldspathic schists from the isograds area to below the peridotite layer. The other suite consists of five quartz veins located in Nome group schists and Kigluaik group schists from the area near the isograds (figures 4.1 and 4.2). Fluid inclusions data is listed in appendix 4.

Pelite Leucosomes

62 fluid inclusions were analyzed from the pelite suite, chosen to represent the spectrum of metamorphic grades exposed. Most samples have the assemblage: Grt + Bt

+ Qtz + Pl + Graph + (Ms + Sta) or (Sil + Kfs) (table 4.1), with the exception of AB90-19, which has the assemblage: Grt + Bt + Qtz + Pl + Kfs + Opx. The inclusions measured occur within quartz, especially in quartz segregations. This inclusion population is dominated by low density CO_2. In the upper part of the stratigraphy (4th pelite) a small population of low-salinity H_2O inclusions occur.

CO_2-rich inclusions

Seven of the nine pelite samples contain CO_2-rich fluid inclusions. Size and abundance vary systematically with stratigraphic location. Inclusions are very abundant and large (5-20 μm diameters) low in the stratigraphic section (0th, 1st, 2nd and 3rd pelites). In the mixed unit and 4th pelite, CO_2 fluid inclusions are rare and not as large (3-10 μm diameters). At room temperature, the inclusions are usually two phase (L + V), dominated by the vapor phase. Rarely, the inclusions are only vapor phase. In one case, a thin meniscus of a second liquid phase was seen at a necked down corner of a carbonic inclusion, indicating that a small amount of H_2O may be present in these inclusions. Because of the dark walls of CO_2 inclusions, up to 20% H_2O may be present in the carbonic inclusions and not visible under the microscope (Roedder 1972). Some inclusions homogenize to liquid, most to vapor; in two samples, critical behavior was observed. The carbonic inclusions are pseudosecondary or secondary in nature. Usually the planes of inclusions do not cross grain boundaries. In samples with abundant carbonic inclusions there are multiple orientations of the planes of inclusions. In samples with rare carbonic inclusions there is generally only one orientation of their planar arrays, perpendicular to schistocity.

H_2O-rich inclusions

Five of the nine pelitic samples contain aqueous fluid inclusions. Aqueous inclusions in schists are smaller than carbonic inclusions (2-10 μm diameters). Aqueous

inclusions are two phase (L + V) with varying proportions of bubble size at room temperature. All inclusions homogenize to liquid. Aqueous inclusions are not present in the 0th, 1st, 2nd and 3rd pelite, and are moderately rare to rare in the mixed unit and 4th pelite. The aqueous inclusions are pseudosecondary to secondary in nature. No trails were observed to cross grain boundaries. These planar arrays are generally limited to one or two orientations. There are three samples in which both CO_2- and H_2O-rich fluid inclusions occur. In these samples, there are more planes of H_2O inclusions than CO_2 inclusions, and the H_2O inclusion planes have more inclusions/mm^2. Due to the rarity of both sets of inclusions, no clear textural or timing relationships were interpreted concerning the two compositions of inclusions.

Qtz vein traverse

35 fluid inclusions from the quartz vein suite were examined in order to assess any variation in fluid composition across the Nome group to Kigluaik group transition. Quartz veins which do not cross cut foliation were chosen in order to examine the earliest generations of fluid inclusions. Fluid inclusions in this suite are low salinity H_2O of varying density. Read and Meinert (1986) also investigated fluid inclusions in quartz veins similar to ones investigated here within Nome Group schists (their type I veins). Along with aqueous inclusions of similar characteristics to the ones reported here, they found mixed H_2O-CO_2 and carbonic inclusions. The CO_2 within these inclusions had characteristics similar to the carbonic inclusions from the 4th pelite discussed in this chapter, namely a depressed melting point (-58.5 to -62.2°C) and homogenization temperatures generally in the teens.

H_2O-rich inclusions

All five of the Qtz vein samples investigated contained H_2O fluid inclusions. CO_2-bearing fluid inclusions were not found in any sample. The Qtz vein aqueous

inclusions are larger (3-15 μm diameters) than their pelite counterparts. All are two phase (L + V) with varying proportions of V to L. The inclusions are very abundant. There are multiple orientations of planar arrays of inclusions in each sample. The inclusions are secondary in nature; inclusions trails cross grain boundaries.

Fluid Inclusion thermobarochemistry

Carbonic inclusions

T_m (temperature at which the solid melts) of CO_2 is slightly depressed below the pure melting temperature of -56.6°C (figure 4.3). The positive correlation between T_m and T_h (temperature at which the inclusion homogenizes to either vapor or liquid) in carbonic inclusions (figure 4.4) indicates that the lowering of T_m is caused by dilution of CO_2 with a small amount of fluid other than H_2O (Thomas et al. 1990), commonly CH_4 or N_2 (Swanenberg 1980, Kreulen and Schuiling 1982, Rudnick et al. 1984, Schreurs 1984, Althaus and Istrate 1990, Samson and Williams-Jones 1991, Winslow et al. 1991). This small amount of lowering (down to -59°C) could be caused by ~20% CH_4 or N_2 (Burruss 1981, Hall and Bodnar 1990, Kerkhof 1990).

T_h for carbonic inclusions that homogenize to liquid ranges from 31 to 12°C with most inclusions above 25°C (figure 4.5), indicating a density of around 0.55 g/cm^3. However, the vast majority of inclusions homogenize to vapor, indicating a density less than 0.47 g/cm^3, similar to low density carbonic inclusions described in forsterite from lower crustal xenoliths by Roedder (1965). In addition, since the inclusions with the lowest homogenization temperature also indicate the highest level of dilution with extra component (figure 4.4), the actual density of inclusions with T_m<-56.6 is less than that calculated if pure CO_2 is assumed (Touret 1981, Touret and Kerkhof 1986). For example, a pure CO_2 inclusion with T_h(liq)=15°C has a density of 0.82 g/cm^3 (Angus et al. 1976), whereas an inclusion that is 80% CO_2 and 20% CH_4

with a $T_h(liq)=15°C$ has a density of 0.45 g/cm^3 (Burruss 1981, Holloway 1981). Therefore, I conclude that carbonic fluid inclusions in pelite leucosomes have a density near that of the critical point, 0.47 g/cm^3. There is a systematic trend toward more pure CO_2 deeper in the stratigraphic section.

21% N_2 was found in one Kigluaik inclusion by laser Raman spectroscopy (Touret written communication 1989), the remainder being 71% CO_2 and 2.4% CH_4. The other inclusions analyzed were 100% CO_2.

Pelite aqueous inclusions

The final melting temperature of this small population of aqueous fluid inclusions is only lowered to about -0.5°C (figure 4.6). This indicates a salinity of about 0.9 wt% NaCl equivalent (Potter and Brown 1977). T_h ranges from ~175° to 250°C with most around 175°C, and all homogenize to liquid (figure 4.7). This corresponds to a density of ~0.90 g/cm^3. Two additional groups of aqueous inclusions were measured in 4th pelite leucosomes (figure 4.8). One has T_m and T_h of -4 and 175°C, found in a pelite from the mixed unit, another has temperatures of -8° and 350°C, found in a 4th pelite from the 2nd Sil isograd ("normal" pelite aqueous inclusions also occur in this sample). These data indicate salinities of 6.4 and 11.7 wt% NaCl equivalent, and corresponding densities of 0.94 and 0.77 g/cm^3, respectively.

Qtz vein aqueous inclusions

These inclusions overlap in composition and density with those of the pelite leucosomes, but have a greater degree of variability in density (figures 4.6, 4.7 and 4.8). T_m in Kigluaik group 4th pelite Qtz veins ranges from -0.2 to -2.2°C (figure 4.6), corresponding to salinities less than 3.7 wt% NaCl equivalent. These fluid inclusions have a range of T_h from ~200° to 325°C, most at about 280°C (figure 4.7), corresponding to a density of 0.78 g/cm^3. Aqueous inclusions in Nome group Qtz

veins cluster more tightly at $T_m = -1.9$ and $T_h = 225°C$ (figure 4.8). This corresponds to a salinity of 3.2 wt% NaCl equivalent and a density of 0.86 g/cm^3. These findings are in agreement with measurements on aqueous fluid inclusions in quartz veins from Nome Group schists investigated by Read and Meinert (1986).

The similarity in composition and density of aqueous inclusions between pelite matrix, pelite quartz vein and Nome Group quartz vein leads to the interpretation that all these inclusions are cogenerational.

Discussion

Calculation of isochores (Nicholls and Crawford 1985) for the carbonic and aqueous inclusions (figure 4.9) leads to some straight-forward conclusions. Isochores for aqueous inclusions from the Sta and Sil+Kfs isograds pass through the estimated P-T conditions of peak metamorphism of their enclosing rocks and may therefore represent peak metamorphic fluids. Isochores for Nome group aqueous inclusions and those for Kigluaik group carbonic inclusions fall well below their respective estimated peak P-T conditions and therefore cannot represent unmodified peak metamorphic fluids. Petrogenetic grid constraints indicate that the P-T path followed by Kigluaik group rocks is clockwise in nature (Ky to Sil, Bt + Sil to Crd, Rt to Ilm, Grt to Opx + Pl). Such a path crosses all the isochores determined in this study, allowing the interpretation that the fluid in inclusions is late and has not been modified since trapping. It is also possible that fluids were trapped at the peak of metamorphism and have since been modified. Modifications could include change in inclusion volume, diffusion of fluid species in/out of or leakage of material out of the inclusion (Roedder 1984). These possibilities are explored in the following sections.

Changes in shape and composition

Changes in volume which would decrease the density of trapped peak fluids include precipitation of daughter minerals, partial decrepitation, and stretching of the inclusions. Since daughter minerals are denser than the fluid from which they precipitate, the remaining fluid must become less dense; however, no daughter minerals were observed. Partial decrepitation of fluid inclusions has been identified in other granulite grade rocks by the distinctive texture of a large central inclusion with a planar cluster of smaller inclusions around it (Touret 1977, Swanenberg 1980). None of these "decrepitation clusters" or "exploded inclusions" were identified in Kigluaik carbonic inclusions. However, this does not preclude the possibility that such features have since annealed into more regular-looking arrays of inclusions. Given a retrograde path of mostly isothermal decompression, fluids trapped at peak conditions would be expected to decrepitate upon a pressure differential of one or two kbar, for the size of inclusions measured in this study (Roedder 1981, Bodnar et al. 1989). This size dependence of decrepitation potential would be manifested in a systematic variation in density with inclusions size, smaller inclusions being more dense. No such systematic variation was observed in Kigluaik carbonic inclusions. Hence, most inclusions have not decrepitated. Stretching via plastic deformation in a host mineral is viable in softer minerals such as halite and fluorite (Roedder 1981, Bodnar and Bethke 1984), and has recently been experimentally established in quartz (Sterner and Bodnar 1989) at temperatures of 600° to 700°C on the time scale of days to weeks. Therefore it must be concluded that Kigluaik carbonic inclusions *could* have undergone a change in volume due to stretching after trapping.

The two most likely candidates for diffusion or leakage out of inclusions are H_2 and H_2O. Diffusion of H_2 into fluid inclusions has experimentally been shown to occur

(Hall et al. 1989, Morgan et al. 1991). Addition of H_2 to CO_2-bearing fluid inclusions would drive the reaction: $CO_2 + 4H_2 = CH_4 + 2H_2O$. Hydrogen is a minor component in most metamorphic fluids, and especially in CO_2 dominated fluids (French 1966, Ohmoto and Kerrick 1977, Frost 1979, Rice and Ferry 1982). However, variation in the fugacities of fluid species along fO_2 buffers on the retrograde path in the matrix pore fluid *can* lead to significant overpressures of fH_2 in the matrix with respect to the inclusion depending on the specific external conditions (Hall and Bodnar 1990). For a retrograde path that is convex to the temperature axis (clockwise), as is the path for Kigluaik rocks, the overpressure in fH_2 calculated by Hall and Bodnar is 30 bars or less for fO_2 conditions one log unit below FMQ, and only a few bars for more oxidizing conditions (one log unit above FMQ). Such a fugacity gradient in H_2 would have promoted diffusive addition of H_2 to Kigluaik inclusion, but the quantity of mass influx at these very low gradients is probably quite small, suggesting that H_2 did not enter the inclusions. Pasteris and Wanamaker (1988) showed experimentally that matrix oxygen fugacity communicated with pure CO_2 inclusions in forsterite by movement of crystal defects, not molecular O_2. The fugacity gradients experimentally imposed were quite large (4-5 log units) and therefore compositional change to Seward Peninsula inclusions due to fO_2 communication with the matrix is unlikely.

Experimental evidence shows that the density of H_2O inclusions can change in response to a pressures gradient between inclusion and confining pressure (Pecher and Boullier 1984, Sterner and Bodnar 1989, Sterner et al. 1988) and may be attributable to diffusive movement of H_2O through the confining quartz. Sterner and Bodnar (1989) concluded that at 600°C diffusion of H_2O through quartz did not occur or was below the detection limits of ~0.5 wt% H_2O loss. However, Sterner et al. (1988) indicate that at higher temperatures (~825°C), H_2O diffusion through quartz may be a viable

mechanism. Hollister (1988, 1989) proposed that H_2O from a *homogeneous* H_2O-CO_2 mixture can preferentially leave the inclusion and diffuse away, leaving CO_2 behind, aided by plastic deformation in the quartz. This process is controversial and has not been experimentally verified.

Figure 4.10 illustrates the magnitude of diffusive loss of H_2O and volume change necessary to convert fluid trapped at 8 kbar and 800°C to pure CO_2 with a density of 0.45 g/cm^3. Ideal mixing of H_2O and CO_2 is assumed, with densities of 0.825 and 1.15 g/cm^3, respectively. The density after diffusive loss of H_2O depends on the amount of H_2O originally in the inclusion. In the Kigluaiks, peak metamorphic XCO_2 is probably in the range 0.5 to 0.8 (Lieberman 1988, this dissertation chapter 3), leading to CO_2 densities of 0.7 to 1.0 g/cm^3 after H_2O loss. The increase in size of the inclusion due to stretching necessary to bring the density to 0.45 g/cm^3 is a 20 to 30% increase in radius, assuming spherical geometry. If the peak fluid was 80% CO_2 and the fluid inclusions hide the 20% H_2O so no diffusive loss of H_2O is needed, then a 37% increase in radius is necessary to bring about the change in density to 0.45 g/cm^3. These calculations indicate that a combination of H_2O loss and stretching could turn mixed volatile inclusions into pure CO_2 with the appropriate density, and that stretching is always necessary to accomplish this.

Timing of inclusion entrapment

Although stretching of fluid inclusions in quartz may occur at temperatures over 800°C, there is no experimental evidence that stretching occurs at temperatures reached in the isograd area (550° to 700°C). If stretching is called upon to explain the low densities of the high-grade carbonic inclusions, then the carbonic inclusions in the isograds should not have stretched, and should display higher densities. This is not the case. If it is argued that on geologic time scales, stretching could occur at the lower

temperatures of the isograds, then H_2O inclusions should have stretched also. However, many aqueous inclusions have higher densities, compatible with peak isograd conditions. The data is reconcilable if the isograd aqueous inclusions were trapped earlier and have not all undergone a substantial amount of stretching, and the carbonic inclusions were simply trapped later at very low pressures. Since peak fluid compositions in the isograds were water-rich (Lieberman 1988) these aqueous inclusions could contain peak Kigluaik isograd fluids.

The array of isochores is interpreted to represent trapping along a clockwise P-T retrograde path. Aqueous inclusions were trapped in rocks of the isograd area near the peak of metamorphism. Additional aqueous fluids were trapped there during decompression, or some peak inclusions were modified (stretched?) along this path. Carbonic inclusions were trapped very late along this retrograde path and do not represent trapped peak metamorphic granulite facies fluids. Carbonic fluid inclusions in the Adirondack granulites are also thought to have been trapped after the peak of metamorphism (Lamb et al. 1987, Morrison and Valley 1988).

Source of aqueous fluids

The ranges of aqueous fluid inclusion salinities and densities overlap among Kigluaik pelites, Kigluaik quartz veins, and Nome group quartz veins. This allows the interpretation that they all have the same source, indicating that the inclusions are late at least with respect to metamorphism in the Nome group. The source of aqueous fluids could be connate, magmatic or metamorphic. Connate waters from continental shelf sediments would likely be more saline than these fluid inclusions (Roedder 1984). Igneous fluids likewise have high salinities (Roedder 1984). Metamorphic fluids have the appropriate low salinity. Substantial dehydration has occurred in Kigluaik group pelites; dehydration-derived fluids would have driven off connate fluids. Therefore I

conclude that aqueous fluid inclusions in the isograd area are metamorphic in origin, rising from local dehydrating sediments.

Source of carbonic fluids

The source of carbonic fluids is more problematic. There are three possible sources of N_2 in fluid inclusions: atmospheric N_2, ammonia released from silicate minerals during dehydration reactions such as: $2(NH_4)Al_3Si_3O_{10}(OH)_2 + \frac{3}{2} O_2 = N_2 + 6H_2O + 3Al_2SiO_5 + 3SiO_2$ (O_2 is supplied by the buffer capacity of the rock, such as $2Fe_2O_3 = 4FeO + O_2$, where iron oxides are components in biotite or iron oxides), and nitrogen compounds released from organic matter during maturation to graphite (Samson and Williams-Jones 1991). None of these sources are completely satisfactory to explain late CO_2-N_2. The possibility that any atmospheric gas could survive an entire granulite grade metamorphic cycle is remote. Ammonia from dehydration and nitrogen from organic maturation are given off during prograde metamorphism, not during the waning stages of uplift. The dehydration scenario is especially difficult to justify because it requires that N_2 is trapped, but not the H_2O given off by the same reaction.

Conclusions

Two generations of fluid inclusions have been identified in Kigluaik Group and Nome Group lithologies. The earlier generation consists of low salinity aqueous inclusions with a density of ~0.9 g/cm^3. These were trapped at and following the time of peak metamorphism in the isograd area of the Kigluaiks. The other generation of fluid inclusions consists of nearly pure CO_2 with low densities (around the critical density of 0.47 g/cm^3). These carbonic inclusions were trapped late in the metamorphic cycle, as was concluded for Adirondack carbonic inclusions (Lamb 1987, Morrison and Valley 1988, Lamb et al. 1991). This contrasts with other granulite grade terranes where (higher density) carbonic inclusions are taken to represent samples of peak fluids

(Newton et al. 1980, Hansen et al. 1984, Touret 1985, Santosh et al. 1991). In the granulite grade rocks of the Kigluaik mountains, no peak metamorphic fluids survived as fluid inclusions.

Table 4.1   Fluid inclusion host rock assemblages.   Arranged stratigraphically

Sample#	Unit	Isograd	Grt	Bt	Qtz	Pl	Kfs	Ms	Sta	Sil	Gr	Op
Pelites												
AB87-218	IV	Sta		X	X			X	X		X	X
AB87-220	IV	Sta	X	X	X			X	X		X	i
AB87-290	IV	Sta	X	X	X	X		X	X			X
AB87-254.2	IV	Sil+Kfs	X	X	X	X	?			X	X	
AB85-208.1	IV	Sil+Kfs	X	X	X	X	X			X	X	
AB89-33.2	mixed	Sil+Kfs	X	X	X	X	?			X		i
AB89-1.1	III	Sil+Kfs	X	X	X	X	X			X	X	
OS-18	I	Sil+Kfs	X	X	X	X	X			X	X	X
AB90-19.1	0	Opx	X	X	X	X	X					

Quartz veins		
AB87-201	Nome	qtz vein lineated subparallel to foliation
AB87-208	Nome	strong pencil structure qtz rods
AB87-212	IV	veined and brechiated qtzite
AB87-217	IV	large quartz pod (1 X 2 m)
AB87-257	IV	qtz vein

Figure 4.1   Fluid inclusion sample location map.   See figure 1.2 for explanation of map patterns.
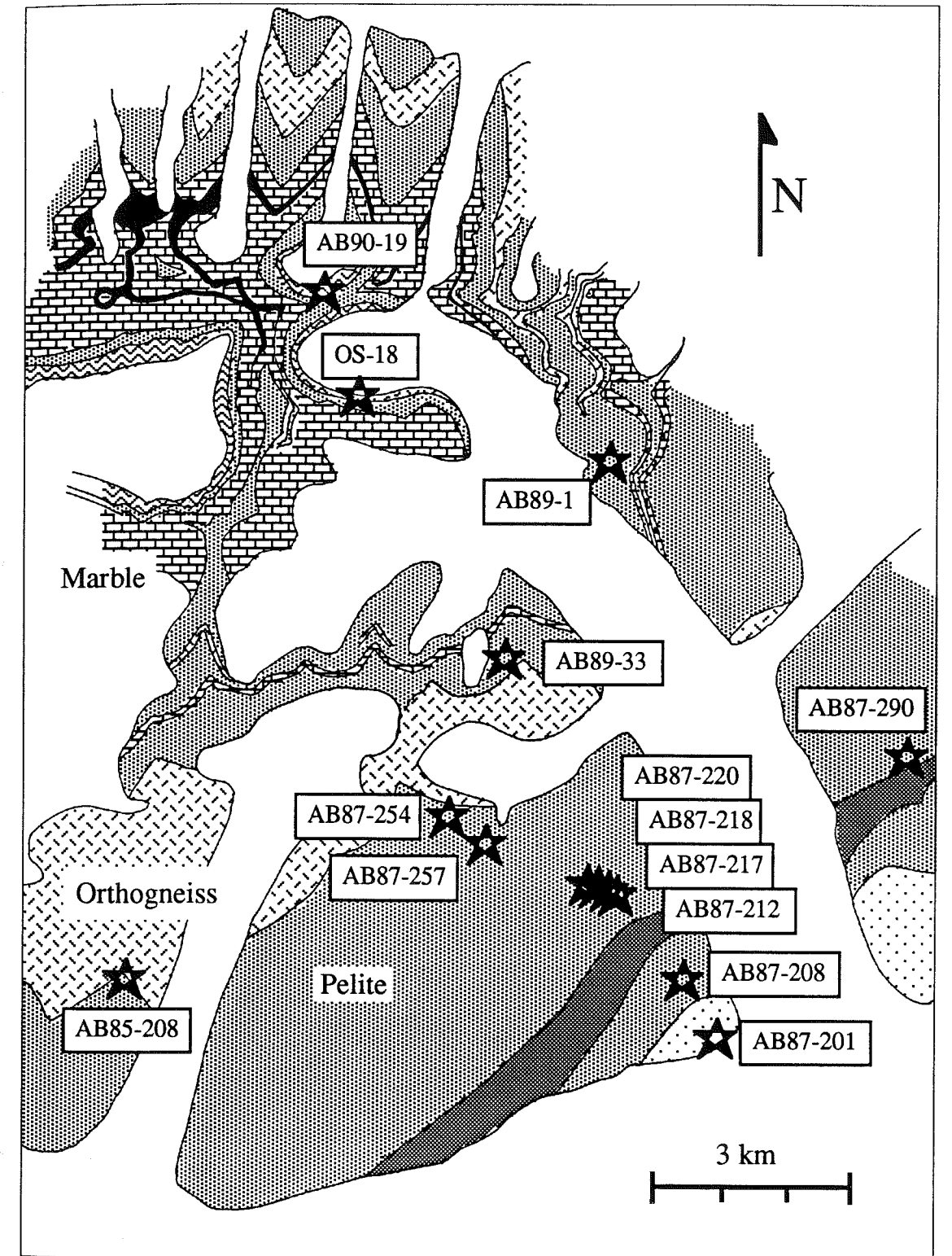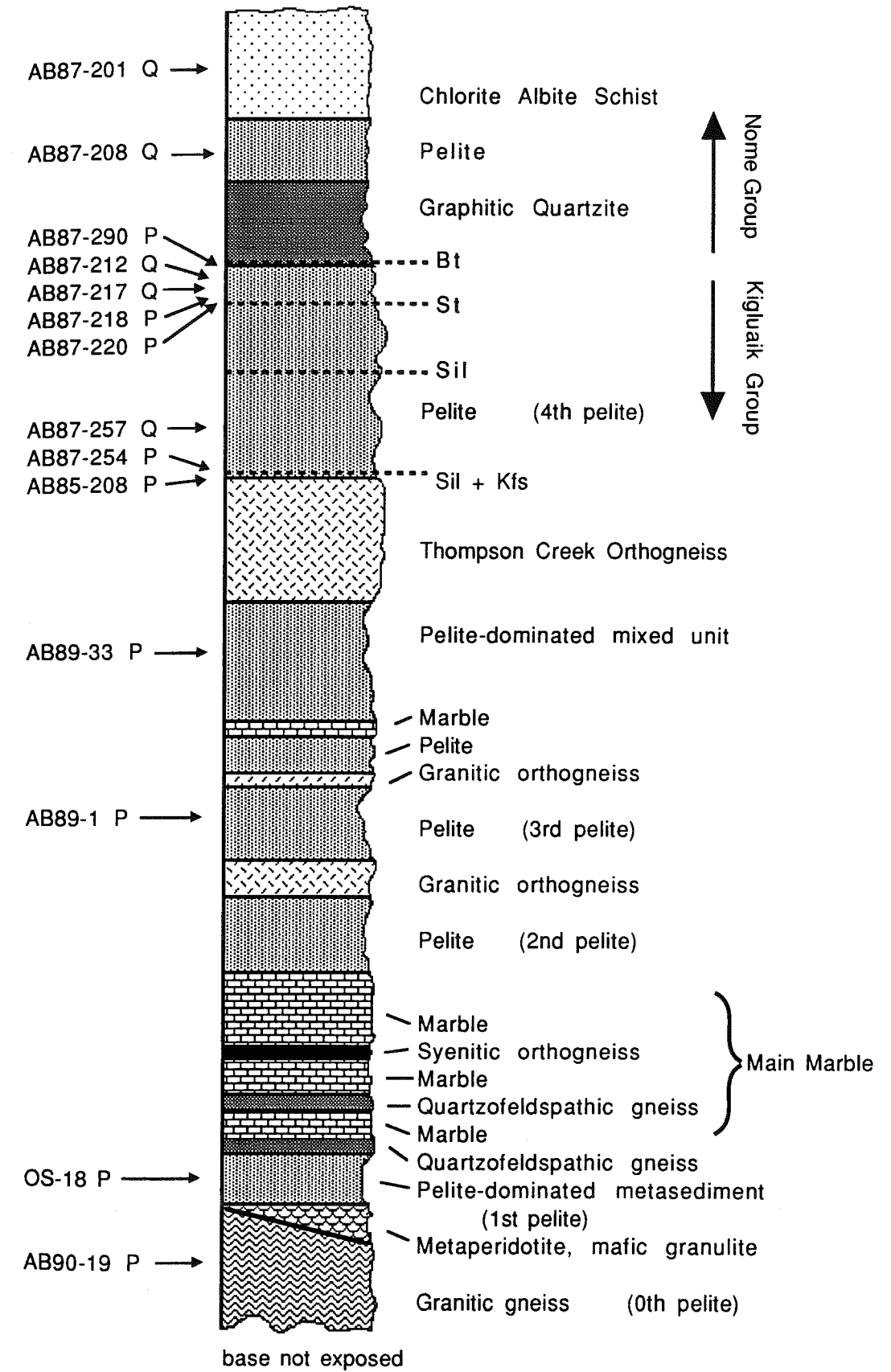
Figure 4.2   Stratigraphic location of fluid inclusion samples.   Q = quartz
vein sample; P = pelite sample. Vertical scale as in figure 1.4.
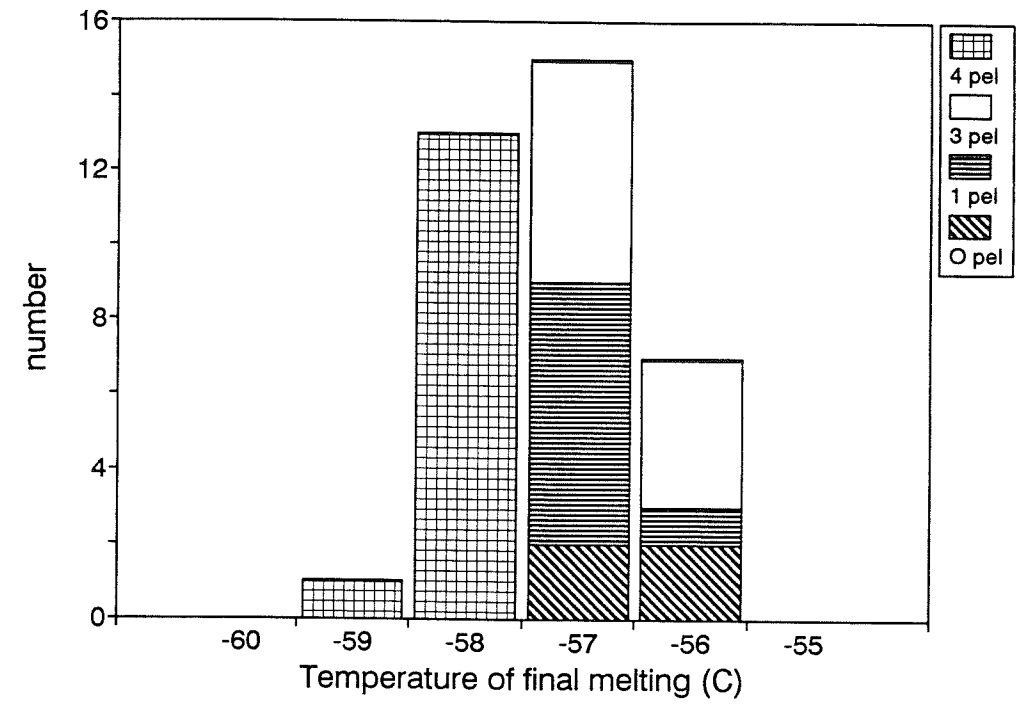
Figure 4.3 T_m carbonic inclusion histogram.
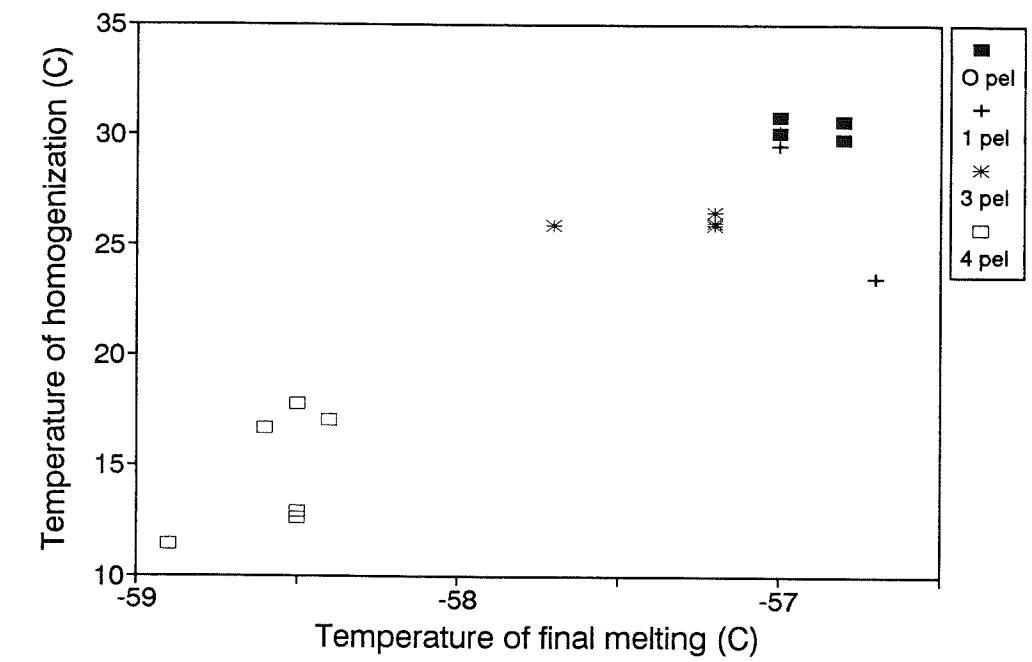
Figure 4.4 T_m vs. T_h for carbonic inclusions.   The positive correlation indicates dilution with up to 20% CH_4 or N_2.
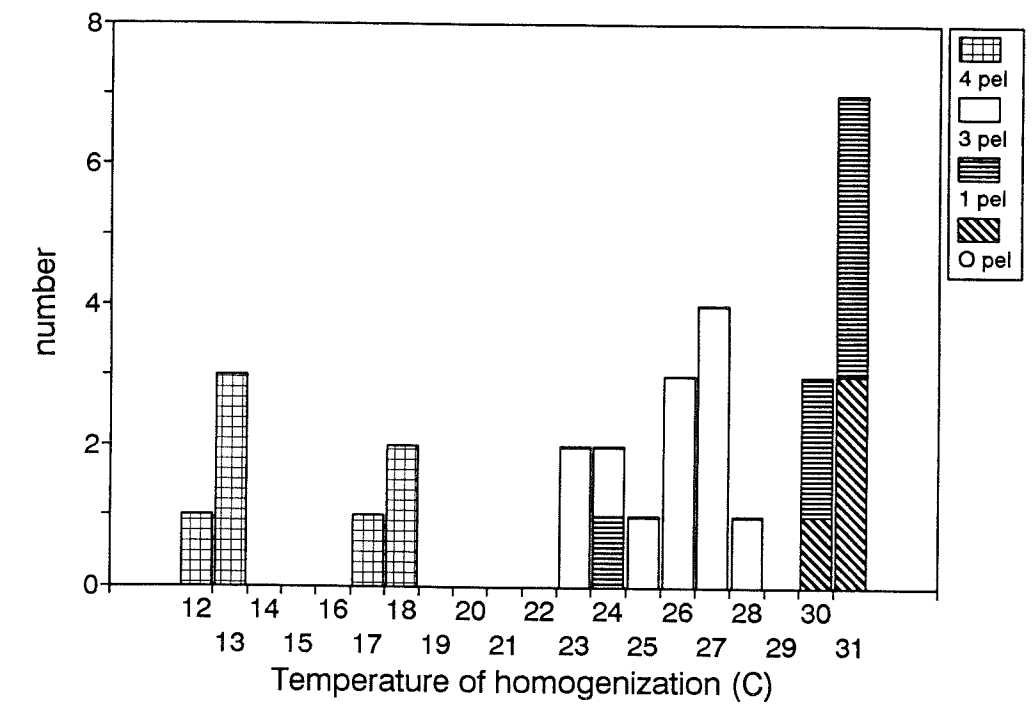
Figure 4.5   T$_h$ carbonic inclusion histogram.
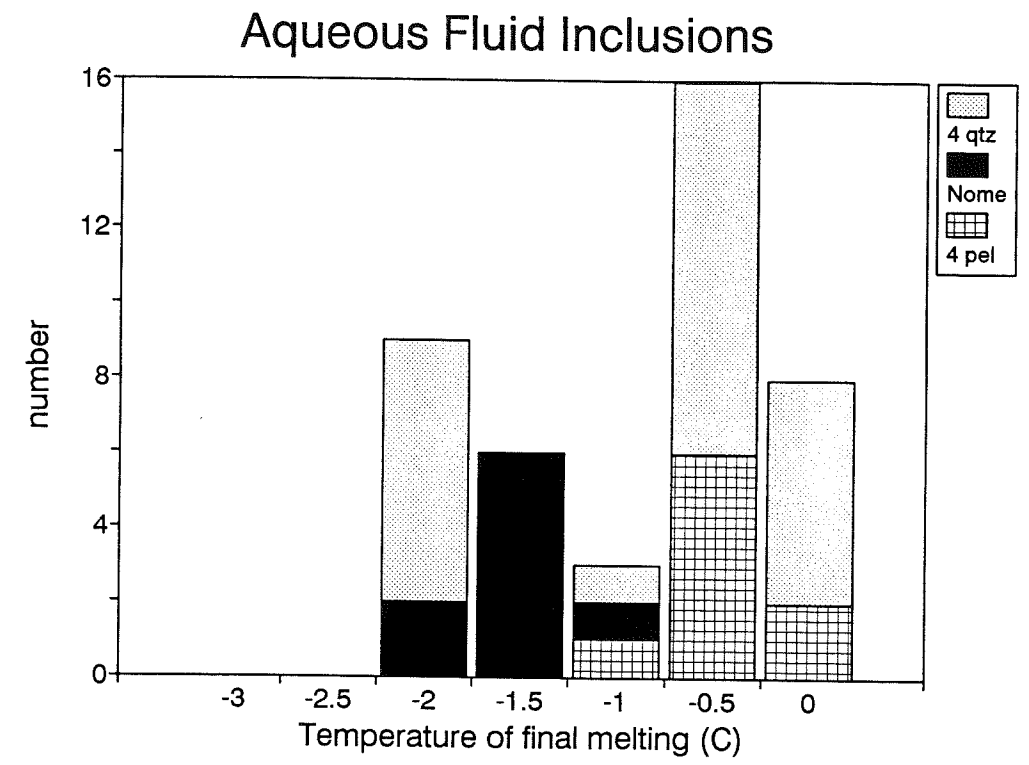
Figure 4.6 T_m aqueous inclusion histogram.

Aqueous Fluid Inclusions
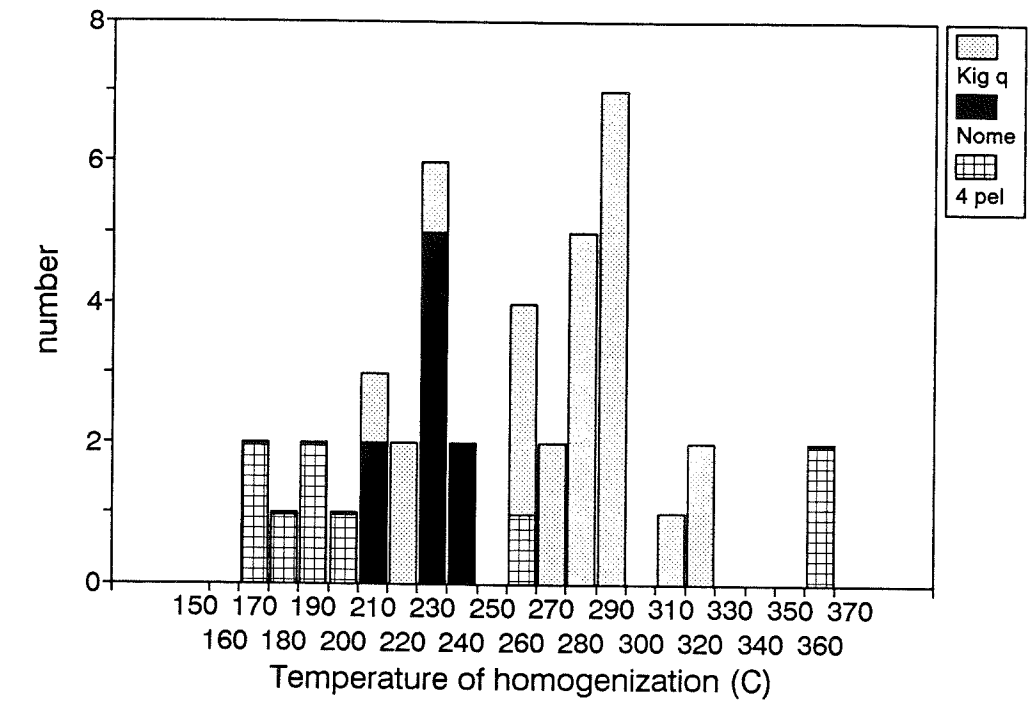
Figure 4.7 T_h aqueous inclusion histogram.
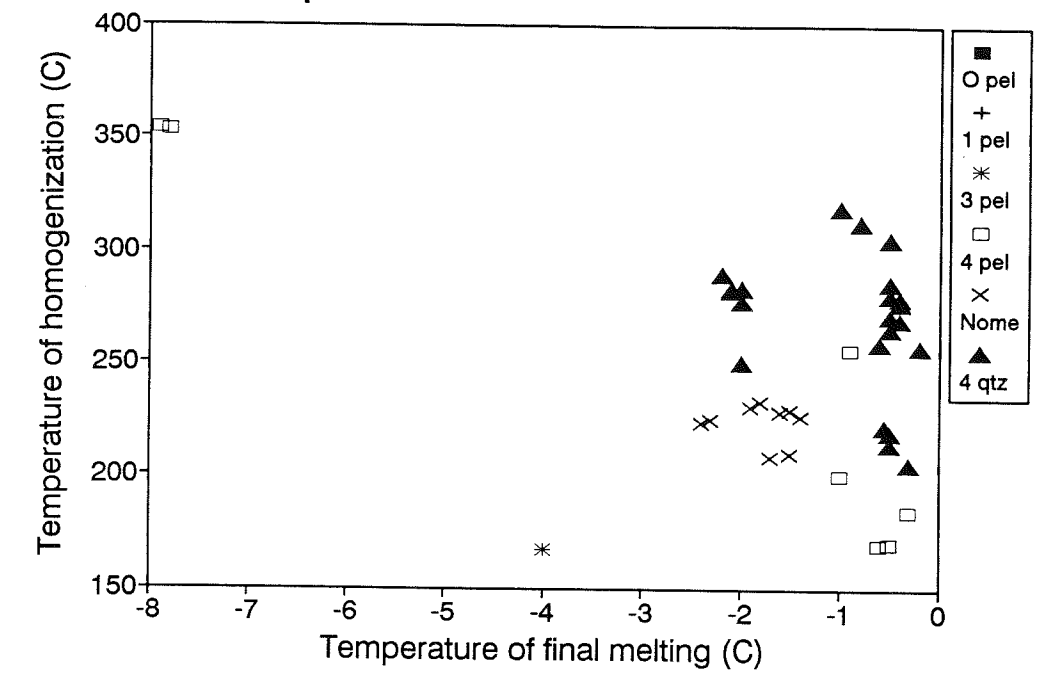
Figure 4.8 T_m vs. T_h for aqueous inclusions.   The high degree of overlap in T_m and T_h of quartz vein and pelite samples suggest that the fluids are cogenerational.
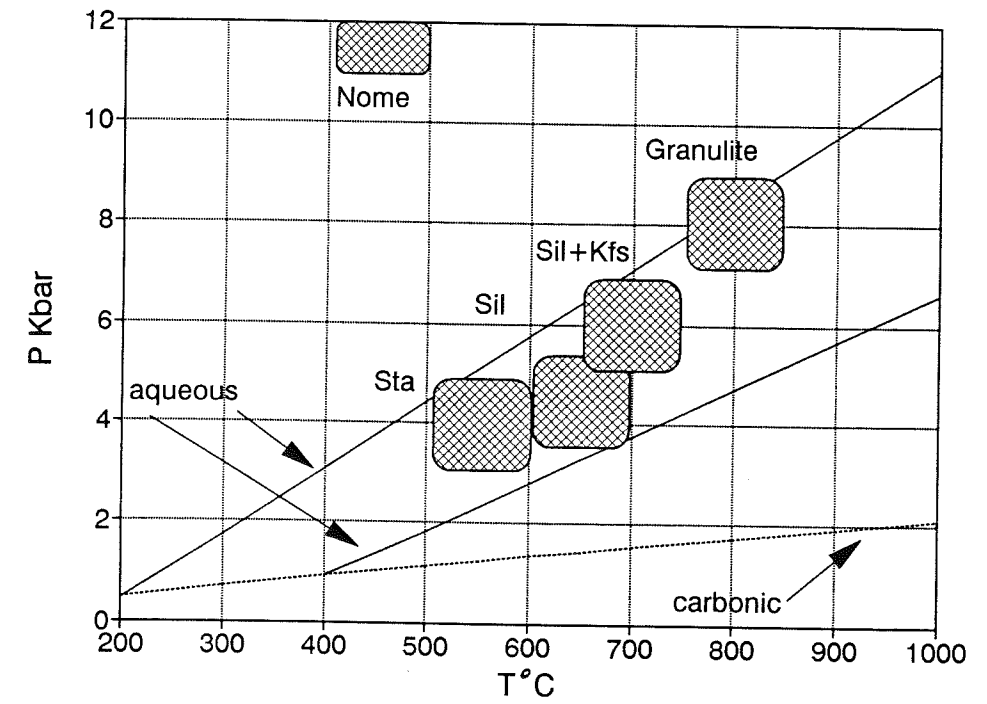
Figure 4.9   P-T diagram showing isochores for fluid inclusions.   The solid lines span the range in aqueous densities measured from 0.9 g/cm^3 (upper) to 0.7 g/cm3 (lower). The dashed line shows the isochore for carbonic fluids of 0.45 g/cm^3 density. The hatchured boxes represent peak metamorphic conditions attained (Lieberman 1988, Patrick and Evans 1989). See chapter 1 for explanation of isograd zones.
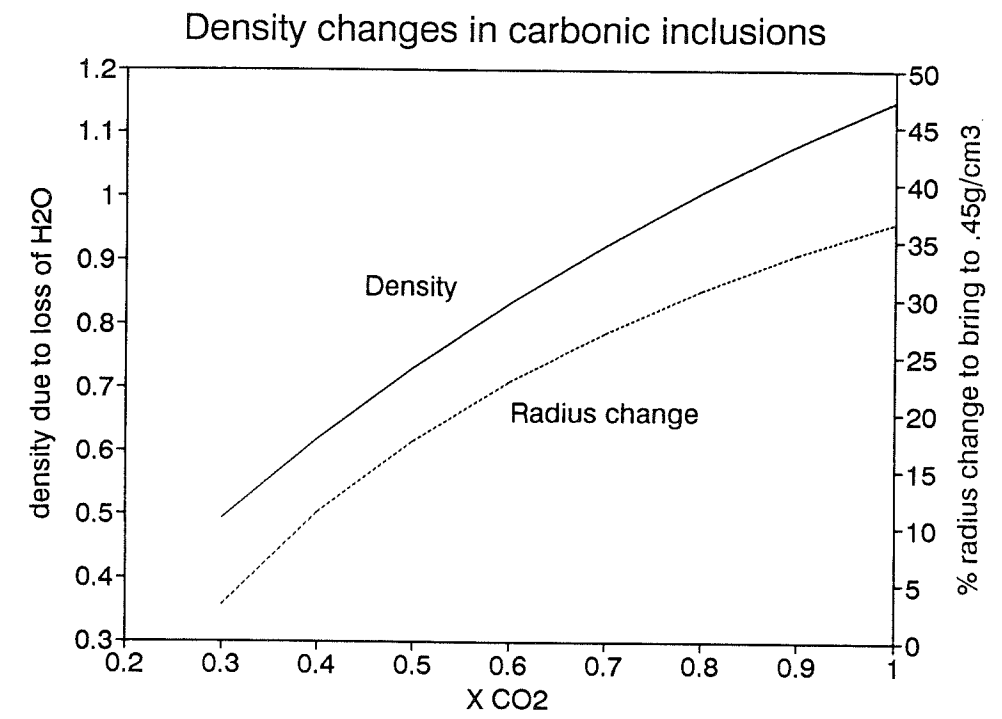
Figure 4.10   Fluid inclusion density change due to change in shape or composition.
See text for details.

Chapter 5: Summary and Conclusions

Stable isotope profiles across lithological boundaries only provide information on the component of transport parallel to the profile. In the main marble unit of the Kigluaik Mountains (transitional amphibolite-granulite facies), steep oxygen and carbon isotope profiles attest to extremely small amount to no time integrated fluid flux across lithological boundaries (see also Baker 1990, Cartwright and Valley 1991 1992). Pervasive upward fluid flow is ruled out. Both marble and gneissic units retain oxygen isotope signatures characteristic of their protolith, indicating that an external fluid did not homogenize rock compositions. The small amount of fluid that did advect across lithologic boundaries is inferred to have been CO_2-rich and derived from marble, moving downwards in two cases out of three. The H_2O evolved during prograde metamorphism of the underlying pelite-bearing layer left no measurable isotopic imprint on the main marble above. This H_2O, and the H_2O released from crystallizing partial melt in the pelites, presumably departed along mainly horizontal channels external to the main marble. The main marble was an effective aquitard. Cross-cutting veins in marble, composed of monomineralic diopside, are extremely rare. Only during the waning stages of metamorphism did the injection of pegmatite dikes permit fluids, in this case H_2O-rich, to penetrate the main marble and, at pegmatite-marble contacts, precipitate garnet, clinopyroxene, epidote, wollastonite, and fluorite. In addition, small amounts of late, channelized H_2O-rich fluid locally converted forsterite to serpentine and diopside to tremolite.

The isotopic profiles are interpreted to be dominated by diffusive processes. The extent of isotopic interaction is related more to lithological type (compare marble at AB89-41 with that at AB89-61) than to stratigraphic horizon (compare AB89-62 + AB90-27 at the base of the main marble with AB89-61 in the interior). Outcrop AB89-

41 involves a relatively pure dolomitic marble whereas marble at AB89-61 has a varied composition with a much higher proportion of silicate phases (table 2.2). AB89-61 would have undergone much more devolatilization during prograde metamorphism than AB89-41. Devolatilization reactions enhance porosity, leading to more extensive interaction with fluid (Rumble and Spear 1983). Other workers have found thick pure carbonate marbles to be very effective barriers to infiltrating fluid (Gerdes et al. 1991; Frueh-Green et al. 1991). The estimate of porosity for AB89-61 based on a 1 Ma time-scale is nevertheless very low and it is questionable that transport of material could have occurred under these circumstances. If fluid was present only during transient devolatilization events (Thompson 1983, Hoernes and Hoffer 1985) in the marble, the corresponding time scale would be much less than 1Ma and calculated porosity increased to levels more appropriate for fluid interconnectivity regardless of solid-fluid dihedral angle (Brenan 1991). Ductile thinning of this section (factor of two?) may have occurred (Miller et al. 1992a), but this amount of thinning would not significantly effect the conclusions presented here.

The estimates of time integrated fluid flux calculated here (0 and 0.01 m^3/m^2) are four to six orders of magnitude less than those calculated for metasedimentary rocks in low to medium grade regional metamorphic terranes (Ferry and Dipple 1991). The method used by Ferry and Dipple is based on reaction progress, whereas the calculations presented here are based on advective-diffusive displacements of stable isotope discontinuities (Bickle and McKenzie 1987). Many stable isotope studies are consistent with estimates of fluid advection monitored by reaction progress (Ferry 1986). The difference in estimated flux may be reconcilable in that the present calculations are for cross-lithology transport and those of Ferry and Dipple represent layer-parallel flux. A difference in crustal level could affect the extent of fluid movement

possible (Baker 1990), but since the *time integrated* fluid flux is small, practically no fluid advected across the main marble units at *any time* during metamorphism. The present flux parameters are one to two orders of magnitude smaller than those calculated by Bickle and Baker (1990a) for outcrops in an amphibolite grade terrane in the Cyclades of Greece using the same methods of calculation.

Granulite facies metamorphic parageneses are usually characterized by a reduced activity of H_2O (e.g. Newton 1986), and this field location is no exception (Lieberman 1988 and figure 2.10 here). The present results render unlikely the possibility that this was caused by an influx of pervasive externally derived H_2O-poor fluid, such as CO_2 streaming from the mantle (Janardhan et al. 1982) or from mantle-derived mafic magma (Frost and Frost 1987). The main marble extends across the entire mountain range (figure 1.3) and formed an impermeable barrier to upward pervasive flow of fluid, CO_2 or otherwise, during metamorphism. Passage of H_2O-undersaturated synmetamorphic plutons (Frost and Frost 1987) can be ruled out because the layering in the Kigluaik Mountains has only been disrupted by *late* plutons and pegmatites. Because orthogneiss units comprise only a small part of the lithologic sequence, heating of previously dry rocks (e.g. Valley and O'Neil 1984) can also be ruled out. There are two internal methods left of altering pore fluid composition: (1) extract H_2O by partial melting (e.g. Crawford and Hollister 1986) and (2) add CO_2 by local decarbonation of graphite or carbonate minerals (Glassley et al. 1989). Both may occur. In the vicinity of marble contacts, it was argued in chapter 3 that (2) operated on a decimeter scale. Fluid movement played a limited role in controlling mineral parageneses in the Kigluaiks.

The retrograde path followed by rocks in the Kigluaik Mountains was dominated by decompression. This is supported by mineral replacements, petrogenetic grid

considerations and fluid inclusion microthermometry. In the lower part of the stratigraphy, no peak metamorphic fluids were trapped. In the isograd area, however, aqueous inclusions may represent fluids trapped at the peak of metamorphism. Rocks at all levels of the Kigluaik Group contain low density CO_2-rich inclusions trapped late along the retrograde path. This is in contrast to other terranes, where carbonic inclusions have been used in support of theories of CO_2 from mantle sources (Newton et al. 1980, Touret 1985).

In view of the above, I conclude that heat was transported into the section by conduction alone. Most likely, the source of heat was syn-metamorphic intrusions below the present level of exposure, or perhaps exposed to the west of this field area (Amato et al. 1992). The data presented here demonstrate the large effect that can be played by lithologic layering during metamorphism. Differing lithologies can control fluid movement deep in the crust just as they do in the near-surface environment.

References

Althaus E, Istrate G (1990) Granulite facies conditions derived from fluid inclusions: Sila massif, Calabria, Italy. N Jb Miner Mh 5: 65-75.

Amato JM, Wright JE, Gans PB (1992) The nature and age of Cretaceous magmatism and metamorphism on the Seward Peninsula, Alaska. GSA Abstr 24: 2.

Anderson TF (1969) Self-diffusion of carbon and oxygen in calcite by isotope exchange with carbon dioxide. J Geophys Res 74: 3918-3932.

Anderson TF (1972) Self-diffusion of carbon and oxygen in dolomite. J Geophys Res 77: 857-861.

Angus S, Armstrong B, deReuck KM (1976) International thermodynamic tables of the fluid state, carbon dioxide. Pergamon Press, pp 1-67.

Armstrong RL, Harakal JE, Forbes RB, Evans BW, Thurston SP (1986) Rb-Sr and K-Ar study of metamorphic rocks of the Seward Peninsula and Southern Brooks Range, Alaska. Geol Soc Amer Mem 164: 185-203.

Baker AJ (1990) Stable isotopic evidence for fluid-rock interactions in the Ivrea Zone, Italy. J Petrol 31: 243-260.

Barnes DF, Hudson T (1977) Bouger gravity map of the Seward Peninsula, Alaska: U.S. Geol Survey Open-file map 77-796C.

Baumgartner LP, Rumble D III (1988) Transport of stable isotopes: I: Development of a kinetic continuum theory for stable isotope transport. Contrib Mineral Petrol 98: 417-430.

Bence AE, Albee AL (1968) Empirical correction factors for the electron microanalysis of silicates and oxides. J Geol 76: 382-403.

Berman RG (1988) Internally-consistent thermodynamic data for minerals in the system $Na_2O-K_2O-CaO-MgO-FeO-Fe_2O_3-Al_2O_3-SiO_2-TiO_2-H_2O-CO_2$. J Petrol 29: 445-522.

Berman RG (1990) Mixing properties of Ca-Mg-Fe-Mn garnets. Am Mineral 75: 328-344.

Berman RG, Brown TH, Perkins EH (1987) GE0-CALC: software for calculation and display of pressure-temperature-composition phase diagrams. Am Mineral 72: 861-862.

Bickle MJ, Baker J (1990a) Advective-diffusive transport of isotopic fronts: an example from Naxos, Greece. Earth Planet Sci Lett 97: 78-93.

Bickle MJ, Baker J (1990b) Migration of reaction and isotopic fronts in infiltration zones: assessments of fluid flux in metamorphic terrains. Earth Planet Sci Lett 98: 1-13.

Bickle MJ, McKenzie D (1987) The transport of heat and matter by fluids during metamorphism. Contrib Mineral Petrol 95: 384-392.

Blattner P, Lassey KR (1989) Stable-isotope exchange fronts, Damkohler numbers, and fluid to rock ratios. Chem Geol 78: 381-392.

Bodnar RJ, Bethke PM (1984) Systematics of stretching of fluid inclusions I: Fluorite and sphalerite at 1 atmosphere confining pressure. Econ Geology 79: 141-161.

Bodnar RJ, Binns PR, Hall KL (1989) Synthetic fluid inclusions. VI. Quantitative assessment of the decrepitation characteristics of fluid inclusions in quartz at one atmosphere confining pressure. J Metam Geology 7: 229-242.

Box SE (1985) Early Cretaceous orogenic belt in northwestern Alaska: internal organization, lateral extent, and tectonic interpretation. In: DG Howell (ed) Tectonostratigraphic terranes of the Circumpacific region, Circumpacific council for energy and mineral resources, Earth Science Series. 1: 137-146.

Bradshaw JY (1989) Early Cretaceous vein-related garnet granulite in Fiordland, Southwest New Zealand: a case for infiltration of mantle-derived, CO_2-rich fluids. J Geol 97: 697-717.

Brady JB (1988) The role of volatiles in the thermal history of metamorphic terranes. J Petrol 29: 1187-1213.

Brenan J (1991) Development and maintenance of metamorphic permeability: implications for fluid transport. Rev Mineral 26: 291-319.

Brooks AH, Richardson GB, Collier AJ (1901) A reconnaissance of the Cape Nome and adjacent gold fields of Seward Peninsula Alaska, in 1900. In: AH Brooks, GB Richardson, AJ Collier, WC Mendenhall (eds) Reconnaissances in the Cape Nome and Norton Bay Regions, Alaska, in 1900. US Geol Surv special publ, 222p.

Burruss RC (1981) Analysis of phase equilibria in C-O-H-S fluid inclusions. In: Hollister LS, Crawford ML (eds) Short course in fluid inclusions: applications to petrology. Mineral Assoc Can Short Course Handbook: 39-74.

Buxton CL (1990) Geology and pre-metamorphic evolution of the Nome Group blueschist terrane, Horton Creek area, Seward Peninsula, Alaska. M.S. thesis, Univ. Washington, 115p.

Cady JW (1977) Aeromagnetic interpretation of Seward Peninsula, Alaska. US Geol Surv Open-file report 76-425.

Calvert AT (1992) Deformational and cooling history of the Cretaceous Kigluaik metamorphic complex, Seward Peninsula, Alaska. M.S. thesis, Stanford Univ.

Cartwright I, Valley JW (1991) Steep oxygen-isotope gradients at marble-metagranite contacts in the northwest Adirondack Mountains, New York, USA: products of fluid-hosted diffusion. Earth Planet Sci Lett 107: 148-163.

Cartwright I, Valley JW (1992) Oxygen-isotope geochemistry of the Scourian Complex, northwest Scotland. J Geol Soc Lond 149: 115-126.

Cathcart SH (1922) Metalliferous lodes in southern Seward Peninsula. US Geol Surv Bull 722-F: 163-261.

Chamberlain CP, Rumble D III (1988) Thermal anomalies in a regional metamorphic terrane: the role of advective heat transport during metamorphism. J Petrol 29: 1215-1232.

Chamberlain CP, Rumble D III (1989) The influence of fluids on the thermal history of a metamorphic terrain: New Hampshire, U.S.A. In: JS Daly, RA Cliff, BWD Yardley (eds) Geol Soc Spec Pub 43: 203-214.

Clayton RN, Goldsmith JR, Mayeda TK (1989) Oxygen isotope fractionation in quartz, albite, anorthite and calcite. Geochim Cosmochim Acta 53: 725-733.

Collier AJ (1902) A Reconnaissance of the northwestern portion of the Seward Peninsula, Alaska. US Geol Surv Prof Paper 2, 70p.

Collier AJ, Hess FL, Smith PS, Brooks AH (1908) The gold placers of parts of the Seward Peninsula, Alaska. US Geol Surv Bull 328.

Crawford ML (1981) Phase equilibria in aqueous fluid inclusions. In: Hollister LS, Crawford ML (eds) Short course in fluid inclusions: applications to petrology. Mineral Assoc Can Short Course Handbook: 75-100.

Crawford ML, Hollister LS (1986) Metamorphic fluids: The evidence from fluid inclusions. In: JV Walther & BJ Wood (eds) Advances in Physical Geochemistry: 1-35.

Dymek RF (1983) Titanium, aluminum, and interlayer cation substitutions in biotite from high-grade gneisses, West Greenland. Am Mineral 68: 880-899.

Essene EJ (1982) Geologic thermometry and barometry. Rev Mineral 10: 153-206.

Etheridge MA, Wall JV, Cox SF (1984) High fluid pressures during regional metamorphism and deformation: implications for mass transport and deformation mechanisms. J Geophys Res 89 B6: 4344-4358.

Evans BW, Irving AJ, Patrick BE (1992) Metamorphosed mafic igneous rocks in the Seward Peninsula. in: G Plafker, DL Jones, HC Berg (eds) Geology of Alaska. GSA Geology of North America G-1: in press.

Evans BW, Patrick BE (1987) Phengite (3T) in high-pressure metamorphosed granitic orthogneisses, Seward Peninsula, Alaska. Can Mineral 25: 141-158.

Ferry JM (1984) A biotite isograd in south-central Maine, U.S.A.: mineral reactions, fluid transfer, and heat transfer. J Petrol 25: 871-893.

Ferry JM (1986) Reaction progress: a monitor of fluid-rock interaction during metamorphic and hydrothermal events. In: JV Walther & BJ Wood (eds) Advances in Physical Geochemistry: 60-88.

Ferry JM (1989) Contact metamorphism of roof pendants at Hope Valley, Alpine County, California, USA. A record of the hydrothermal system of the Sierra Nevada batholith. Contrib Mineral Petrol 101: 402-417.

Ferry JM (1991) Dehydration and decarbonation reactions as a record of fluid infiltration. Rev Mineral 26: 351-393.

Ferry JM, Dipple GM (1991) Fluid flow, mineral reactions, and metasomatism. Geology 19: 211-214.

Fisher GW (1989) Matrix analysis of metamorphic mineral assemblages and reactions. Contrib Mineral Petrol 102: 69-77.

Forbes RB, Evans BW, Thurston SP (1984) Regional progressive high-pressure metamorphism, Seward Peninsula, Alaska. J Metam Geol 2: 43-54.

French BM (1966) Some geological implications of equilibrium between graphite and a C-H-O gas phase at high temperatures and pressures. Rev Geophys 4: 223-253.

Frost BR (1979) Mineral equilibria involving mixed-volatiles in a C-O-H fluid phase: The stabilities of graphite and siderite. Am J Sci 279: 1033-1059.

Frost BR, Frost CD (1987) CO_2, melts and granulite metamorphism. Nature 327: 503-506.

Frueh-Green GL, Olgaard DL, Coli M (1991) Controls on fluid flow in metacarbonates during metamorphism and deformation: Examples from the Carrara Marbles, Apuane Alps, N Italy. Terra Abstr 3: 436-437.

Fuhrman ML, Lindsley DH (1988) Ternary-feldspar modeling and thermometry. Am Mineral 73: 201-215.

Fyfe WS (1973) The granulite facies, partial melting and the Archean crust. Philos Trans R Soc London A 273: 457-461.

Fyfe WS, Price NJ, Thompson AB (1978) Fluids in the Earth's crust. Elsevier, Amsterdam, 583 p.

Ganor J, Matthews A, Paldor N (1989) Constraints on effective diffusivity during oxygen isotope exchange at a marble-schist contact, Sifnos (Cyclades), Greece. Earth Planet Sci Lett 94: 208-216.

Gerdes ML, Valley JW, Baumgartner LP (1991) Fluid evolution and mass transport at the Valentine wollastonite mine, Adirondack Mountains, N.Y. GSA Abstr. 23: A334.

Glassley WE (1983) Deep crustal carbonates as CO_2 fluid sources: Evidence from metasomatic reactions zones. Contrib Mineral Petrol 84: 15-24.

Glassley W, Ryerson R, Shaw H (1989) Chemical changes associated with formation of granulite and migration of complex C-O-H-S fluids, Sri Lanka. In: D Bridgwater (ed) Fluid movements-element transport and the composition of the deep crust, NATO ASI series C 281: 39-50.

Gottschalk RR (1990) Structural evolution of the Schist Belt, south-central Brooks Range fold and thrust belt, Alaska. J Struct Geol 12: 453-470.

Greenwood HJ (1967) The N-dimensional tie-line problem. Geochim Cosmochim Acta 31: 467-490.

Greenwood HJ (1975) Buffering of pore fluids by metamorphic reactions. Am J Sci 275: 573-593.

Griffin WL (1969) Replacement antiperthites in gneisses of the Babbitt-Embarrass area, Minnesota, USA. Lithos 2: 171-186.

Hall DL, Bodnar RJ (1990) Methane in fluid inclusions from granulites: A product of hydrogen diffusion? Geochim Cosmochim Acta 54: 641-651.

Hall DL, Sterner SM, Bodnar RJ (1989) Experimental evidence for hydrogen diffusion into fluid inclusions in quartz. GSA Abstr 21: A358.

Hansen EC, Newton RC, Janardhan AS (1984) Fluid inclusions in rocks from the amphibolite-facies gneiss to charnockite progression in southern Karnataka, India: direct evidence concerning the fluids of granulite metamorphism. J Metam Geol 2: 249-264.

Harrington GL (1919a) Graphite mining in Seward Peninsula. US Geol Surv Bull 692-G: 363-367.

Harrington GL (1919b) Tin mining in Seward Peninsula. US Geol Surv Bull 692-G: 353-361.

Harris NBW, Bickle MJ (1989) Advective fluid transport during charnockite formation; an example from southern India. Earth Planet Sci Lett 93: 151-156.

Hitzman MW, Proffett JM, Schmidt JM, Smith TE (1986) Geology and mineralization of the Ambler district, northwestern Alaska. Econ Geol 81: 1592-1618.

Hoernes S, Hoffer E (1985) Stable isotope evidence for fluid-present and fluid-absent metamorphism in metapelites from the Damara Orogen, Namibia. Contrib Mineral Petrol 90: 322-330.

Hoisch TD (1991) The thermal effects of pervasive and channelized fluid flow in the deep crust. J Geol 99: 69-80.

Holdaway MJ, Dutrow BL, Shore P (1986) A model for the crystal chemistry of staurolite. Am Mineral 71: 1142-1159.

Hollister LS (1988) On the origin of CO_2-rich fluid inclusions in migmatites. J Metam Geol 6: 467-474.

Hollister LS (1989) Enrichment of CO_2 in fluid inclusions in quartz by removal of H_2O during crystal plastic deformation. Geol Soc Am Abstr 21: A357.

Hollocher K (1991) Prograde amphibole dehydration reactions during high-grade regional metamorphism, central Massachusetts, USA. Am Mineral 76: 956-970.

Holloway JR (1981) Compositions and volumes of supercritical fluids in the earth's crust. In: Hollister LS, Crawford ML (eds) Short course in fluid inclusions: applications to petrology. Mineral Assoc Can Short Course Handbook: 13-38.

Hudson T (compiler) (1977) Geologic map of Seward Peninsula, Alaska. US Geol Surv Open-file map OF 77-796A.

Hummel CH (1962a) Preliminary geologic map of the Nome C-1 quadrangle, Seward Peninsula, Alaska. US Geol Surv Map MF-247.

Hummel CH (1962b) Preliminary geologic map of the Nome D-1 quadrangle, Seward Peninsula, Alaska. US Geol Surv Map MF-248.

Janardhan AS, Newton RC, Hansen EC (1982) The transformation of amphibolite facies gneiss to charnockite in Southern Karnataka and Northern Tamil Nadu, India. Contrib Mineral Petrol 79: 130-149.

Kay SM (1977) The origin of antiperthites in anorthosites. Am Mineral 62: 905-912.

Kerkhof AM van den (1990) Isochoric phase diagrams in the systems CO_2-CH_4 and CO_2-N_2: Applications to fluid inclusions. Geochim Cosmochim Acta 54: 621-629.

Kretz R (1983) Symbols for rock-forming minerals. Am Mineral 68: 277-279.

Kreulen R, Schuiling RD (1982) N_2-CH_4-CO_2 fluids during formation of the Dome de l'Agout, France. Geochim Cosmochim Acta 46: 193-203.

Kronenberg AK, Yund RA, Giletti BJ (1984) Carbon and oxygen diffusion in calcite: effects of Mn content and P_{H_2O}. Phys Chem Mineral 11: 101-112.

Lamb WM, Brown PE, Valley JW (1991) Fluid inclusions in Adirondack granulites: implications for the retrograde P-T path. Contrib Mineral Petrol 107: 472-483.

Lamb WM, Valley JW (1985) C-O-H fluid calculations and granulite genesis. In: Tobi AC, Touret JSR (eds) The deep Proterozoic crust of the north Atlantic Provinces. Reidel, Dordrecht: 119-131.

Lamb WM, Valley JW, Brown PE (1987) Post-metamorphic CO_2-rich fluid inclusions in granulites. Contrib Mineral Petrol 96: 485-495.

Leake BE (1978) Nomenclature of amphiboles. Am Mineral 63: 1023-1052.

Lieberman JE (1988) Metamorphic and structural studies of the Kigluaik Mountains, Western Alaska. Ph.D. dissertation, Univ. of Washington, 192p.

Lieberman JE, Petrakakis K (1992) TWEEQU thermobarometry: analysis of uncertainties and applications to granulites from Western Alaska and Austria. Can Mineral 29: 857-887.

Lindsley DH (1983) Pyroxene thermometry. Am Mineral 68: 477-493.

McMullin DW, Berman RB, Greenwood HJ (1992) Calibration of the SGAM thermobarometer for pelitic rocks using data from phase-equilibrium experiments and natural assemblages. Can Mineral 29: 889-908.

Miller EL, Calvert AT, Little TA (1992a) Strain-collapsed metamorphic isograds in a sillimanite gneiss dome, Seward Peninsula, Alaska. Geology in press.

Miller EL, Amato J, Calvert A, Dumitru T, Gans, P, Hannula K, Lee J, Little T, Rubin C (1992b) Structural evolution of the Seward Peninsula, Alaska: A progress report. GSA Abstr 24: 70.

Miller TP, Grybeck DG, Elliott RL, Hudson T (1972) Preliminary Geologic map of the eastern Solomon and southeastern Bendeleben quadrangles, eastern Seward Peninsula, Alaska. US Geol Surv Open-file report 72-256, 11p.

Moffit FH (1913) Geology of the Nome and Grand Central quadrangles. US Geol Surv Bull 533, 140p.

Morgan GB VI, Chou I-M, Pasteris JD, Olsen S (1991) Controlled-atmosphere experiments with CO_2 fluid inclusions: Monitoring H_2 diffusion and mechanisms of re-equilibration. GSA Abstr. 23: A336.

Morrison J, Valley JW (1988) Post-granulite facies fluid infiltration in the Adirondack Mountains. Geology 16: 513-516.

Murck BW, Burruss RC, Hollister LS (1978) Phase equilibria in fluid inclusions in ultramafic xenoliths. Am Mineral 63: 40-46.

Nabelek PI, Labotka TC, O'Neil JR, Papike JJ (1984) Contrasting fluid/rock interaction between Notch Peak granitic intrusion and argillites and limestones in western Utah: Evidence from stable isotopes and phase assemblages. Contrib Mineral Petrol 86: 25-34.

Newton RC (1986) Fluids of granulite facies metamorphism. In: JV Walther & BJ Wood (eds) Advances in Physical Geochemistry, 36-59.

Newton RC, Smith JV, Windley BF (1980) Carbonic metamorphism, granulites and crustal growth. Nature 288: 45-50.

Nicholls J, Crawford ML (1985) FORTRAN programs for calculation of fluid properties from microthermometric data on fluid inclusions. Computers and Geoscience 11: 619-645.

Northrop DA, Clayton RN (1966) Oxygen isotope fractionation in systems containing dolomite. J Geol 74: 174-196.

Ohmoto H, Kerrick D (1977) Devolatilization equilibria in graphitic systems. Am J Sci 277: 1013-1044.

Pasteris JD, Wanamaker BJ (1988) Laser raman microprobe analysis of experimentally re-equilibrated fluid inclusions in olivine: Some implications for mantle fluids. Am Mineral 73: 1074-1088.

Patrick BE (1987) Petrological and structural studies in the Seward Peninsula blueschist terrane, Alaska. Ph.D. dissertation, Univ. of Washington, 118p.

Patrick BE (1988) Synmetamorphic structural evolution of the Seward Peninsula Blueschist terrane. J Struct Geol 10: 555-565.

Patrick BE, Evans BW (1989) Metamorphic evolution of the Seward Peninsula Blueschist Terrane. J Petrol 30: 531-556.

Patrick BE, Lieberman JE (1988) Thermal overprint on the Seward Peninsula Blueschist terrane: the Lepontine in Alaska. Geology 16: 1100-1103.

Pattison DRM (1991) Infiltration-driven dehydration and anatexis in granulite facies metagabbro, Grenville Province, Ontario, Canada. J Metam Geol 9: 315-332.

Peacock SM (1991) Metamorphic Geology. Contributions in Volcanology, Geochemistry and Petrology, U.S. National Report 1987-1990: 486-499.

Pecher A, Boullier AM (1984) Evolution a pression et temperature elevees d'inclusions fluides dans un quartz synthetique. Bull Mineral 107: 139-153.

Pollock SM (1982) Structure, petrology and metamorphic history of the Nome Group Blueschist Terrane, Salmon Lake are, Seward Peninsula, Alaska. M.S. thesis, Univ Washington, 222p.

Potter RW II, Brown DL (1977) The volumetric properties of aqueous sodium chloride solutions from $0°$ to $500°C$ at pressures up to 2000 bars based on a regression of the available literature data. USGS Bull 1421-C, 36p.

Read JJ, Meinert LD (1986) Gold-bearing quartz vein mineralization at the Big Hurrah Mine, Seward Peninsula, Alaska. Economic Geol 81: 1760-1774.

Rice JM (1980) Calculated equilibria involving humite minerals in impure dolomitic limestones. Part I. Calculated stability of clinohumite. Contrib Mineral Petrol 71: 219-235.

Rice JM, Ferry JM (1982) Buffering, infiltration and the control of intensive variables during metamorphism. Rev Mineral 10: 263-326.

Robinson MS, Stevens DL (compilers) (1984) Geologic map of Seward Peninsula, Alaska. Alaska division of geological and geophysical surveys special report 34.

Robinson P, Spear FS, Schumacher JC, Laird J, Klein C, Evans BW, Doolan BL (1982) Phase relations of metamorphic amphiboles: natural occurrence and theory. Rev Mineral 9B: 1-228.

Roedder E (1965) Liquid CO_2 inclusions in olivine-bearing nodules and phenocrysts from basalts. Am Mineral 50: 1746-1782.

Roedder E (1972) The compositions of fluid inclusions. US Geol Surv Prof Paper 440JJ.

Roedder E (1981) Origin of fluid inclusions and changes that occur after trapping. In: Hollister LS, Crawford ML (eds) Short course in fluid inclusions: applications to petrology. Mineral Assoc Can Short Course Handbook: 103-137.

Roedder E (1984) Fluid inclusions. Rev Mineral 12: 1-644.

Rubie DC (1986) The catalysis of mineral reactions by water and restrictions on the presence of aqueous fluid during metamorphism. Min Mag 50: 399-415.

Rudnick RL, Ashwal LD, Henry DJ (1984) Fluid inclusions in high-grade gneisses of the Kapuskasing structure zone, Ontario: metamorphic fluids and uplift/erosion path. Contrib Mineral Petrol 87: 399-406.

Rumble D III (1982) Stable isotope fractionation during metamorphic devolatilization reactions. Rev Mineral 10: 327-353.

Rumble D III, Ferry JM, Hoering TC, Boucot AS (1982) Fluid flow during metamorphism of the Beaver Brook fossil locality, New Hampshire. Am J Sci 282: 886-919.

Rumble D III, Hoering TC (1986) Carbon isotope geochemistry of graphite vein deposits from New Hampshire, USA. Geochim Cosmochim Acta 50: 1239-1247.

Rumble D III, Spear FS (1983) Oxygen-isotope equilibration and permeability enhancement during regional metamorphism. J Geol Soc 140: 619-628.

Rye RO, Schuiling RD, Rye DM, Jansen JBH (1976) Carbon, hydrogen and oxygen isotope studies of the regional metamorphic complex at Naxos, Greece, Geochim Cosmochim Acta 40: 1031-1049.

Sainsbury CL (1969) Geologic map of the Teller C-4 and the southern part of the Teller B-4 quadrangles, western Seward Peninsula, Alaska. US Geol Surv Map I-572.

Sainsbury CL, Kachadoorian R, Hudson T, Smith TE, Richard TR, Todd WE (1969) Reconnaissance geologic maps and sample data, Teller A-1, A-2, A-3, B-1, B-2, B-3, C-1, and Bendeleben A-6, B-6, C-6, D-5, D-6 quadrangles, Seward Peninsula, Alaska. US Geol Surv Open-file report 69-236, 49p.

Sainsbury CL (1972) Geologic map of the Teller quadrangle, Alaska. US Geol Surv Map I-685.

Sainsbury CL, Hudson T, Ewing R, Marsh WR (1972a) Reconnaissance geologic map of the Nome C-3 quadrangle, Seward Peninsula, Alaska. US Geol Surv Open-file report 72-322, 9p.

Sainsbury CL, Hudson T, Ewing R, Marsh WR (1972b) Reconnaissance geologic maps of the Solomon D-5 and C-4 quadrangles, Seward Peninsula, Alaska. US Geol Surv Open-file report 72-323, 10p.

Sainsbury CL, Hudson T, Ewing R, Marsh WR (1972c) Reconnaissance geologic map of the western half of the Solomon quadrangle, Alaska. US Geol Surv Open-file report 72-324, 10p.

Sainsbury CL, Hudson T, Ewing R, Richards T (1972d) Geologic map of the Solomon D-6 quadrangle, Seward Peninsula, Alaska. US Geol Surv Open-file report 72-325, 17p.

Sainsbury CL, Hummel CH, Hudson T (1972e) Reconnaissance geologic map of the Nome quadrangle, Seward Peninsula, Alaska. US Geol Surv Open-file report, 28p.

Sainsbury CL, Smith TE, Kachadoorian R (1972f) Reconnaissance geologic map of the Nome D-3 quadrangle, Seward Peninsula, Alaska. US Geol Surv Open-file report 72-327, 10p.

Samson IM, William-Jones AE (1991) C-O-H-N-salt fluids associated with contact metamorphism, McGerrigle Mountains, Quebec: a Raman spectroscopic study. Geochim Cosmochim Acta 55: 169-177.

Santosh M, Harris NBW, Jackson DH, Mattey DP (1990) Dehydration and incipient charnockite formation: a phase equilibria and fluid inclusion study from southern India. J Geol 98: 915-926.

Santosh M, Jackson DH, Harris NBW, Mattey DP (1991) Carbonic fluid inclusions in south Indian granulites: evidence for entrapment during charnockite formation. Contrib Mineral Petrol 108: 318-330.

Schreurs J (1984) The amphibolite-granulite facies transition in West Uusimaa, S.W. Finland. A fluid inclusion study. J Metam Geol 2: 327-341.

Schwarcz HP, Clayton RN, Mayeda T (1970) Oxygen isotopic studies of calcareous and pelitic metamorphic rocks, New England. Geol Soc Amer Bull 81: 2299-2316.

Sharp ZD (1991) Determination of oxygen diffusion rates in magnetite from natural isotopic variations. Geology 19: 653-656.

Sheppard SMF, Schwarcz HP (1970) Fractionation of carbon and oxygen isotopes and magnesium between coexisting metamorphic calcite and dolomite. Contrib Mineral Petrol 26: 161-198.

Skippen GB (1974) An experimental model for low pressure metamorphism of siliceous dolomitic marble. Am J Sci 274: 487-509.

Smith PS (1908) Investigations of the mineral deposits of Seward Peninsula, Alaska. US Geol Surv Bull 345-E: 206-250.

Smith PS (1910) Geology and mineral resources of the Solomon and Casadepaga quadrangles, Seward Peninsula, Alaska. US Geol Surv Bull 433, 234p.

Steidtmann E, Cathcart SH (1922) Geology of the York Tin deposits, Alaska. US Geol Surv Bull 733, 130p.

Sterner SM, Bodnar RJ (1989) Synthetic fluid inclusions - VII. re-equilibration of fluid inclusions in quartz during laboratory-simulated metamorphic burial and uplift. J Metam Geol 7: 243-260.

Sterner SM, Hall KL, Bodnar RJ (1988) Post-entrapment compositional changes in fluid inclusions: Experimental evidence for water diffusion in quartz GSA Abstr. 20: A100.

Sturnick MA (1984) Metamorphic petrology, geothermo-barometry and geochronology of the eastern Kigluaik Mountains, Seward Peninsula, Alaska. M.S. thesis, Univ. of Alaska, Fairbanks.

Swanenberg HEC (1980) Fluid inclusions in high-grade metamorphic rocks from S.W. Norway. Geologica Ultraiectina 25, 147p.

Thompson AB (1983) Fluid-absent metamorphism. J Geol Soc Lond 140: 533-548.

Thompson JB (1982a) Composition space: an algebraic and geometric approach. Rev Mineral 10: 1-31.

Thompson JB (1982b) Reaction space: an algebraic and geometric approach. Rev Mineral 10: 33-52.

Thurston SP (1985) Structure, petrology and metamorphic history of the Nome group blueschist terrane, Salmon Lake area, Seward Peninsula, Alaska. Geol Soc Amer Bull 96: 600-617.

Till AB (1980) Crystalline rocks of the Kigluaik Mountains, Seward Peninsula, Alaska. M.S. thesis, Univ. Washington, 97p.

Till AB, Dumoulin JA (1992) Geology of Seward Peninsula and Saint Lawrence Island. in: G Plafker, DL Jones, HC Berg (eds) Geology of Alaska. GSA Geology of North America G-1: in press.

Till AB, Dumoulin JA, Gamble B, Kaufman D, Carroll PE (1986) Preliminary geologic map and fossil data, Solomon, Bendeleben and Southern Kotzebue quadrangles, Seward Peninsula, Alaska, U.S. Geol Surv Open-file report 86-276, 71p.

Thomas AV, Pasteris JD, Bray CJ, Spooner ETC (1990) H_2O-CH_4-NaCl-CO_2 inclusions from the footwall contact of the Tanco granitic pegmatite: Estimates of internal pressure and composition from microthermometry, laser Raman spectroscopy, and gas chromatography. Geochim Cosmochim Acta 54: 559-573.

Todd CS (1990) Bleaching of limestones in the Notch Peak contact-metamorphic aureole, Utah. Geology 18: 83-86.

Touret JLR (1971) Le facies granulite in Norvege meridionale II. Les inclusions fluides. Lithos 4: 423-436.

Touret JLR (1977) The significane of fluid inclusions in metamorphic rocks. In: DG Fraser (ed) Thermodynamics in Geology. Reidel, Dordrecht: 203-227.

Touret JLR (1981) Fluid inclusions in high grade metamorphic rocks. In: Hollister LS, Crawford ML (eds) Short course in fluid inclusions: applications to petrology. Mineral Assoc Can Short Course Handbook: 182-208.

Touret JLR (1985) Fluid regimes in southern Norway: the record of fluid inclusions. In: Tobi AC, Touret JSR (eds) The deep Proterozoic crust of the north Atlantic Provinces. Reidel, Dordrecht: 517-549.

Touret JLR, van den Kerkhof AM (1986) High density fluids in the lower crust and upper mantle. Physica 139 and 140B: 834-840.

Touret JLR, Olsen SN (1985) Fluid inclusions in migmatites. In: JR Ashworth (ed) *Migmatites*: 265-288.

Tracy RJ, Rye DM, Hewitt A, Schiffries CM (1983) Petrologic and stable-isotopic studies of fluid-rock interactions, south-central Connecticut: I. The role of infiltration in producing reaction assemblages in impure marbles. Am J Sci 283-A: 589-616.

Turner DL, Forbes RB, Dillon JT (1979) K-Ar geochronology of the southwestern Brooks Range, Alaska. Can J Earth Sci 16: 1789-1804.

Valley JW (1986) Stable isotope geochemistry of metamorphic rocks. Rev Mineral 16: 445-492.

Valley JW, O'Neil JR (1984) Fluid heterogeneity during granulite facies metamorphism in the Adirondacks: Stable isotope evidence. Contrib Mineral Petrol 85: 158-173.

Walther JV, Orville PM (1983) The extraction-quench technique for determination of the thermodynamic properties of solute complexes: application to quartz solubility in fluid mixtures. Am Mineral 68: 731-741.

Wickham SM, Taylor HP Jr (1985) Stable isotopic evidence for large-scale seawater infiltration in a regional metamorphic terrane; the Trois Seigneurs Massif, Pyrenees, France. Contrib Mineral Petrol 91: 122-137.

Wickham SM, Taylor HP Jr (1987) Stable isotope constraints on the origin and depth of penetration of hydrothermal fluids associated with Hercynian regional metamorphism and crustal anatexis in the Pyrenees. Contrib Mineral Petrol 95: 255-268.

Winslow DM, Erickson CJ, Tracy RJ, Bodnar RJ (1991) Evidence for nitrogen-rich metamorphic fluids in the central Maine terrane of south-central Massachusetts. GSA Abstr. 23: A134.

Appendix 1:   Mineral assemblages in Kigluaik group pelites

This appendix is organized into two parts; one where the information is arranged by sample number, the other where the information is organized by stratigraphic horizon. Mineral identifications were made petrographically or by electron microprobe. Samples were collected by Alison Till (XXX KT78), Steve Pollack (SL81-XXX), Josh Leiberman (OS-XX, AB85-XXX, AB86-XXX, AB87-XXX), Brian Patrick (AB84-XXX) and Clifford Todd (AB89-XX, AB90-XX). Unit refers to the stratigraphic horizon from which the sample came (see figure 1.4): 0th, 1st, 2nd, 3rd, and 4th refer to pelite units; TGOC refers to the Thompson Creek Orthogneiss; mixed refers to the mixed metasedimentary unit between the TGOC and the 3rd pelite; syen refers to the metasyenite unit within the main marble. The Isograd column denotes the isograd zone from which the sample was taken (see chapter 1 for explanation of isograd zones). Mineral abbreviations are listed in table 1.1, with the exception of "Tourm" tourmoline, and "Op", which stands for opaque, usually ilmenite. "X" signifies that the mineral is present. "inc" signifies that the mineral is present only as an inclusion within another mineral, usually garnet. "lt" signifies that the mineral is texturally late. "tr" signifies a trace amount of the mineral. An exclamation point means that the mineral is very abundant. "fib" refers to fibrolite, the fine grained fibrous form of sillimanite. "A" in the Ky column stands for andalusite, instead of kyanite. "Lithol" describes the lithology of the sample: gqtzite = graphitic quartzite, btgneiss = biotite gneiss.

Sample#	Unit	Isograd	Gt	Bt	Qz	Pl	Kfs	Mu	Sta	Sil	Ky	Crd	Gr	Opq	Rut	Lithol	Access
028 KT78	4th	Sil	X	X	X	X		X		fib	X					pelite	eggshell
030 KT78	4th	Sil/Sta		X	X	X		X		fib						pelite	
038 KT78	4th	Sil+Kfs	X	X	X	X				X						pelite	
039 KT78	4th	Sil+Kfs	X	X	X	X				X fib						pelite	
042 KT78	4th	Sil+Kfs		X	X	X	?			X			X			gqtzite	Ap
043 KT78	4th	Sil+Kfs		X	X	X	X			X			X			gqtzite	Tourm
055 KT78	4/TGOC	Sil+Kfs		X	X	X	X			X			X			pelite	Sph, Allan
063 KT78	mixed	Sil+Kfs	X	X	X	X								inc	inc	granitic	Tourm
066 KT78	mixed/TG	Sil+Kfs	X	X	X	X				fib					inc	pelite	
068 KT78	mixed/TG	Sil+Kfs	X	X	X	X				X						pelite	Tourm
076 KT78	mixed	Sil+Kfs	X	X	X	X										qtzite	
082 KT78	mixed	Sil+Kfs	X	X	X	X				X fib			X			pelite	
085 KT78	mixed	Sil+Kfs	X	X	X	X	X	tr		X		?	X	X		pelite	
096 KT78	3rd	Sil+Kfs	X	X	X	X	X			X			X	X		pelite	
098 KT78	3rd	Sil+Kfs	X	X	X	X				X			X	X		pelite	Tourm
099 KT78	3rd	Sil+Kfs	X	X	X	X	X			X			X	X		pelite	Tourm
100 KT78	3rd	Sil+Kfs	X	X	X	X	X			X		?	X			pelite	
101 KT78	3rd	Sil+Kfs	X	X	X	X	X			X			X			pelite	
117 KT78	1st	Sil+Kfs	X	X	X	X	X					tt	X			pelite	
147 KT78	4th	Sil	X	X	X	X		X		fib			X	X	X	pelite	
150 KT78	4th	Sil		X	X			X	X	tr	one		X		X	btschist	
155 KT78	4th	Sta	X	X	X	X				X fib	tr		X			pelite	Ap
156 KT78	3rd	Sil+Kfs	X	X	X	X	X			X			X			qtzite	
170 KT78	2nd	Sil+Kfs	X	X	X	X	X						X			pelite	
SL81-425.1	4th	Sta	X	X	X	X		X	X		tr			X		pelite	Tourm
SL81-483.1	4th	Sta	X	X	X			X	X					X		pelite	
SL81-483.2	4th	Sta	X	X	X			X	X					X		pelite	
SL81-484.1	4th	Sta	X	X	X	X		X	X		X			X		pelite	
SL81-485.1	4th	Sta	X	X	X	X		X	X					X		pelite	Tourm
SL81-486.1	4th	Sta	X	X	X			X	X		X			X		pelite	
SL81-487.1	4th	Sta	X	X	X	X		X	X					X		pelite	
SL81-488.1	4th	Sta	X	X	X			X	X				X	X		pelite	
SL81-491.1	4th	Sta	X	X	X			X	X				X	X		pelite	
SL81-491.3	4th	Sta	X	X	X			X	X								
SL81-492	4th	Sta	X	X	X			X	X		A	?					
SL81-497.1	4th	Sta		X	X	X	X	X	X					X		pelite	Ap, Zircon
SL81-504.1	4th	Sil	X	X	X		X	X		fib				X		pelite	

Sample#	Unit	Isograd	Gt	Bt	Qz	Pl	Kfs	Mu	Sta	Sil	Ky	Crd	Gr	Opq	Rut	Lithol	Access
SL81-504.2	4th	Sil	X	X	X	X		X		fib				X			
SL81-506.1	4th	Sil	X	X	X	X		tr	X	fib				X			Tourm
SL81-512.1	4th	Sil	X	X	X	X		X	X	X fib				X		pelite	Tourm
SL81-515.1	4th	Sta	X	X				X	X		X				X		pelite	Tourm
SL81-516.1	4th	Sta		X	X	X		tr					X					
OS 06	1st	Sil+Kfs	X	X	X	X	X	X		X				X		pelite	
OS 18	1st	Sil+Kfs	X	X	X	X	X	X		X	inc?		X	X		pelite	
OS 19	1st	Sil+Kfs	X	X	X	X		X		X				X		pelite	Ap
OS 30	3/2	Sil+Kfs	X	X	X	X		X		X				X		pelite	
OS 30.1	3/2	Sil+Kfs	X	X	X	X	X	X		X		tt		X	inc	pelite	
OS 35	2/syen	Sil+Kfs	X	X	X	X		X		X			X	X	inc	pelite	Tourm
OS 36	2/syen	Sil+Kfs	X	X	X	X		X		X			X	X	inc	pelite	Tourm
OS 39	2nd	Sil+Kfs	X	X	X	X		X		X				X		pelite	
OS 40	2nd	Sil+Kfs	X	X	X	X	X	X		X			X	X		pelite	
OS 41.2	2nd	Sil+Kfs	X	X	X	X	X	X	inc	X		tt	X	X		pelite	
OS 42	3/2	Sil+Kfs	X	X	X	X	X	X		X fib			X	X		pelite	
OS 43	3/2	Sil+Kfs	X	X	X	X	X	?		X		tt	X	X		pelite	Tourm
OS 52.1	1st	Sil+Kfs	X	X	X	X		X		X				X	X	pelite	
OS 56	1st	Sil+Kfs	X	X	X	X	X	X		X				X		pelite	
OS 60	2/syen	Sil+Kfs	X	X	X	X	X	X	inc	X				X		pelite	
OS 63	3rd	Sil+Kfs	X	X	X	X		X		X fib	inc			X		pelite	
OS 70	1st	Sil+Kfs	X	X	X	X		X	inc	X				X		pelite	
OS 76	syen	Sil+Kfs	X	X	X	X		X		X						pelite	
OS 78	3rd	Sil+Kfs	X	X	X	X	X						X			pelite	
OS 91	4th	Sil+Kfs	X	X	X	X	X		inc	X		tt	X	X	inc	pelite	
OS 92	3rd	Sil+Kfs	X	X	X	X				X			X	X		pelite	
OSW 2	1st	Sil+Kfs	X	X	X	X	?							X			
AB84-149	4th	Sta	X	X	?	?		X	X							pelite	
AB84-152	4th	Sta	X	X	X	X		X	X		X		X			pelite	Tourm
AB85-005	4th	Sta	X	X	X	X		X	X					X		pelite	
AB85-021	4th	Sta	X	X	X	X		X	X					X		pelite	
AB85-022.1	4th	Sta	X	X	X	X											
AB85-023	4th	Sta	X	X	X	X		X	X							schist	
AB85-026	4th	Sta	X	X	X	X		X	X				X		X	pelite	
AB85-033	4th	Sta															

Sample#	Unit	Isograd	Gt	Bt	Qz	Pl	Kfs	Mu	Sta	Sil	Ky	Crd	Gr	Opq	Rut	Lithol	Access
AB85-034.1	4th	Sta	X	X	X	X							X	X		gqtzite	
AB85-034.2	4th	Sta	X	X	X	X			X		X	X	X	X			Tourm
AB85-036	4th	Sta		X	X	X		X	X	fib		X	X			qtzitic	Tourm
AB85-036.2	4th	Sta	X	X	X	X		X	X	fib			X	X			
AB85-037.1	4th	Sta	X	X	X	X		X	X	tr	A		X	X		btschist	Tourm, Ap
AB85-041	4th	Sta		X	X	X	?		X				X			gqtzite	Tourm
AB85-049.2	4th	Sta	X	X	X	X		X		?			X			pelite	
AB85-050	4th	Sil		X	X	X			X	fib			X	X		gqtzite	
AB85-051	4th	Sil		X	X	X		tr	X	fib			X	X			Tourm
AB85-065	4th	Sta	X	X	X	X		X	X		A		X	X			
AB85-067.1	4th	Sta	X	X	X	X		X	X				X	X			
AB85-067.2	4th	Sta	X	X	X	X		X	X				X	X			
AB85-067.3	4th	Sta	X	X	X	X		X	X				X	X			
AB85-069	4th	Sta	X	X	X	X		X	X				X	X			
AB85-070	4th	Sta		X	X					X			X				Tourm
AB85-071	4th	Sta		X	X	X				X			X	X			
AB85-072	4th	Sta	X	X	X	X			X		A						Tourm
AB85-073	4th	Sta		X	X	X			X	fib							
AB85-076	4th	Sta		X	X							X					
AB85-077.2	4th	Sil	X						inc								Ap
AB85-085	4th	Sil	X	X	X	X	X			fib			X				Tourm
AB85-208.1	4th	Sil+Kfs	X	X	X	X	X			fib			X				Tourm
AB85-208.2	4th	Sil+Kfs	X	X	X	X				fib			X				Tourm
AB85-210.2	4th	Sil	X	X	X	X				X fib			X			pelite	
AB85-215.1	4th	Sil+Kfs	X	X	X	X	X			fib			X	X			
AB85-217	4th	Sil+Kfs	X	X	X	X		X		X fib			X	X			
AB85-222.2	4th	Sta	X	X	X	X			X				X				
AB85-226.2	4th	Sil		X	X	X		tr		X fib				X		pelite	
AB85-226.3	4th	Sil	X	X	X					X fib				X		pelite	
AB85-227.1	4th	Sil+Kfs	X	X	X	X	X			fib				X		pelite	
AB85-228.1	4th	Sil+Kfs	X	X	X	X		X		fib				X	inc		Tourm
AB85-229	4th	Sil+Kfs		X	X	X		X	X	fib				X			Tourm
AB85-249	4th	Sta	X	X	X	X		X	X				X				
AB86-006	4th	Sta	X	X	X	X		X									
AB86-007.2	4th	Sta	X	X	X	X		X						relic			chlorite
AB86-104.1	1st	Sil+Kfs	X	X	X	X	?			X	?	It				pelite?	
AB86-105.1	1st	Sil+Kfs	X	X	X	X	X			X						pelite	

Sample#	Unit	Isograd	Gt	Bt	Qz	Pl	Kfs	Mu	Sta	Sil	Ky	Crd	Gr	Opq	Rut	Lithol	Access
AB86-105.2	1st	Sil+Kfs	X	X	X	X	X	X	X	X		It		X		pelite	
AB86-105.3		see Josh Table 5.2															
AB86-118.2	1st	Sil+Kfs		X	X	X	X			X		It	X	X		pelite	
AB86-123	1st	Sil+Kfs	X	X	X	X	X			X			Xl	X		pelite	
AB87-213.1	4th	Sta	X	X	X	X			tr					X			
AB87-218	4th	Sta	X	X	X	X		X	X				X	X			
AB87-220.1	4th	Sta	X	X	X	X		X	X				X	X			Tourm
AB87-220.3	4th	Sta	X	X	X	X		X	X				X	inc			
AB87-221.2	4th	Sta		X	X	X		X	X		Xl		X	X		pelite	Tourm
AB87-222	4th	Sta		X	X	X		X	X	fib	X					pelite	Tourm
AB87-224	4th	Sil	X	X	X	X		X	one	fib		Xl		X		pelite	
AB87-225.1	4th	Sil	X	X	X	X		X	X					X		pelite	
AB87-244.1	4th	Sta	X	X	X	X		X						X			Tourm
AB87-246	4th	Sta		X	X	X		X			X	It?		X		pelite	
AB87-247	4th	Sta		X	X	X		X	Xl		X		X	X		pelite	
AB87-250	4th	Sil	one	X	X	X		X		fib							
AB87-252.1	4th	Sil	X	X	X	X		X		fib						pelite	
AB87-252.2	4th	Sil	X	X	X	X		X		fib						pelite	Tourm
AB87-252.3	4th	Sil	X	X	X	X		X		fib						gqzite	Tourm
AB87-253.1	4th	Sil+Kfs		X	X	X	?	X		fib			X			gqzite	
AB87-253.2	4th	Sil+Kfs		X	X	X	X	X	X	fib			X			gqzite	Tourm
AB87-253.3	4th	Sil+Kfs		X	X	X	X	X	X	fib			X				Tourm
AB87-254.1	4th	Sil+Kfs		X	X	X	X			X fib		It	X				Tourm
AB87-254.2	4th	Sil+Kfs		X	X	X	??			fib			X				Tourm, Alla
AB87-255	4th	Sil		X	X	X		tr		fib						pelite	
AB87-256	4th	Sil	X	X	X	X			X	fib				X			
AB87-257	4th	Sil	X	X	X	X		X	X	fib							
AB87-257.2	4th	Sil	X	X	X	X			X	fib							Tourm
AB87-257.3	4th	Sil	X	X	X				X						inc		Tourm
AB87-271	4th	Sta	X	X	X	X		X	X					X			
AB87-272.1	4th	Sta	X	X	X	X			X					X			Tourm
AB87-272.2	4th	Sta	X	X	X	X			X					X			Tourm
AB87-273	4th	Sil	X	X	X	X		X	X	fib				inc			
AB87-274	4th	Sil	X	X	X	X		X		fib	A?			X		pelite	Tourm
AB87-275	4th	Sil	X	X	X	X				fib	?					pelite	Tourm
AB87-277	4th	Sil+Kfs	X	X	X	X		X				X				pelite	Tourm
AB87-278	4th	Sil+Kfs		X	X	X	X			fib			X			gqzite	

Sample#	Unit	Isograd	Gt	Bt	Qz	Pl	Kfs	Mu	Sta	Sil	Ky	Crd	Gr	Opq	Rut	Lithol	Access
AB87-281	4th	Sil+Kfs	X	X	X	X	?	?		fib							
AB87-282	4th	Sil+Kfs	X	X	X	X	X			fib							
AB87-283.2	4th	Sil+Kfs	X	X	X	X	X	lt		fib			X			gqtzite	
AB87-285	4th	Sil	X	X	X	X			relic	fib		lt		X			Tourm
AB87-286	4th	Sil	X	X	X	X			Xinc	fib		lt?		X		pelite	Tourm
AB87-287	4th	Sil	X	X	X	X			X	fib				X			
AB87-289	4th	Sta	X	X	X	X		X	X					X		pelite	Tourm
AB87-290	4th	Sta	X	X	X	X		X	X					X		pelite	Tourm
AB89-01.1	3rd	Sil+Kfs	X	X	X	X	X			X			X		inc	pelite	Tourm
AB89-01.2	3rd	Sil+Kfs	X	X	X	?			inc	X fib			X		inc	pelite	Ap
AB89-01.3	3rd	Sil+Kfs	X	X	X	X	X			X			X			pelite	
AB89-02	3rd	Sil+Kfs	X	X	X	X	?			X		?		X		pelite	Tourm, Ap
AB89-07	3rd	Sil+Kfs	X	X	X	X				X						pelite	
AB89-10.1	1st	Sil+Kfs	X	X	X	X	X			X fib	inc		X		inc	pelite	
AB89-10.3	1st	Sil+Kfs	X	X	X	X			inc	X	inc		X		X	pelite	
AB89-10.4	1st	Sil+Kfs	X	X	X	X										pelite?	
AB89-10.5	1st	Sil+Kfs	X	X	X	X	X			X fib	inc		X	X	inc	pelite	
AB89-11.1	1st	Sil+Kfs	X	X	X	X	X			X fib		tr		?		pelite	
AB89-11.2	1st	Sil+Kfs	X	X	X	X	X			X fib		lt		?	X	pelite	
AB89-13	syen	Sil+Kfs	X	X	X	X	X			X				X	X	pelite	Tourm
AB89-15	syen	Sil+Kfs	X	X	X	X	X			X				X	X	qtzite	Ap
AB89-16	2nd	Sil+Kfs	X	X	X	X				X				X		pelite	
AB89-20	3rd	Sil+Kfs	X	X	X	X			inc	X fib				X	inc	pelite	
AB89-21.1	3rd	Sil+Kfs	X	X	X	X	X			X fib			X	X	inc	pelite	Ap
AB89-21.2	3rd	Sil+Kfs	X	X	X	X	X		inc	inc		lt	X	X	inc	pelite	Ap
AB89-23.3	1st	Sil+Kfs	X	X	X	X				X			X	X	X	btgneiss	Ap
AB89-29	mixed	Sil+Kfs	X	X	X	X	X			X					inc	pelite	Ap, Tourm
AB89-33.1	mixed	Sil+Kfs	X	X	X	X			inc	X		lt		X		pelite	Ap
AB89-33.2	mixed	Sil+Kfs	X	X	X	X				X	inc					pelite	
AB89-35	3rd	Sil+Kfs	X	X	X	?		inc		X fib			X		inc	pelite	
AB89-37.1	3rd	Sil+Kfs	X	X	X	X	?			X			X	X	X	grphsch	
AB89-40.03	3rd	Sil+Kfs	X	X	X	?				X			X			gqtzite	
AB89-40.07	3rd	Sil+Kfs	X	X	X	?				X			X			pelite	
AB89-40.08	3rd	Sil+Kfs	X	X	X	?			inc	X fib			X	X		pelite	
AB89-40.09	3rd	Sil+Kfs	X	X	X	?				X			X			pelite	Tourm
AB89-40.10	3rd	Sil+Kfs	X	X	X	X				X fib			X		inc	pelite	Ap
AB89-40.11	3rd	Sil+Kfs	X	X	X	X				X fib	inc?		X			pelite	Ap

Sample#	Unit	Isograd	Gt	Bt	Qz	Pl	Kfs	Mu	Sta	Sil	Ky	Crd	Gr	Opq	Rut	Lithol	Access
AB89-48.3	3rd	Sil+Kfs	X	X	X	X	X			X		Xl	X				
AB89-57.2	3/2	Sil+Kfs	X	X	X	X	X			X			X				Ap
AB89-58	3/2	Sil+Kfs	X	X	X	X	X			X		X	X	X	inc	pelite	
AB89-60.3	1st	Sil+Kfs	X	X	X	X	X			X	inc	?	X	X	inc		Tourm
AB89-64.2	1float	Sil+Kfs		X	X	X	X			X		X	X	X		pelite	
AB89-64.3	1float	Sil+Kfs	X	X	X	X	X			X	inc	X	X	X	inc	pelite	
AB89-64.5	1float	Sil+Kfs	X	X	X	X	X			X	inc		X	X		pelite	
AB89-65.2	1float	Sil+Kfs	X	X	X	X	X			X	inc					pelite	
AB89-65.6	1float	Sil+Kfs		X	X	X			inc	X						?	
AB89-65.8	1float	Sil+Kfs		X	X	X	?			tr		Xl	X	X	X		Tourm, Ap,
AB89-67.1	mixed	Sil+Kfs		X	X	X	?			tr		Xl	X	X	X		Tourm
AB89-67.2	mixed	Sil+Kfs		X	X	X		lt				X	X				
AB89-71	mixed	Sil+Kfs	X	X	X	X	?			X		X	X	X			
AB89-77.1	3rd	Sil+Kfs		X	X	X				X							
AB89-78.1	3rd	Sil+Kfs	X	X	X	X	X			X			X				
AB89-78.2	3rd	Sil+Kfs	X	X	X	X	X			X				X			
AB89-82.2	2nd	Sil+Kfs	X	X	X	X	X			X							
AB90-04.1	1st	Sil+Kfs	X	X	X	X	X			X	inc	lt		tr		pelite	
AB90-04.2	1st	Sil+Kfs	X	X	X	X	X			tr						pelite	
AB90-07	1st	Sil+Kfs	X	X	X	X	X			X						pelite	
AB90-17	1st	Sil+Kfs	X	X	X	X	X			X						pelite	
AB90-18.3B	1st	Sil+Kfs	X	X	X	X	X									pelite	
AB90-19.1	0th	Sil+Kfs	X	X	X	X	X									pelite	
AB90-19.5	0th	Sil+Kfs	X	X	X	X	X									pelite	
AB90-19.6	0th	Sil+Kfs	X	X	X	X	X			X						pelite	
AB90-19.7	0th	Sil+Kfs	X	X	X	X	X									pelite	
AB90-19.9	0th	Sil+Kfs	X	X	X	X				X			X			pelite	
AB90-23.2	3rd	Sil+Kfs	X	X	X	X	X					lt				pelite	
AB90-23.7	3rd	Sil+Kfs	X	X	X	X	X			X		lt				pelite	
AB90-26.06	3rd	Sil+Kfs	X	X	X	X	X						X			pelite	
AB90-26.12	3rd	Sil+Kfs	X	X	X	X										pelite	
AB90-35.5	0th	Sil+Kfs	X	X	X	X	X						?		X	pelite	Tourm, Sul
AB90-39.1	2nd	Sil+Kfs	X	X	X	X				X						pelite	
AB90-39.2	2nd	Sil+Kfs	X	X	X	X	X			X			X			pelite	
AB90-40.1	2float	Sil+Kfs	X	X	X	X	X		inc	X		lt				pelite	Tourm
AB90-44	2nd	Sil+Kfs	X	X	X	X	X			X		X				pelite	
AB90-61.1	2nd	Sil+Kfs	X	X	X	X	X			X		X	X			pelite	

Sample#	Unit	Isograd	Gt	Bt	Qz	Pl	Kfs	Mu	Sta	Sil	Ky	Crd	Gr	Opq	Rut	Lithol	Access
AB90-61.2	2nd	Sil+Kfs	X	X	X	X	X		inc	X		X				pelite	
AB90-65A	0th	Sil+Kfs	X	X	X	X	?					?				pelite	
AB90-65B	0th	Sil+Kfs	X	X	X	X										pelite	
AB90-67	1st	Sil+Kfs	X	X	X	X	X			X					inc	pelite	
AB90-70.3	4th	Sta	X	X	X	X		X	inc	fib		tr	X		inc	pelite	
AB90-78.2	4th	Sil	X	X	X	X		X	X	X fib						pelite	
AB90-79	4th	Sil	X	X	X	X		tr	inc	fib		X	X	X		pelite	
AB90-80	4th	Sil	X	X	X	X				fib						pelite	Tourm
AB90-81	4th	Sil	X	X	X	X	?			fib						pelite	Tourm

Sample#	Unit	Isograd	Gt	Bt	Qz	Pl	Kfs	Mu	Sta	Sil	Ky	Crd	Gr	Opq	Rut	Lithol	Access
AB85-005	4th	Sta	X	X	X	X		X	X					X		pelite	
155 KT78	4th	Sta	X	X	X	X		X	X							pelite	
AB84-149	4th	Sta	X	X	X	?		X	X				X			pelite	
AB84-152	4th	Sta		X	X	X										pelite	Tourm
AB85-021	4th	Sta	X	X	X	X		X	X		X		X	X		pelite	
AB85-022.1	4th	Sta	X	X	X	X											
AB85-023	4th	Sta	X	X	X	X		X	X							schist	
AB85-026	4th	Sta	X	X	X	X		X	X							pelite	
AB85-033	4th	Sta															
AB85-034.1	4th	Sta	X	X	X	X		X	X				X	X		gqtzite	Tourm
AB85-034.2	4th	Sta	X	X	X	X		X	X				X	X		qtzitic	Tourm
AB85-036	4th	Sta								fib	X	X	X	X			
AB85-036.2	4th	Sta	X	X	X	X		X	X	fib		X	X	X			Tourm, Ap
AB85-037.1	4th	Sta	X	X	X	X		X	X	tr	A		X	X		btschist	Tourm
AB85-041	4th	Sta								?			X	X		gqtzite	
AB85-049.2	4th	Sta		X	X	X		tr	X				X	X			Tourm
AB85-065	4th	Sta	X	X	X	X		X	X	X			X	X			Tourm
AB85-067.1	4th	Sta	X	X	X	X		X	X	X	A		X	X			
AB85-067.2	4th	Sta	X	X	X	X		X	X				X	X			
AB85-067.3	4th	Sta	X	X	X	X		X	X				X	X			
AB85-069	4th	Sta	X	X	X			X	X								
AB85-070	4th	Sta	X	X	X			X	X				X				
AB85-071	4th	Sta	X	X	X	X		X	X	X	A			X			Tourm
AB85-072	4th	Sta		X	X	X		X	X	fib							
AB85-073	4th	Sta		X	X	X		X	X			X					Tourm
AB85-076	4th	Sta								fib							
AB85-077.2	4th	Sta		X	X	X		X	X				X	X			
AB85-222.2	4th	Sta	X	X	X	X		X	X				X	X			
AB85-249	4th	Sta	X	X	X	X		X	X								
AB86-006	4th	Sta															
AB86-007.2	4th	Sta	X	X	X	X		X	X								
AB87-213.1	4th	Sta		X	X	X		X	tr								
AB87-218	4th	Sta															Tourm
AB87-220.1	4th	Sta	X	X	X	X		X	X		Xl		X	X			
AB87-220.3	4th	Sta	X	X	X	X		X	X		X		X	X		pelite	
AB87-221.2	4th	Sta		X	X			X				Xl	X	inc			
AB87-222	4th	Sta		X	X	X		X	X		Xl		X	X		pelite	Tourm
AB87-244.1	4th	Sta	X	X	X	X		X	X				X	X		pelite	Tourm

Sample#	Unit	Isograd	Gt	Bt	Qz	Pl	Kfs	Mu	Sta	Sil	Ky	Crd	Gr	Opq	Rut	Lithol	Access
AB87-246	4th	Sta		X	X	X		X	X		X	It?		X		pelite	Tourm
AB87-247	4th	Sta		X	X	X		X	X		X			X		pelite	
AB87-271	4th	Sta		X	X			X	X					X	inc	pelite	Tourm
AB87-272.1	4th	Sta	X	X	X	X			X					X		pelite	Tourm
AB87-272.2	4th	Sta	X	X	X	X		X	X		A?	?		X		pelite	Tourm
AB87-273	4th	Sta	X	X	X			X	X					X		pelite	Tourm
AB87-289	4th	Sta	X	X	X	X		X	X					X			
AB87-290	4th	Sta	X	X	X	X		X	X								
AB90-70.3	4th	Sta		X	X			X	X		tr			X		pelite	Tourm
SL81-425.1	4th	Sta	X	X	X			X	X					X		pelite	
SL81-483.1	4th	Sta	X	X	X	X		X	X					X		pelite	
SL81-483.2	4th	Sta	X	X	X			X	X		X			X		pelite	Tourm
SL81-484.1	4th	Sta	X	X	X	X		X	X					X		pelite	
SL81-485.1	4th	Sta	X	X	X	X		X	X		X			X		pelite	
SL81-486.1	4th	Sta	X	X	X			X	X					X		pelite	
SL81-487.1	4th	Sta	X	X	X			X	X				X	X		pelite	
SL81-488.1	4th	Sta	X	X	X	X		X	X				X	X		pelite	
SL81-491.1	4th	Sta		X	X			X	X								
SL81-491.3	4th	Sta		X	X	X											
SL81-492	4th	Sta		X	X												
SL81-497.1	4th	Sta	X	X	X	X		X	X			?		X		pelite	Ap, Zrn
SL81-515.1	4th	Sta	X	X	X	X		tr	X		A			X		pelite	Tourm
SL81-516.1	4th	Sta		X	X			tr						X			
030 KT78	4th	Sil/Sta		X	X	X		X		fib	X					pelite	
028 KT78	4th	Sil		X	X	X		X		fib	X					pelite	
147 KT78	4th	Sil		X	X					fib			X	X	X	btschist	
150 KT78	4th	Sil		X	X	X	?			tr	one					pelite	
AB85-050	4th	Sil	X	X	X	X		X		fib			X	X		gqtzite	
AB85-051	4th	Sil	X	X	X	X		inc		fib			X	X		pelite	Ap
AB85-085	4th	Sil	X	X	X					X fib			X				
AB85-210.2	4th	Sil		X	X					X fib						pelite	Tourm
AB85-226.2	4th	Sil		X	X	X			one	fib				X		pelite	
AB85-226.3	4th	Sil		X	X			tr		fib				X		pelite	
AB85-227.1	4th	Sil	X	X	X	X		X	Xl	fib				X		pelite	
AB87-224	4th	Sil	one	X	X	X		X		fib							
AB87-225.1	4th	Sil	X	X	X	X		X		fib							
AB87-250	4th	Sil		X	X					fib							
AB87-252.1	4th	Sil		X	X					fib						pelite	

Sample#	Unit	Isograd	Gt	Bt	Qz	Pl	Kfs	Mu	Sta	Sil	Ky	Crd	Gr	Opq	Rut	Lithol	Access
AB87-252.2	4th	Sil	x	x	x	x		x		fib						pelite	
AB87-252.3	4th	Sil	x	x	x	x	??	x		fib						pelite	Tourm
AB87-256	4th	Sil	x	x	x	x				fib							
AB87-257	4th	Sil	x	x	x	x		tr		fib				x			
AB87-257.2	4th	Sil	x	x	x	x				fib						pelite	Tourm
AB87-257.3	4th	Sil	x	x	x	x				fib						pelite	Tourm
AB87-274	4th	Sil	x	x	x	x		x	x	fib				inc		pelite	
AB87-275	4th	Sil	x	x	x	x		x	x	fib				x		pelite	Tourm
AB87-285	4th	Sil	x	x	x	x			relic	fib				x		pelite	Tourm
AB87-286	4th	Sil	x	x	x	x			X inc	fib		It?		x		pelite	
AB87-287	4th	Sil	x	x	x	x		x	x	fib						pelite	Tourm
AB90-78.2	4th	Sil	x	x	x	x				x fib		It?				pelite	
AB90-79	4th	Sil	x	x	x	x	?			fib		x	x	x		pelite	Tourm
AB90-80	4th	Sil	x	x	x	x			inc	fib						pelite	Tourm
AB90-81	4th	Sil	x	x	x	x		tr		fib				x			
SL81-504.1	4th	Sil	x	x	x	x		x	x	fib				x		pelite	Tourm
SL81-504.2	4th	Sil	x	x	x	x		x	x	fib				x		pelite	Tourm
SL81-506.1	4th	Sil	x	x	x	x		tr		fib							
SL81-512.1	4th	Sil	x	x	x			x	x	X fib				x		pelite	Tourm
038 KT78	4th	Sil+Kfs	x	x	x	x			x	x						pelite	
039 KT78	4th	Sil+Kfs	x	x	x	x	?			X fib						pelite	
042 KT78	4th	Sil+Kfs		x	x	x	x			x			x			gqtzite	Ap
043 KT78	4th	Sil+Kfs		x	x	x	x			x			x			gqtzite	Tourm
AB85-208.1	4th	Sil+Kfs	x	x	x	x	x			fib			x				Tourm
AB85-208.2	4th	Sil+Kfs	x	x	x	x	x			fib			x				Tourm
AB85-215.1	4th	Sil+Kfs	x	x	x	x	x			X fib			x				Tourm
AB85-217	4th	Sil+Kfs	x	x	x	x	x			fib			x				Tourm
AB85-228.1	4th	Sil+Kfs	x	x	x	x				fib			x	x			Tourm
AB85-229	4th	Sil+Kfs		x	x	x		x		fib				x			Tourm
AB87-253.1	4th	Sil+Kfs	x	x	x	x	x			fib			x				Tourm
AB87-253.2	4th	Sil+Kfs	x	x	x	x	?			fib			x				Tourm
AB87-253.3	4th	Sil+Kfs	x	x	x	x	x			fib			x			gqtzite	Tourm
AB87-254.1	4th	Sil+Kfs	x	x	x	x	x			X fib		It	x		inc	gqtzite	Tourm
AB87-254.2	4th	Sil+Kfs	x	x	x	x	x			fib			x			gqtzite	Tourm
AB87-255	4th	Sil+Kfs	x	x	x	x	x			fib			x			gqtzite	Tourm
AB87-277	4th	Sil+Kfs		x	x	x				fib				x		pelite	Tourm
AB87-278	4th	Sil+Kfs	x	x	x	x	?			fib						gqtzite	Tourm, Allanite
AB87-281	4th	Sil+Kfs	x	x	x	x	?	?		fib							

Sample#	Unit	Isograd	Gt	Bt	Qz	Pl	Kfs	Mu	Sta	Sil	Ky	Crd	Gr	Opq	Rut	Lithol	Access
AB87-282	4th	Sil+Kfs	X	X	X	X	X			fib						gqtzite	
AB87-283.2	4th	Sil+Kfs	X	X	X	X	X			fib						pelite	
OS 91	4th	Sil+Kfs	X	X	X	X	X	lt	inc	X		lt	X	X	inc	pelite	
055 KT78	4/TGOC	Sil+Kfs		X	X	X	X			X			X			pelite	
066 KT78	mixed/TG	Sil+Kfs		X	X	X				fib				inc	inc	pelite	Tourm
068 KT78	mixed/TG	Sil+Kfs	X	X	X	X										pelite	
063 KT78	mixed	Sil+Kfs		X	X	X	X			fib						granitic	Sph, Aln
076 KT78	mixed	Sil+Kfs		X	X	X		tr		X						pelite	Tourm
082 KT78	mixed	Sil+Kfs	X	X	X	X	X		X	X fib						qtzite	
085 KT78	mixed	Sil+Kfs	X	X	X	X	X			X		?	X	X		pelite	
AB89-29	mixed	Sil+Kfs		X	X	X				X			X	X		btgneiss	Ap
AB89-33.1	mixed	Sil+Kfs	X	X	X	X	X			X	inc	lt	X	inc	inc	pelite	Ap
AB89-33.2	mixed	Sil+Kfs	X	X	X	X	?			tr		Xl	X				Ap, Tourm
AB89-67.1	mixed	Sil+Kfs		X	X	X	X	lt		tr		Xl					Tourm,Ap,Sulph
AB89-67.2	mixed	Sil+Kfs		X	X	X				X							
AB89-71	mixed	Sil+Kfs		X	X	X	X			X			X	X		pelite	Tourm
096 KT78	3rd	Sil+Kfs	X	X	X	X				X			X	X		pelite	
098 KT78	3rd	Sil+Kfs	X	X	X	X	X			X		?	X	X		pelite	
099 KT78	3rd	Sil+Kfs	X	X	X	X	X			X			X	X		pelite	Tourm
100 KT78	3rd	Sil+Kfs	X	X	X	X				X fib			X		inc	pelite	Tourm
101 KT78	3rd	Sil+Kfs	X	X	X	X	X			X fib			X		inc	qtzite	Ap
156 KT78	3rd	Sil+Kfs	X	X	X	X	X		inc	X			X			pelite	Tourm
AB89-01.1	3rd	Sil+Kfs	X	X	X	?				X fib		?	X			pelite	Ap
AB89-01.2	3rd	Sil+Kfs	X	X	X	?	?			X fib			X	X		pelite	
AB89-01.3	3rd	Sil+Kfs	X	X	X	X	?			X		?	X			pelite	Tourm, Ap
AB89-02	3rd	Sil+Kfs	X	X	X	X				X			X			pelite	
AB89-07	3rd	Sil+Kfs	X	X	X	X			inc	X fib			X	X	inc	pelite	
AB89-20	3rd	Sil+Kfs	X	X	X	X				X			X	X	inc	pelite	
AB89-21.1	3rd	Sil+Kfs	X	X	X	X	X		inc	X fib			X	X	inc	pelite	Ap
AB89-21.2	3rd	Sil+Kfs	X	X	X	X			inc	X fib		lt	X	X		pelite	Ap
AB89-35	3rd	Sil+Kfs	X	X	X	X	X			X			X			grphsch	
AB89-37.1	3rd	Sil+Kfs		X	X	X	?			X			X			gqtzite	
AB89-40.03	3rd	Sil+Kfs	X	X	X	X	?			X fib			X	X	X	pelite	
AB89-40.07	3rd	Sil+Kfs	X	X	X	?	?			X			X			pelite	
AB89-40.08	3rd	Sil+Kfs	X	X	X	?	?	inc		X fib			X			pelite	
AB89-40.09	3rd	Sil+Kfs	X	X	X	X				X			X	X	X	pelite	Tourm
AB89-40.10	3rd	Sil+Kfs	X	X	X	X				X fib			X	X	inc	pelite	Ap
AB89-40.11	3rd	Sil+Kfs	X	X	X	X				X fib	inc?		X			pelite	Ap

Sample#	Unit	Isograd	Gt	Bt	Qz	Pl	Kfs	Mu	Sta	Sil	Ky	Crd	Gr	Opq	Rut	Lithol	Access
AB89-48.3	3rd	Sil+Kfs	X	X	X	X				X				X			
AB89-77.1	3rd	Sil+Kfs	X	X	X	X	?			X		X					
AB89-78.1	3rd	Sil+Kfs	X	X	X	X	X			X			X				
AB89-78.2	3rd	Sil+Kfs	X	X	X	X				X							
AB90-23.2	3rd	Sil+Kfs	X	X	X	X				X		lt				pelite	Tourm,sulphide
AB90-23.7	3rd	Sil+Kfs	X	X	X	X	X			X		lt	X			pelite	
AB90-26.06	3rd	Sil+Kfs	X	X	X	X										pelite	
AB90-26.12	3rd	Sil+Kfs	X	X	X	X								X		pelite	
OS 63	3rd	Sil+Kfs	X	X	X		X		inc	X							
OS 78	3rd	Sil+Kfs	X	X	X	X				X						pelite	
OS 92	3rd	Sil+Kfs	X	X	X	X				X							
AB89-57.2	3/2	Sil+Kfs	X	X	X	X	X			X		Xl					Ap
AB89-58	3/2	Sil+Kfs	X	X	X	X	X			X			X			pelite	
OS 30	3/2	Sil+Kfs	X	X	X	X				X			X			pelite	
OS 30.1	3/2	Sil+Kfs	X	X	X	X	X			X			X			pelite	
OS 42	3/2	Sil+Kfs	X	X	X	X		?		X fib			X			pelite	
OS 43	3/2	Sil+Kfs	X	X	X	X				X		lt	X	X		pelite	
170 KT78	2nd	Sil+Kfs	X	X	X	X	X			X							
AB89-16	2nd	Sil+Kfs	X	X	X	X	X			X				X			
AB89-82.2	2nd	Sil+Kfs	X	X	X	X				X		X		X			
AB90-39.1	2nd	Sil+Kfs	X	X	X	X	X			X		X				pelite	Tourm
AB90-39.2	2nd	Sil+Kfs	X	X	X	X			inc	X		X	X	X		pelite	
AB90-44	2nd	Sil+Kfs	X	X	X	X				X						pelite	
AB90-61.1	2nd	Sil+Kfs	X	X	X	X			inc	X						pelite	
AB90-61.2	2nd	Sil+Kfs	X	X	X	X				X				X		pelite	
OS 39	2nd	Sil+Kfs	X	X	X	X	X			X			X			pelite	
OS 40	2nd	Sil+Kfs	X	X	X	X	X		inc	X		lt	X	X		pelite	
OS 41.2	2nd	Sil+Kfs	X	X	X	X				X		lt		X		pelite	
AB90-40.1	2float	Sil+Kfs	X	X	X	X	X			X			X	X	inc	pelite	
OS 35	2/syen	Sil+Kfs	X	X	X	X	X			X			X	X	inc	pelite	Tourm
OS 36	2/syen	Sil+Kfs	X	X	X	X				X			X	X		pelite	Tourm
OS 60	2/syen	Sil+Kfs	X	X	X	X				X fib		lt	X	X		pelite	Tourm
AB89-13	syen	Sil+Kfs	X	X	X	X	X			X				X	X	qtzite	Ap
AB89-15	syen	Sil+Kfs	X	X	X	X	X			X				X	X	pelite	
OS 76	syen	Sil+Kfs	X	X	X	X						lt	X			pelite	
117 KT78	1st	Sil+Kfs	X	X	X	X	X				?	lt	X			pelite?	
AB86-104.1	1st	Sil+Kfs	X	X	X	X	?							relic			
AB86-105.1	1st	Sil+Kfs	X	X	X	X	X			X	?	lt				pelite	

Sample#	Unit	Isograd	Gt	Bt	Qz	Pl	Kfs	Mu	Sta	Sil	Ky	Crd	Gr	Opq	Rut	Lithol	Access
AB86-105.2	1st	Sil+Kfs	X	X	X	X	X			X		tt		X		pelite	
AB86-118.2	1st	Sil+Kfs			X	X	X			X		tt	X	X		pelite	
AB86-123	1st	Sil+Kfs			X	X	X			X			Xl			pelite	
AB89-10.1	1st	Sil+Kfs	X	X	X	X				Xfib	inc		X		inc	pelite	
AB89-10.3	1st	Sil+Kfs	X	X	X	X	X			X	inc		X		X	pelite?	
AB89-10.4	1st	Sil+Kfs	X	X	X	X										pelite?	
AB89-10.5	1st	Sil+Kfs	X	X	X	X	X			Xfib	inc		X	?	inc	pelite	
AB89-11.1	1st	Sil+Kfs	X	X	X	X	X			Xfib			?	?	X	pelite	
AB89-11.2	1st	Sil+Kfs	X	X	X	X	X			Xfib		tr		?	X	pelite	
AB89-23.3	1st	Sil+Kfs	X	X	X	X	X			inc				X	X	pelite	Ap
AB89-60.3	1st	Sil+Kfs	X	X	X	X	X			X	inc	X	X	X	inc	pelite	
AB90-04.1	1st	Sil+Kfs	X	X	X	X	X			X				X	tr	pelite	
AB90-04.2	1st	Sil+Kfs	X	X	X	X				tr	inc	tt				pelite	
AB90-07	1st	Sil+Kfs	X	X	X	X	X			X						pelite	
AB90-17	1st	Sil+Kfs	X	X	X	X	X			X			X		inc	pelite	
AB90-18.3B	1st	Sil+Kfs	X	X	X	X	X		inc	X	inc?			X		pelite	
AB90-67	1st	Sil+Kfs	X	X	X	X	X			X		tt	X	X	X	pelite	Ap
OS 06	1st	Sil+Kfs	X	X	X	X	X			X				X	X		
OS 18	1st	Sil+Kfs		X	X	X			inc	X			X	X			Tourm
OS 19	1st	Sil+Kfs	X	X	X	X	X			Xfib	inc	tt		X	X	pelite	
OS 52.1	1st	Sil+Kfs	X	X	X	X				X			X	X	X	pelite	
OS 56	1st	Sil+Kfs	X	X	X	X	X			X						pelite	
OS 70	1st	Sil+Kfs	X	X	X	X	?		inc	X	inc			X	X		
OSW 2	1st	Sil+Kfs	X	X	X	X	X			X		?	X	X			Tourm
AB89-64.2	1float	Sil+Kfs		X	X	X	X			X		X					
AB89-64.3	1float	Sil+Kfs	X	X	X	X	X			X	inc	X	X	X	inc	pelite	
AB89-64.5	1float	Sil+Kfs	X	X	X	X	X			X	inc		X	X		pelite	
AB89-65.2	1float	Sil+Kfs	X	X	X	X	X			X	inc					?	
AB89-65.6	1float	Sil+Kfs	X	X	X	X				X		tt				pelite	
AB89-65.8	1float	Sil+Kfs			X	X											
AB90-19.1	0th	Sil+Kfs	X	X	X	X	X						X	X	X	pelite	
AB90-19.5	0th	Sil+Kfs	X	X	X	X	X						X	X	X	pelite	
AB90-19.6	0th	Sil+Kfs	X	X	X	X	X									pelite	
AB90-19.7	0th	Sil+Kfs	X	X	X	X	X			X						pelite	
AB90-19.9	0th	Sil+Kfs	X	X	X	X	X						?			pelite	
AB90-35.5	0th	Sil+Kfs	X	X	X	X	X							X			
AB90-65A	0th	Sil+Kfs	X	X	X	X	X								inc		
AB90-65B	0th	Sil+Kfs	X	X	X	X	?					?				pelite	

Appendix 2:   Major element mineral compositions

Microprobe analyses of minerals were carried out on a JEOL Superprobe 733 at the University of Washington, Department of Geological Sciences. The accelerating voltage was 15 kvolts and sample current 15 namps for biotite, feldspar and carbonate and 25 namps for all other phases. Natural minerals and synthetic glasses were used as standards. Data were reduced using the method of Bence and Albee (1968).

Biotites were normalized to 11 oxygens assuming all Fe measured is Fe^{2+}, so that the solution model of McMullin et al. (1992) could be used for thermodynamic calculations. (OH) was determined by the formula (OH) = 2 - F - Cl, and a wt% H_2O calculated accordingly. Definition of exchange vectors (Thompson 1982, Dymek 1983) and formulas used to caclulate them are defined as follows: $X_{tlc} = K_{-1}Al_{-1}\square Si = 1 - K - Na - Ca$; $X_{an} = K_{-1}Si_{-1}CaAl = Ca$; $X_{tispl} = Al_{-2}TiMg = Ti$; $X_{dioct} = Mg_{-3}\square Al_2 = 3 - Mg - Fe - Mn - Al^{vi} - Ti$; $X_{tk} = Mg_{-1}Si_{-1}Al_2 = 3 - Si - X_{an} - X_{tlc}$.

Feldspars were normalized to Ca + Na + K = 1.

Garnets were normalized to 8 cations. Fe^{3+} was calculated so as to bring the number of oxygens to 12.

Hornblende stoichiometry calculated from microprobe data is dependent on the normalization scheme used (Robinson et al. 1982). I have chosen to normalize to the average of 15 (excluding K and Na) and 13 (excluding K, Na and Ca) cations (Hollocher 1991). Niether F nor Cl were measured; (OH) was assumed to be 2. Wt% H_2O was calculated based on this stoichiometry. Definition of exchange vectors (Thompson 1982) and formulas used to caclulate them are defined as follows: $X_{ed} = \square_{-1}Si_{-1}(Na,K)Al = (Na + K)^A$; $X_{tspl} = Al_{-2}TiMg = Ti$; $X_{ab} = Ca_{-1}Al_{-1}NaSi = Na^{M4}$; $X_{tk} = Mg_{-1}Si_{-1}Al_2 = 8 - Si - X_{ed} + X_{ab}$. "xsO" is the oxygen wt% correction for Fe^{2+} to Fe^{3+} conversion.

Olivine was normalized to 3 cations, clinohumite to 13 cations and chondrodite to 7 cations, assuming all Fe measured is Fe^{2+}. The (OH) content of clinohumite and chondrodite was determined by the formula (OH) = 2 - F - 2Ti, and a wt% H_2O calculated accordingly.

Pyroxenes were normalized to 4 cations. Fe^{3+} was calculated so as to bring oxygens to 6. "xsO" is the oxygen wt% correction for Fe^{2+} to Fe^{3+} conversion.

Spinels were normalized to 3 cations. Fe^{3+} was calculated so as to bring oxygens to 4. "xsO" is the oxygen wt% correction for Fe^{2+} to Fe^{3+} conversion.

Staurolites were normalized to Si + Al = 25.53 (Holdaway et al. 1986). Fe^{3+} is assumed to be 0.25; lithium is assumed to be 0.2; hydrogen is assumed to be 3.06 (Holdaway et al. 1986). Wt% Li_2O and H_2O was calculated accordingly.

	Bt	Bt	Bt	Bt	Bt	Bt	Bt	Bt	Bt //	Bt	Bt AB90-13	Bt	Bt	Bt
	87-220	87-218	81-425	85-222	81-506	78-85	89-78	90-19.5	+15 cm	+18 cm	+61 cm	+86 cm	+244 cm	+594 cm
SiO2	34.44	35.55	35.33	33.94	36.23	35.21	35.03	36.29	36.69	37.78	38.11	36.39	36.40	38.09
TiO2	1.80	1.37	2.08	2.77	2.34	3.99	3.93	6.63	7.32	4.48	3.58	4.08	3.55	3.58
Al2O3	19.16	19.40	18.75	18.84	18.93	17.46	17.71	14.04	13.42	14.98	14.59	14.04	14.19	14.41
FeO	22.40	17.89	16.85	22.53	16.46	17.95	18.43	17.30	17.07	15.13	14.63	18.81	18.95	15.93
MnO	0.02	0.11	0.09	0.01	0.40	0.06	0.07	0.04	0.05	0.07	0.11	0.18	0.22	0.01
MgO	7.20	10.18	10.97	5.82	10.82	10.19	9.66	11.10	11.68	14.00	14.83	11.81	12.39	14.11
CaO	0.03	0.03	0.01	0.02	0.01	0.02	0.05	0.01		0.04	0.03	0.02	0.07	0.01
Na2O	0.30	0.30	0.24	0.27	0.19	0.23	0.15	0.09	0.03	0.03	0.09	0.06	0.09	0.06
K2O	8.78	8.76	8.78	8.39	9.10	9.37	8.92	9.71	9.88	9.78	9.60	9.78	9.33	9.78
F	0.45	0.38	0.34	0.43	0.30	0.33	0.34	0.43	0.03	0.26	0.10	0.35	0.32	0.45
Cl	0.01	0.01	0.01	0.02	0.01	0.04	0.02	0.01	0.02	0.07	0.07	0.05	0.01	0.05
F,Cl=O	-0.19	-0.16	-0.14	-0.18	-0.13	-0.15	-0.15	-0.18	-0.02	-0.12	-0.06	-0.16	-0.14	-0.20
H2O*	3.63	3.73	3.74	3.57	3.83	3.75	3.73	3.74	3.96	3.91	3.97	3.73	3.77	3.80
Total	98.02	97.53	97.04	96.39	98.48	98.46	97.91	99.19	100.14	100.41	99.67	99.15	99.15	100.08
Si	2.689	2.724	2.712	2.696	2.735	2.694	2.694	2.758	2.761	2.795	2.831	2.789	2.784	2.836
Aliv	1.311	1.276	1.288	1.304	1.265	1.306	1.306	1.242	1.239	1.205	1.169	1.211	1.216	1.164
Alvi	0.453	0.475	0.408	0.459	0.420	0.268	0.298	0.016	-0.049	0.101	0.108	0.057	0.062	0.101
Ti	0.106	0.079	0.120	0.165	0.133	0.230	0.227	0.379	0.414	0.249	0.200	0.235	0.204	0.200
Fe	1.463	1.146	1.082	1.496	1.040	1.148	1.185	1.100	1.074	0.936	0.909	1.205	1.212	0.992
Mn	0.001	0.007	0.006	0.001	0.025	0.004	0.004	0.003	0.003	0.004	0.007	0.012	0.014	0.001
Mg	0.838	1.162	1.255	0.689	1.218	1.162	1.108	1.258	1.310	1.544	1.643	1.349	1.412	1.566
Ca	0.002	0.002	0.001	0.001	0.000	0.002	0.004	0.000	0.000	0.003	0.002	0.002	0.006	0.001
Na	0.045	0.044	0.036	0.041	0.028	0.034	0.023	0.013	0.004	0.004	0.014	0.009	0.013	0.009
K	0.875	0.856	0.860	0.850	0.877	0.915	0.875	0.941	0.948	0.924	0.910	0.956	0.910	0.929
F	0.110	0.092	0.082	0.108	0.071	0.079	0.084	0.104	0.008	0.061	0.025	0.085	0.077	0.106
Cl	0.001	0.001	0.001	0.002	0.001	0.005	0.003	0.001	0.003	0.009	0.008	0.006	0.001	0.006
OH*	1.889	1.907	1.917	1.890	1.929	1.916	1.913	1.895	1.989	1.931	1.967	1.909	1.921	1.888
cations	7.783	7.772	7.768	7.703	7.742	7.764	7.726	7.710	7.706	7.766	7.792	7.825	7.835	7.800
Xllc	0.077	0.098	0.103	0.108	0.094	0.049	0.098	0.046	0.048	0.069	0.074	0.033	0.071	0.061
Xtk	0.386	0.372	0.390	0.411	0.359	0.354	0.400	0.287	0.286	0.270	0.241	0.243	0.281	0.224
Xan	0.002	0.002	0.001	0.001	0.000	0.002	0.004	0.000	0.000	0.003	0.002	0.002	0.006	0.001
Xtispl	0.106	0.079	0.120	0.165	0.133	0.230	0.227	0.379	0.414	0.249	0.200	0.235	0.204	0.200
Xdioct	0.139	0.130	0.129	0.190	0.164	0.187	0.177	0.244	0.247	0.165	0.134	0.142	0.095	0.139

	Bt AB89-41 -33 cm	Bt AB89-41 -24 cm	Bt AB89-41 +3cm
SiO2	35.41	35.32	39.77
TiO2	5.00	4.10	1.45
Al2O3	13.48	13.66	16.12
FeO	24.23	23.94	0.43
MnO	0.31	0.27	-
MgO	8.10	8.62	26.48
CaO	0.00	0.03	-
Na2O	0.08	0.06	0.06
K2O	9.61	9.57	10.57
F	0.66	0.69	1.56
Cl	0.16	0.16	0.75
F,Cl=O	-0.31	-0.33	-0.83
H2O*	3.49	3.46	3.35
Total	100.22	99.54	99.70
Si	2.763	2.770	2.789
Aliv	1.237	1.230	1.211
Alvi	0.002	0.033	0.121
Ti	0.293	0.242	0.077
Fe	1.581	1.570	0.025
Mn	0.020	0.018	0.000
Mg	0.942	1.008	2.769
Ca	0.000	0.002	0.000
Na	0.012	0.009	0.008
K	0.957	0.958	0.946
F	0.163	0.171	0.346
Cl	0.021	0.021	0.089
OH*	1.816	1.808	1.565
cations	7.808	7.840	7.945
Xllc	0.031	0.030	0.046
Xlk	0.268	0.258	0.257
Xan	0.000	0.002	0.000
Xtispl	0.293	0.242	0.077
Xdioct	0.160	0.129	0.009

	Pl +18 cm plag-host	Kfs +18 cm bleb	Pl +18 cm reintegrate	Pl +18 cm unexsol	Pl +61 cm	Pl AB90-13 +86 cm	Pl +244 cm	Pl +594 cm	Kfs //89-41 -33 cm	Pl -33 cm	Kfs 89-41 -24 cm	Pl -24 cm
SiO_2	55.48	65.65	57.42	50.08	57.14	57.01	57.71	55.78	64.42	59.82	64.82	59.96
Al_2O_3	28.49	18.82	26.09	31.77	27.49	27.54	26.80	27.88	18.96	25.43	18.94	25.58
CaO	10.72	0.18	8.36	15.00	9.44	9.61	8.67	10.08	0.22	6.98	0.14	7.22
Na_2O	5.38	1.21	3.81	3.00	5.86	5.88	6.33	5.56	1.82	7.38	1.51	7.20
K_2O	0.25	15.07	4.27	0.12	0.38	0.25	0.47	0.32	13.98	0.34	14.38	0.36
Total	100.33	100.94	99.95	99.98	100.31	100.29	99.98	99.62	99.40	99.95	99.79	100.32
Si	2.494	3.016	2.635	2.271	2.602	2.590	2.604	2.537	2.983	2.692	3.026	2.706
Al	1.509	1.019	1.411	1.698	1.475	1.474	1.425	1.494	1.035	1.349	1.042	1.361
Ca	0.516	0.009	0.411	0.729	0.461	0.468	0.419	0.491	0.011	0.337	0.007	0.349
Na	0.469	0.108	0.339	0.264	0.517	0.518	0.554	0.490	0.163	0.644	0.137	0.630
K	0.015	0.883	0.250	0.007	0.022	0.014	0.027	0.019	0.826	0.020	0.856	0.021

	Grt	Grt	Grt	Grt	Grt	Grt	Grt	Grt AB89-41	Grt AB89-41	Grt AB90-13
	87-220	90-19	89-78	78-85	81-506	89-35	89-10.3	-33 cm	-24 cm	+18 cm
SiO2	37.55	38.87	38.91	38.39	38.00	37.80	38.51	37.99	37.88	38.45
TiO2	0.03	0.03	0.02	0.00	0.03	0.03	0.04	0.04	0.06	0.01
Al2O3	20.56	20.24	20.46	20.42	20.07	21.23	21.59	21.32	21.11	21.57
FeO*	35.50	28.44	32.25	32.12	25.12	32.17	29.76	26.68	26.30	25.68
MnO	1.14	1.56	1.43	1.93	10.40	0.70	0.62	4.41	4.08	2.43
MgO	2.04	5.77	5.56	5.31	3.14	5.68	7.60	2.51	2.76	6.49
CaO	2.91	4.58	1.30	1.31	2.66	1.74	1.59	7.75	8.28	5.20
xs oxy	0.00	0.00	0.00	0.00	0.00	0.00	0.00	0.00	0.03	0.02
Total	99.72	99.49	99.92	99.48	99.42	99.37	99.71	100.69	100.50	99.86
Si	3.046	3.067	3.085	3.063	3.070	3.004	3.008	3.002	2.994	2.996
Ti	0.002	0.002	0.001	0.000	0.002	0.002	0.002	0.002	0.003	0.000
Al	1.966	1.883	1.912	1.920	1.911	1.988	1.987	1.986	1.966	1.981
Fe3+	0.000	0.000	0.000	0.000	0.000	0.001	0.000	0.005	0.040	0.026
Fe2+	2.408	1.877	2.139	2.143	1.697	2.137	1.943	1.758	1.698	1.648
Mn	0.079	0.104	0.096	0.131	0.711	0.047	0.041	0.295	0.273	0.161
Mg	0.247	0.679	0.657	0.631	0.378	0.673	0.885	0.296	0.326	0.754
Ca	0.253	0.387	0.110	0.112	0.230	0.148	0.133	0.656	0.701	0.434
Mg#	0.093	0.266	0.235	0.228	0.182	0.239	0.313	0.144	0.161	0.314
Xalm	0.806	0.616	0.712	0.710	0.563	0.711	0.647	0.585	0.566	0.550
Xspess	0.026	0.034	0.032	0.043	0.236	0.016	0.014	0.098	0.091	0.054
Xpyr	0.083	0.223	0.219	0.209	0.125	0.224	0.295	0.098	0.109	0.252
Xgros	0.085	0.127	0.037	0.037	0.076	0.049	0.044	0.218	0.234	0.145

	Hbl +15 cm	Hbl AB90-13 +61 cm	Hbl +86 cm	Hbl +244 cm	Hbl +594 cm	Hbl 90-13 +86 cm Tr vein	Hbl 89-41 -33 cm	Hbl 90-65 inc	Hbl 90-65 inc
SiO2	43.14	49.63	43.07	42.77	43.40	52.29	40.43	44.09	44.46
TiO2	3.73	0.68	1.62	1.43	1.58	0.16	2.03	1.71	1.58
Al2O3	10.24	7.15	11.39	11.14	11.32	4.19	11.71	12.44	12.06
FeO*	14.15	12.18	17.50	17.30	15.63	13.98	22.68	11.98	12.31
MnO	0.09	0.26	0.41	0.41	0.31	0.57	0.54	0.05	0.04
MgO	11.29	15.24	10.25	10.62	11.41	14.52	6.38	14.62	14.22
CaO	11.48	11.59	11.23	11.34	11.43	12.12	11.06	9.65	9.66
Na2O	1.33	0.88	1.33	1.28	1.31	0.32	1.56	2.02	2.34
K2O	1.67	0.66	1.49	1.38	1.40	0.13	1.80	0.40	0.48
Subtotal	97.12	98.30	98.27	97.67	97.80	98.29	98.20	96.96	97.15
xs O *	0.00	0.15	0.16	0.22	0.15	0.13	0.11	0.32	0.22
H2O*	2.00	2.10	2.01	2.01	2.02	2.09	1.94	2.08	2.07
Total	99.12	100.54	100.45	99.90	99.97	100.51	100.26	99.36	99.44
Si	6.471	7.101	6.418	6.393	6.439	7.501	6.247	6.360	6.447
Aliv	1.529	0.899	1.582	1.607	1.561	0.499	1.753	1.640	1.553
Alvi	0.281	0.307	0.417	0.356	0.419	0.210	0.379	0.475	0.507
Ti	0.420	0.074	0.182	0.161	0.176	0.017	0.236	0.185	0.172
Fe3+ *	0.011	0.316	0.357	0.492	0.342	0.290	0.261	0.692	0.482
Fe2+	1.765	1.142	1.824	1.671	1.597	1.388	2.670	0.754	1.011
Mn	0.011	0.031	0.051	0.052	0.039	0.070	0.071	0.006	0.005
Mg	2.512	3.235	2.266	2.355	2.512	3.090	1.462	3.129	3.059
Ca	1.845	1.777	1.792	1.816	1.818	1.862	1.831	1.491	1.501
(Na)vi	0.155	0.119	0.110	0.098	0.097	0.074	0.090	0.288	0.263
(Na)A	0.231	0.127	0.273	0.273	0.280	0.016	0.376	0.297	0.394
K	0.320	0.121	0.283	0.263	0.265	0.023	0.356	0.073	0.088
H*	2	2	2	2	2	2	2	2	2
Xtk	1.133	0.770	1.137	1.169	1.113	0.533	1.112	1.537	1.333
Xed	0.551	0.248	0.555	0.536	0.545	0.039	0.732	0.370	0.483
Xtixpl	0.420	0.074	0.182	0.161	0.176	0.017	0.236	0.185	0.172
Xab	0.155	0.119	0.110	0.098	0.097	0.074	0.090	0.268	0.263

	Ol 89-41 Cal+Fo	Ol 89-41 Dol zone	Chu 89-41	Chond 89-41 Chond vien	Chu 89-12.1
SiO2	41.22	41.540	37.54	34.37	37.44
TiO2	0.01	0.010	1.47	2.27	1.42
Al2O3	0.02	0.02			
FeO	6.710	5.350	3.86	2.96	5.19
MnO	0.120	0.080	0.09	0.04	0.14
MgO	50.610	52.140	53.40	54.57	53.54
CaO	0.080	0.050	0.08	0.04	0.01
F			2.53	4.85	2.27
Subtotal	98.770	99.200	98.97	99.10	100.01
H2O*			1.27	2.33	1.44
F = O			-1.07	-2.04	-0.96
Total			99.18	99.39	100.49
Si	1.007	1.004	4.012	2.005	3.964
Ti	0.000	0.000	0.118	0.100	0.113
Al	0.001	0.001			
Fe	0.137	0.108	0.345	0.144	0.460
Mn	0.003	0.002	0.008	0.002	0.013
Mg	1.843	1.879	8.508	4.746	8.450
Ca	0.002	0.001	0.009	0.003	0.001
F			0.855	0.895	0.760
OH			0.909	0.906	1.014

	Cpx AB90-13 +61 cm	Opx AB90-13 +61 cm	Opx AB90-13 +18 cm	Cpx AB90-13 +15 cm	Opx AB90-13 +15 cm	Cpx AB89-41 -33 cm	Cpx AB89-41 -24 cm
SiO2	52.13	51.13	51.29	51.77	51.36	51.02	51.03
TiO2	0.13	0.05	0.04	0.21	0.11	0.09	0.05
Al2O3	2.09	0.88	1.32	1.55	0.79	0.93	0.67
FeO	9.11	25.45	26.13	10.86	28.69	17.43	16.06
MnO	0.50	1.07	0.74	0.22	0.50	0.92	1.04
MgO	13.52	20.04	20.15	13.07	18.71	8.81	9.10
CaO	21.87	0.70	0.39	21.96	0.77	20.53	21.35
Na2O	0.28	0.01	0.01	0.28	0.01	0.29	0.21
xs O	0.05	0.20	0.20	0.18	0.21	0.06	0.06
Total	99.67	99.52	100.26	100.09	101.16	100.07	99.58
Si	1.953	1.950	1.942	1.945	1.949	1.978	1.982
Aliv	0.047	0.050	0.058	0.055	0.051	0.022	0.018
Alvi	0.046	-0.010	0.000	0.013	-0.016	0.021	0.013
Ti	0.004	0.001	0.001	0.006	0.003	0.003	0.002
Fe3+	0.014	0.058	0.056	0.050	0.061	0.017	0.018
Fe2+	0.271	0.754	0.771	0.291	0.850	0.548	0.504
Mn	0.016	0.035	0.024	0.007	0.016	0.030	0.034
Mg	0.751	1.134	1.132	0.728	1.053	0.507	0.524
Ca	0.878	0.029	0.016	0.884	0.031	0.853	0.889
Na	0.020	0.000	0.000	0.020	0.001	0.022	0.016

129

	Spl by Sta 1 83-91 inc	Spl by Sta 2 83-91 inc	Spl 83-41 inc	Spl 89-35 inc	Spl AB89-41 Cal+Fo	Spl Dol zone
SiO2	0.03	0.03	0.01	0.04	0.03	0.02
TiO2					0.06	0.07
Al2O3	60.50	60.48	60.65	59.45	68.01	69.08
Cr2O3					0.17	0.10
FeO*	27.85	24.99	27.16	23.80	6.86	5.51
MnO	0.05	0.10	0.05	0.03	0.07	0.06
MgO	5.08	4.50	6.06	6.26	23.69	24.32
ZnO	6.08	9.12	5.70	9.29		
xs O	0.00	0.00	0.02	0.09	0.01	0.00
	99.57	99.21	99.65	98.97	98.91	99.17
Si	0.000	0.000	0.000	0.000	0.001	0.001
Ti	0.001	0.001	0.000	0.001	0.001	0.001
Al	2.005	2.023	1.995	1.979	1.982	1.996
Cr	0.000	0.000	0.000	0.000	0.003	0.002
Fe3+	0.000	0.000	0.004	0.019	0.002	0.000
Fe2+	0.655	0.593	0.630	0.543	0.139	0.113
Mg	0.213	0.190	0.252	0.263	0.873	0.888
Mn	0.001	0.002	0.001	0.001	0.001	0.001
Zn	0.126	0.191	0.117	0.194	0.000	0.000

	Sta 85-222	Sta 87-220	Sta 81-425	Sta 87-218	Sta // 89-10.3 1 inc	Sta 89-10.3 2 inc	Sta // 89-35 inc	Sta // 83-41 1 inc	Sta 83-41 2 inc	Sta 3 inc	Sta // 83-91 1 inc	Sta 2 inc
SiO2	28.40	27.92	27.87	27.89	25.43	25.30	25.51	25.62	25.45	25.65	25.67	25.59
TiO2	0.69	0.50	0.63	0.66	1.34	1.23	1.16	0.96	1.14	1.13	1.18	0.88
Al2O3	54.69	54.19	54.07	53.97	57.50	57.42	57.02	56.42	55.97	55.31	56.66	57.11
FeO*	12.92	13.96	13.00	13.25	10.50	10.69	11.81	12.30	11.39	12.18	12.25	12.09
MnO	0.05	0.07	0.27	0.32	0.04	0.04	0.06	0.07	0.06	0.09	0.06	0.04
MgO	0.81	1.31	1.95	1.57	2.93	2.93	2.39	2.44	2.59	2.00	1.75	2.07
ZnO	0.01	0.09	0.08	0.18	1.49	1.50	1.26	0.63	1.28	1.27	0.90	1.17
Li2O*	0.18	0.18	0.18	0.18	0.18	0.18	0.18	0.18	0.18	0.18	0.18	0.18
H2O*	1.67	1.65	1.65	1.64	1.67	1.67	1.67	1.66	1.64	1.63	1.66	1.67
	99.43	99.87	99.69	99.65	101.09	100.97	101.05	100.26	99.70	99.45	100.30	100.79
Si	7.81	7.76	7.77	7.78	6.97	6.95	7.03	7.10	7.11	7.21	7.09	7.03
Ti	0.14	0.10	0.13	0.14	0.28	0.25	0.24	0.20	0.24	0.24	0.24	0.18
Al	17.72	17.77	17.76	17.75	18.56	18.58	18.50	18.43	18.42	18.32	18.44	18.50
Fe3+ *	0.25	0.25	0.25	0.25	0.25	0.25	0.25	0.25	0.25	0.25	0.25	0.25
Fe2+	2.72	3.00	2.78	2.84	2.16	2.20	2.47	2.60	2.41	2.61	2.58	2.53
Mn	0.01	0.02	0.06	0.08	0.01	0.01	0.01	0.02	0.01	0.02	0.01	0.01
Mg	0.33	0.54	0.81	0.65	1.19	1.20	0.98	1.01	1.08	0.84	0.72	0.85
Zn	0.00	0.02	0.02	0.04	0.30	0.30	0.26	0.13	0.26	0.26	0.18	0.24
Li*	0.20	0.20	0.20	0.20	0.20	0.20	0.20	0.20	0.20	0.20	0.20	0.20
H*	3.06	3.06	3.06	3.06	3.06	3.06	3.06	3.06	3.06	3.06	3.06	3.06

Appendix 3:   Stable isotope mineral compositions

Stable isotope analyses were carried out on a Finnigan Mat Delta E spectrometer at Department of Geosciences, New Mexico Tech, Socorro, New Mexico. Carbonates were dissolved in phosphoric acid overnight in a 25°C water bath; silicates were reacted with ClF_3 at 450°C for 10 hours, and liberated oxygen was then reacted with a glowing carbon rod. The CO_2 was then isolated by standard cryogenic techniques. $\delta^{18}O$ values are reported relative to SMOW, $\delta^{13}C$ relative to PDB. One sigma precision for extraction and mass spectrometry is estimated at 0.3 ‰.

AB89-41

dist cm	18O	13C	mineral	d18O biot
-31	14.9		fspar	
-25	11.9		fspar	6.3
-18	10.4		fspar	
-11	9.9		fspar	7.0
-5.1	10.8		fspar	7.0
0	11.0		fspar	
0.3	12.7	-2.0	calcite	
0.75	13.0	-2.2	calcite	
1.25	13.1	-2.3	calcite	
1.6	13.5	-2.3	calcite	
2.2	16.4	-1.3	dolomite	
2.6	18.3	-0.9	dolomite	
3.2	20.6	-0.5	dolomite	
3.7	22.5	-0.3	dolomite	
4.2	22.7	-0.2	dolomite	
4.8	23.3	-0.3	dolomite	
5.4	23.1	-0.4	dolomite	
5.9	23.1	-0.3	dolomite	
6.35	22.7	-0.4	dolomite	
11	22.4	-0.5	dolomite	
30	22.3	-0.4	dolomite	
244	22.9	-0.7	dolomite	
396	22.4	-0.5	dolomite	

AB89-62

cm	d18O	d13C		
183	21.4	-2.1	calcite	
43	22.2	-1.6	calcite	
2.5	20.6	-2.5	calcite	
-6.35	19.4		quartz	
-35.5	20.2		quartz	
-63.5	19.1		quartz	
-234	18.9		quartz	

AB89-44

cm				
55	18.8	3.7	calcite	
35	19.4	4.3	calcite	
3	18.2	3.6	calcite	
-1	15.1		quartz	
-7	16.3		quartz	
-16	14.2		quartz	
-60	15.6		quartz	

AB89-61

cm	d18O	d13C		
670	24.3	0.1	calcite	
366	23.7	-1.2	calcite	
366	23.4	-1.2	calcite	1/2 hr
366	23.8	-1.2	calcite	2 hr
366	24.0	-1.2	calcite	overnight
135	20.7	-0.7	calcite	
107	19.6	-1.3	calcite	
102	19.8	-1.3	calcite	
94	19.3	-1.6	calcite	
71	19.5	-1.3	calcite	
53	18.9	-1.1	calcite	

41	18.6	-1.5	calcite	
33	20.1	-0.8	dolomite	
33	20.4	-0.8	dolomite	
15	16.9	-1.2	calcite	
11	16.5	-1.3	calcite	
10	16.8	-1.6	calcite	1 hr
10	16.6	-1.6	calcite	overnight
7.6	16.9	-1.6	calcite	
5	16.6	-1.8	calcite	
2.5	16.3	-1.8	calcite	
-24	15.9		quartz	
-60	16.5		quartz	

AB90-27

cm	d18O	d13C	mineral
2621	22.7	-0.6	calcite
1676	22.8	-0.9	calcite
701	22.6	-1.0	calcite
183	21.8	-0.7	calcite
51	20.9	-1.5	calcite
25	21.3	-0.6	calcite
6	18.8	-1.9	calcite

Nome Group Marbles

AB80-4.1	21.9	4.8	calcite
AB80-4.3	18.3	3.9	calcite
AB80-90.	13.8	3.0	calcite
AB80-91.	13.4	4.6	calcite
AB81-18	15.9	4.7	calcite

AB90-13

cm	Ox Qtz	Ox Hbld	Ox Biot	Ox cc	Carb cc
594	15.1	12.1	8.3		
381	14.9	12.2	8.9		
170	15.1	12.2	7.4		
86	15.1	11.7	7.4		
61	15.3	11.9	7.1		
57	14.8				
41	16.0		7.6		
38	16.2				
23	16.1				
18	16.0		8.2		
15	15.7		11.1		
10	16.2		11.1		
6	16.2				
0				20.9	-0.9
-18				21.7	-0.8
-61				22.2	-1.0
-152				22.2	-0.9
-366				18.1	-0.2

Kigluaik Pelites

	Qtz	Biot	Wh Mica
85-215.1	19.4	13.2	
89-16	18.7	13.0	
89-82.2	17.5	11.4	
89-20	16.2	11.0	

89-13	15.4	7.6		
89-11.1	14.3	9.6		
87-220.1	16.3		13.9	

AB90-26

cm	Ox cc	Carb cc	Ox Qtz	Ox Biot
1389			14.3	8.2
1361	28.0	-0.8		
1323	28.3	-1.6		
992	23.1	5.2		
543	27.3	0.3		
283	16.5	0.9		
104	25.0	4.7		
-28			13.1	7.2

Appendix 4:   Fluid inclusion measurements

Doubly polished thin sections (100-200 μm thick) were prepared from the sample material. Microthermometry was performed on a Fluid Inc. stage in the School of Oceanography, University of Washington, Seattle, WA. The thermocouple was calibrated by a synthetic pure CO_2 fluid inclusion. Accuracy is taken to be $\pm 0.1°C$ for temperatures near or below $0°C$ increasing to $\pm 1°C$ for temperatures above $200°C$. Isochores were calculated using the programs of Nicholls and Crawford (1985).

		Tm	Th		
PELITES					
OS-18	Pel I			Qtz in pelite	
		-57.1	28	vap	others to vap
		-56.7	23.5	liq	
		-57.0	30.2	crit	
			30.2	crit	
			30.2	crit	
			30.2	crit	
			29.3	liq	
		-57.0	29.5	liq	
AB89-1.1	Pel III			Qtz in pelite	
		-57.2	26	liq	
		-57.2	25.9	liq	
		-57.2	26.5	liq	
		-57.1		vap	
		-56.6		vap	
		-57.7	25.9	liq	
			26.1	liq	
			26.1	liq	
			26.2	liq	
			27.8	liq	
			22.4	liq	
			23.7	liq	
			24.6	liq	
			22.9	liq	
AB85-208.1			Pel IV	Qtz in pelite	
area 1		-0.3	184	liq	
		-0.2		vap	
area 2		-7.8	352.5	liq	
		-7.9	353.7	liq	
AB87-220.1			Pel IV	Qtz in pelite	
area 1		-58.6		vap	
		-58.6		vap	
		-0.7			
		-0.8			
area 2		-0.5			
		-59.0		vap	
area 3		-0.6	169.5		
		-0.5	170		
			171		
			182		
AB89-33.2			Pel III	Qtz in schist	
area 1		-56.9		vap	
		-56.8		vap	
		-56.8		vap	
		-4.0	167	liq	
			185	liq	
area 2		-57.0		vap	
area 3			31	vap	
			31	vap	
AB87-218			Pel IV	Qtz in pelite	

area 1	-58.9	11.4	liq	medium bubble at -56
	-58.6	16.7	liq	
	-58.5	17.8	liq	
	-58.5	12.9	liq	small bubble at -56
	-58.4	17.1	liq	large bubble at -56
area 2	-58.1	20	vap	
	-58.1	20	vap	
	-58.1	20	vap	
area 3	-58.5	12.6	liq	most to bubble
	-58.5	12.9	crit	
	-58.2	16	vap	
AB87-254.2		Pel IV	vap	CO_2
AB87-290		Pel IV	Qtz in schist	
area 1	-0.9	256	liq	
	-1.0	200	liq	
		260	liq	
AB90-19.1		Pel O	Qtz in 'charnokite'	
	-57.0	30.8	liq	others to vapor 29+
	-57.0	30.1	liq	
	-56.8	29.8	liq	
	-56.8	30.6	liq	
QTZ VEINS				
AB87-257.2		Pel IV	Qtz in qtz vien	
	-2.1	283.3	liq	
	-2.2	289.8	liq	
	-2.0	277.7	liq	
	-2.1	282.7	liq	
	-2.1	283.4	liq	
	-2.0	250.7	liq	
	-2.0	283.4	liq	
AB87-217		Pel IV	Qtz in qtz vien	
plane 1	-1.0	318.6	liq	
	-0.6	259	liq	
	-0.8	312.2	liq	
	-0.2	257.1	liq	
plane 2	-0.5	271	liq	
	-0.4	279.2	liq	
	-0.5	265.7	liq	
	-0.5	280.3	liq	
	-0.4	277.3	liq	
	-0.4	269.5	liq	
	-0.4	277	liq	
	-0.5	285.6	liq	
	-0.5	305	liq	
AB87-212.1		Pel IV	Qtz in qtz vien	
	-0.3	205.4	liq	
	-0.5	219.5	liq	
	-0.5	214.1	liq	
	-0.6	221.8	liq	

AB87-201.1		Nome	Qtz in qtz vien
plane 1	-1.9	230.8	liq
	-1.7	208.5	liq
	-1.5	229.5	liq
	-1.6	228.3	liq
plane 2	-2.4	223.7	liq
		230.4	liq
		228.3	liq
	-2.3	224.9	liq
	-1.8	233.3	liq

AB87-208.3		Nome	Qtz in qtz vien
	-1.4	226.3	liq
	-1.5	210	liq